Functional coupling of thermo-receptors and fatty acid-related enzymes in regulation of thermal preference in *Drosophila*

Deng, Xiangmei (鄧 香梅)

Doctor of Philosophy

Department of Physiological Sciences
School of Life Science

The Graduate University for Advanced Studies, SOKENDAI

September 2023

Table of contents

Summary 4

1 Introduction 6

1.1 Thermal sensation is critical for insects. 6

1.2 Thermo-sensory molecules in *Drosophila*. 6

1.2.1 TRP channels are involved in thermosensation. 7

1.2.2 IRs and GR are involved in thermosensation. 8

1.3 Potential correlation of fatty acid metabolism with thermal sensation. 8

2 Materials and Methods 10

2.1 Fly strains and rearing condition 10

2.2 Generation of $CG8893^{KO}$, $MGAT\text{-}1^{KO}$, $MGAT\text{-}2^{KO}$, and $MGAT\text{-}3^{KO}$ flies 10

2.3 Generation of *MGAT-2* and *MGAT-3* transgenic flies 12

2.4 Quantitative PCR (qPCR) 13

2.5 Temperature gradient assays 14

2.6 Thermal two-way choice assay 16

2.7 Evaluation of developmental rate 16

2.8 Locomotion assay 17

2.9 *in vivo* GCaMP-imaging 17

2.10 Statistical analysis 19

3 Results 20

3.1 FAAHs displayed potential involvements in warm avoidance of *Drosophila* larvae. 20

3.2 DAGL (*inaE*) played a potential role in temperature gradient discrimination of *Drosophila* larvae. 21

3.3 *MGAT-2* and *MGAT-3* were involved in the cool avoidance of *Drosophila* larvae. 22

3.3.1 *Drosophila MGATs* were possible orthologs of human monoacylglycerol O-acyltransferase 2 (MOGATs). 22

3.3.2 *MGAT-2/MGAT-3* supported the discrimination between optimal and lower temperatures. 22

3.3.3 Impaired cool avoidance in *MGAT-2/-3* were not due to the changes in development. 24

3.3.4 Role of *MGAT-1/-2/-3* in temperature-dependent locomotion activities. 25

3.3.5 *MGAT-2* and *MGAT-3* functioned in TRP channel expressing neurons. 25

3.3.6 *MGAT-2* primarily functioned in DOCCs to mediate cool avoidance. 26

3.3.7 *MGAT-2* functioned in cool avoidance was compensated by human MOGAT2. 28
3.3.8 Loss of *MGAT-2* caused the deterioration of cooling responses in DOCCs and warming responses in DOWCs. 28
3.3.9 *MGAT-2* maintained *Ir25a* and *Ir21a* mRNA levels. 29
3.3.10 mRNA level of broad was affected by *MGAT-2*. 29
4 Discussion 32
5 References 37
6 Figures 47
7 Tables 103
8 Acknowledgement 107

Summary

Elucidating the mechanism underlying temperature sensation of animals is one of the keys to coping with recent extreme climate changes. Especially for insects, whose body temperature rely on ambient temperatures, sensing and responding to temperature changes are critical for their survival. Insects such as *Drosophila* have developed abilities to precisely discriminate milli-degree per second and this requires a delicate and accurate temperature sensing system.

Thermal sensation in *Drosophila* relies on receptors including Transient receptor potential (TRP) channels, a gustatory receptor (GR), and ionotropic receptors (IRs). TRPA1 and GR28b(D) are activated by temperature increase over 25°C and are involved in warm avoidance, while TRPC (TRPL) and TRPV (Iav) contribute to cool avoidance. IRs are structurally related to mammalian glutamate receptors (GluRs), and *Ir25a*, *Ir93a,* and *Ir21a* are involved in cool avoidance, while *Ir25a*, *Ir93a, and Ir68a* are involved in warm avoidance.

Fatty acids and the conjugates are known to associate with thermo-sensory systems. Polyunsaturated fatty acids (PUFA) are involved in the regulation of TRP channels and triacylglycerol (TAG) contributes to the protection of TRP channel sensitization under oxidative stress. At animal level, fatty acid saturation level affects temperature preference of *Drosophila* larvae and they preferentially consume PUFA containing food under cold environment. However, identity of enzymes involved in this process remains unknown.

Our research aim is to investigate the functional correlation between temperature sensation and fatty acid metabolisms. In this aspect, I sought candidate enzymes that are related to fatty acid metabolism and found multiple genes involved in larval thermotaxis. Those include *CG8839* and *CG5112,* which are putative fatty acid amide hydrolase (FAAH) coding genes catalyzing fatty acid release from anandamide, and inactivation no afterpotential E (*inaE*), a diacylglycerol lipase (DAGL) coding gene hydrolyzing diacylglycerol (DAG) to release PUFA.

I also identified a cluster of genes encoding putative monoacylglycerol acyl transferases (MGATs) and named them *MGAT-1/-2/-3*. These genes are predicted to function in TAG synthesis based on their molecular functions. I observed that *MGAT-2* and *MGAT-3* knockout larvae accumulated in cooler regions on a thermal gradient plate. In a two-way temperature choice assay, *MGAT-2* and *MGAT-3* knockout larvae showed defects in discriminating between optimal 24°C and cooler temperatures. Less preference for 24°C was also observed when these

two genes were knocked down in neurons, suggesting the roles of *MGAT-2/-3* in cool avoidance in the nervous system.

I sought responsible thermo-sensitive neurons and observed less preference for 24°C versus 20°C when knocking down *MGAT-2* or *MGAT-3* in *iav-expressing* chordotonal organs. Meanwhile, a shift in temperature preference towards warmer regions was observed when *MGAT-3* was knocked down in neurons expressing *trpA1-AB* isoforms, suggesting a role of *MGAT-3* in warm avoidance. I also observed that knocking down *MGAT-2* in dorsal organ cool cells (DOCCs) resulted in a defect in discrimination between 24°C and 20°C, where *Ir25a, Ir21a,* and *Ir93a* function for cool avoidance. The defect in cool avoidance in *MGAT-2* KO was compensated by overexpressing *MGAT-2* or human *MOGAT2* in DOCCs, suggesting the primary role of *MGAT-2* in DOCCs.

Using *in vivo* GCaMP imaging, I observed that both the cooling-induced responses in DOCCs and the warming-induced responses of dorsal organ warm cells (DOWCs) were reduced in the absence of *MGAT-2*, and this reduction could be partially rescued by overexpressing *MGAT-2* in the DOCCs. One of the mechanisms of the decreased cool responses was downregulation in the expression level of *Ir25a* and *Ir21a* in DOCCs. After searching database and quantifying expression levels by qPCR, I identified a transcription factor *broad* for *Ir25a* as a candidate for the regulation of the expression level of *Ir25a* and *Ir21a*.

Taken together, I conclude that *MGATs*, which are well-known as an energy storage enzyme, contribute to cool temperature sensing processes by maintaining the transcriptional level of *Irs* in cool-sensing neurons. Proper expression of *Irs* may stabilize the temperature responses of DOCCs and DOWCs, thereby contributing to optimal temperature preference in *Drosophila* larvae.

1 Introduction

1.1 Thermal sensation is critical for insects.

Body temperature serves as a vital indicator of homeostatic stability and therefore has profound effects on the development, growth, survival, and reproduction of living organisms. Insects are ectotherms that exclusively rely on ambient temperatures to maintain their body temperature and achieve homeostasis (Barbagallo and Garrity, 2015). They have developed a large surface-to-volume ratio with small body size and their core temperatures change by environmental temperature rapidly (Garrity et al., 2010), and this temperature fluctuation impacts long-term survival (Dillon et al., 2010) and reproduction (Porcelli et al., 2017).

Since the fluctuation of ambient temperature is unavoidable, insects such as *Drosophila* developed precise temperature detecting mechanisms to discriminate within a milli-degree per second (Fowler and Montell, 2013; Klein et al., 2015), which is hundreds of times higher resolution than that in humans (Luo et al., 2020). This accurate temperature sensation requires a delicate and sophisticated sensory system.

For studying the mechanism for temperature sensation in insects, *Drosophila melanogaster* is a good model. It is a classic model organism that has been studied for more than a hundred years, with complete genome information, profound background knowledge in neuroscience and mature techniques for genetic modifications. These enable researchers to explore the mechanism in sensory neurons at a molecular level.

1.2 Thermo-sensory molecules in *Drosophila.*

Thermotaxis in *Drosophila* has been studied in larval and adult stages. Adult flies prefer temperatures around 25°C, while temperature preference of larvae depends on development (Barbagallo and Garrity, 2015; Sokabe et al., 2016). *Drosophila* larvae seek 24°C from 1st (24 h after egg laying [AEL]) to the early 3rd instar stage (72 h AEL), and their preferred temperature dropped significantly to 18°C at the late 3rd instar stage (120 h AEL) (Sokabe et al., 2016; Wat et al., 2020). These thermotactic phenotypes depend on temperature sensation, which is regulated by multiple thermo-receptors including transient receptor potential (TRP) channels, ionotropic receptors (IRs) and a gustatory receptor (Gr) (Fig. 1) (Li and Gong, 2017).

1.2.1 TRP channels are involved in thermosensation.

TRP channels are non-selective cation channels that have been first identified and characterized in *Drosophila* phototransduction (Montell, 2011). After several decades of study, they have been classified into seven superfamilies including TRPC, TRPV, TRPM, TRPN, TRPA, TRPP, and TRPML, and their functions have been reported in a remarkable number of sensory processes (Cabezas-Bratesco et al., 2022). In thermal sensation, multiple thermosensitive TRPs have been identified in various species, including insects (Li and Gong, 2017).

In *Drosophila*, TRP channels function in various sensory processes including phototransduction, olfaction, gustation, mechanosensation, thermosensation, nociception, and auditory-sensation (Fowler and Montell, 2013; Montell, 2021). In thermosensation, subtypes of TRPA, TRPV, TRPC, TRPP, TRPM, and TRPN subfamilies have been identified in responding to different temperatures (Fig. 1).

In both larval and adult stages, TRPA1 functions as a heat sensor and triggers warm avoidance over 25°C (Hamada et al., 2008; Kwon et al., 2008). It also contributes to avoidance behaviors under noxious heat (Neely et al., 2011; Khuong et al., 2019). There are five identified TRPA1 splicing variants (A, B, C, D, and E). Two of the isoforms, A and D, have been identified as primary heat sensors (Zhong et al., 2012). Isoforms A and B are expressed in the central nervous system (CNS) (Hamada et al., 2008; Li and Montell, 2021), while isoforms C and D are expressed in the peripheral nervous system (PNS) (Zhong et al., 2012). Activation of these TRPA1 isoforms leads to firing of *trpA1-expressing* neurons, facilitating warm avoidance in both larval and adult stages (Gu et al., 2019; Hamada et al., 2008). E isoform is identified as a byproduct of alternative splicing and is expressed in neurons, but its function is still unknown (Gu et al., 2019). In addition to TRPA1, other TRPA subfamily members, *Painless* and *Pyrexia,* have been identified as noxious heat sensors that trigger noxious heat avoidance (Lee et al., 2005; Sokabe et al., 2008; Neely et al., 2011).

Although cold-activated TRPs have not been clarified in *Drosophila*, the involvement of several TRP channels in cool temperature avoidance has been observed. In adults, Brivido 1-3 (Brv1-2, TRPPs) are required for cool sensing (Gallio et al., 2011). In larvae, TPRL (TRPC) and Inactive (Iav, TRPV) are involved in innocuous cold avoidance (Kwon et al., 2010), whereas polycystic kidney disease 2 (Pkd2, TRPP), no mechanoreceptor potential C (NompC, TRPN), and TRPM (TRPM) are expressed in Class III multidendritic sensory neurons to mediate noxious cold aversive behaviors (Turner et al., 2016).

1.2.2 IRs and GR are involved in thermosensation.

IRs belong to a highly divergent subfamily of ionotropic glutamate-like receptors (iGluR) that are conserved across protostomes, including insects (Benton et al., 2009; Ni, 2021). In *Drosophila*, IRs are broadly expressed in PNS and support multiple sensory processes, including olfaction, gustation, thermosensation and hygrosensation (Van Giesen and Garrity, 2017). There are more than 63 IR proteins in *Drosophila*, including four co-receptors (*Ir8a*, *Ir25a*, *Ir76b* and *Ir93a*) and 59 tuning receptors (Benton et al., 2009; Koh et al., 2014; Van Giesen and Garrity, 2017). Most receptors function by forming a complex between individual stimulus-specific tuning receptors and one or two co-receptors (Van Giesen and Garrity, 2017). As for the temperature sensation in adults, *Ir21a/Ir93a/Ir25a* are expressed in the cooling cells (CCs) located in the antenna arista, regulating cool sensation (Knecht et al., 2016; Budelli et al., 2019) (Fig. 1). In larvae, IRs are expressed in two clusters of cells located in the dorsal organ ganglions (DOGs): dorsal organ cooling cells (DOCCs) (Klein et al., 2015) and dorsal organ warm cells (DOWCs) (Hernandez-Nunez et al., 2021). DOCCs require *Ir21a*/*Ir93a*/*Ir25a* to respond cooling while DOWCs require *Ir68a*/*Ir93a*/*Ir25a* to respond warming, which exhibit a cross-inhibition and contribute to thermal homeostasis (Fig. 1) (Ni et al., 2016; Hernandez-Nunez et al., 2021; Tyrrell et al., 2021). Additionally, protein levels of IRs determine responsiveness to cool in DOCCs, which leads to distinctive temperature preference during the 3rd instar stages (Tyrrell et al., 2021).

GRs form a large gene family, which has been widely studied in insect gustation and olfaction (Montell, 2021). One GR, GR28b(D), is activated by temperature increase over 25°C and required for rapid response to increasing temperature in adults (Ni et al., 2013).

1.3 Potential correlation of fatty acid metabolism with thermal sensation.

Fatty acids are well known as energy storage sources, but they also exhibit various functions being associated with channels and receptors (Falomir-Lockhart et al., 2019). Polyunsaturated fatty acids (PUFAs) have been reported as ligands or activators for multiple TRP channels (Yoo et al., 2014) and glutamate receptors (Dec et al., 2023). Additionally, fatty acids play key roles in triacylglycerol (TAG) synthesis and TAG storage within lipid droplets, shielding TRP channels from cellular oxidative stress (Circu and Aw, 2010; Kozai et al., 2014; Jiang et al., 2023). At a behavioral level in *Drosophila*, a shift of temperature preference is observed when a significant increase of PUFA is induced in multiple sensory neurons by an ectopic expression of exogenous fatty acid desaturase (Suito et al., 2020). Moreover,

Drosophila larvae preferentially consume PUFA containing food under cold environment (Brankatschk et al., 2018). However, the involvement of endogenous fatty acid-related enzymes in thermotaxis remains unknown.

I expected that fatty acids and correlated lipid enzymes are involved in the mechanism of temperature preference in *Drosophila* based on the previous findings. Therefore, my study aims to identify lipid enzymes that modulate thermal sensation in *Drosophila* larvae, as well as their potential regulatory mechanisms. I selected several genes encoding fatty acid metabolizing enzymes particularly correlated with PUFA metabolisms or TAG synthesis. The selected genes and their putative or reported molecular functions are as follows. 1) *CG8839* and *CG5112* encode fatty acid amide hydrolases (FAAHs), which hydrolyze anandamide and release PUFA. 2) Inactivation no afterpotential E (*inaE*) encode a diacylglycerol lipase (DAGL), which hydrolyzes diacylglycerol (DAG) into monoacylglycerol (MAG) and PUFA. 3) *MGAT-1/-2/-3* (the name given to *CG1941/CG1942/CG1946* in this study) encode monoacylglycerol acyltransferases (MGATs), which are involved in the TAG synthesis processed by producing intermediate products DAG from MAG.

As a result, I observed potential roles of *CG8839*, *CG5112*, and *inaE* in thermotaxis at a behavioral level. In addition, I performed behavioral assays in multiple set-ups and observed the involvement of *MGAT-2* and *MGAT-3* in cool avoidance in multiple sensory neurons. Additionally, I conducted *in vivo* GCaMP-imaging and qPCR to investigate the physiological mechanism of *MGAT-2* in cool sensation. The results suggested that *MGAT-2* supported the transcriptional level of *Ir25a* transcription factor *broad,* which impacted *Ir25a* expression level in DOCCs/DOWCs. This reduction led to a deteriorated cooling and warming responses in DOCC/DOWCs and an alternation in cool temperature avoidance.

2 Materials and Methods

2.1 Fly strains and rearing condition

Flies were reared on glucose-yeast-cornmeal media: 2,500 ml of reverse osmosis water, 180 g of cornmeal (Oriental Yeast), 100 g of dry brewer's yeast Ebios (#128-297405, Mitsubishi Tanabe Pharma), 19 g of agarose (#RSU-AL01, RIKAKEN), 250 g of glucose (#TDH, San-ei Sucrochemical), 24 ml of Methyl 4-hydroxybenzoate (10% in 70% ethanol; #H5501, Sigma-Aldrich) and 8 ml of propionic acid (#81910, Sigma-Aldrich). Flies were raised in vials or bottles at 25°C under 12-hour light/12-hour dark cycle.

The following flies were obtained from the Bloomington Stock Center (stock numbers are indicated): *vas-cas9 (X)* (#51324), *CG8839^{EP}* (#26990), *CG5112^{PC}* (#16284), *inaE^{N125}* (#42243), *{MGAT-1/-2/-3}* (#90443), *UAS-dicer2* (#24650), *elav-GAL4* (#8760), *iav-GAL4* (#52273), *TRPL-GAL4* (#29134), *Ir25a-GAL4* (#41728), *R11F02-GAL4* (#49828), *UAS-hMOGAT2* (#82252), *UAS-hMOGAT3* (#84925), *UAS-hDGAT2* (#84854), and *UAS-GCaMP8m* (#92591). Two RNAi lines were obtained from the Vienna *Drosophila* RNAi Center: *UAS-MGAT-2-RNAi* (#7942) and *UAS-MGAT-3-RNAi* (#108495). The following stocks were provided by the indicated investigators: *trpA1-AB-GAL4*, *trpA1-CD-GAL4* (Dr. C. Montell) and *Ir21a-GAL4*, *Ir68a-GAL4* (Dr. P. Garrity). The following stocks were created in our laboratory: *CG8893^{KO}*, *MGAT-1^{KO}*, *MGAT-2^{KO}*, *MGAT-3^{KO}*, *UAS-MGAT-2* and *UAS-MGAT-3*. All stocks expected for *UAS-GCaMP8m* were outcrossed for at least five generations to the *w^{1118}* genetic background as a control.

2.2 Generation of *CG8893^{KO}*, *MGAT-1^{KO}*, *MGAT-2^{KO}*, and *MGAT-3^{KO}* flies

CG8893^{KO}, *MGAT-1^{KO}*, *MGAT-2^{KO}* and *MGAT-3^{KO}* fly lines were generated using the CRISPR/Cas9 technique. *MGAT-1* was generated through non-homologous end joining (NHEJ), while *CG8839, MGAT-2* and *MGAT-3* were generated through homology directed repair (HDR).

Guide RNAs (gRNAs) target the coding region of *CG8839, MGAT-1*, *MGAT-2,* and *MGAT-3* were designed using the 'Find CRISPRs' online tool (http://www.flyrnai.org/crispr2/) (Housden et al., 2016) and listed as follows [protospacer adjacent motifs (PAMs) were underlined]:

CG8839: AGAATGGCATCTGTGATCGGTGG

MGAT-1: GCGTCGCCAGACGTTTGCCATGG

MGAT-2: ATCTGCAGTCGGCGTTCCAGAGG

MGAT-3: GGCTCCTCTCCGGGTTCCGCTGG

gRNAs were constructed into gRNA vector pU19_U6_wukong (Dr. C. Montell) by PCRs, which were performed using gRNA vector Phusion High-Fidelity DNA Polymerase (#M0530S, Invitrogen), sense and antisense gRNA primers (Primers #1-8, Table 1) and pU19_U6_wukong as a template. PCR products were phosphorylated by T4 Polynucleotide Kinase (#TKR-2021S, Takara) following the manufacturer's standard protocol. Phosphorylated PCR products were ligated by Ligation High Ver. 2 ((#LGK-201, Toyobo) for 2 hours and transformed into *E. coli*. *E. coli* culture was plated on LB agar (#20067-85, nacalai tesque) containing 100 µg/mL Ampicillin (#016-23301, Wako) in a 10-cm petri dish (#SH90-15, Iwaki) and incubated overnight at 37°C. The colonies were inoculated into Plusgrow II (#08202-75, nacalai tesque) containing 100 µg/mL Ampicillin and cultured overnight in a 37°C shaker. Plasmids were extracted using NucleoSpin Plasmid EasyPure (#U0727C, Takara). The presence of gRNAs in plasmids was confirmed by sequencing.

For generating *CG8839, MGAT-2* and *MGAT-3* knockouts through HDR, additional constructs with two genomic DNA fragments (~1 kb) flanking each side of the cas9 cleavage region were generated.

To amplify genomic DNA templates from *vas-cas9 (X)* flies, DNA extraction solution was freshly prepared with a 50 µl squishing buffer (10 mM Tris-HCl, pH =8.3; 1 mM EDTA; 25 mM NaCl) and 0.5 µl 200 ug/ml Proteinase K (#169-21041, Wako). 3-10-days-old adult flies were anesthetized on ice and homogenized in the DNA extraction solution with a 100-µl pipette tip and incubated at 37°C for 30 minutes followed by 85°C for 1.5 minutes. After cooling down and 10-times diluted with Milli-Q water, genomic DNA solution was stored at -20°C until further use. To subclone the DNA fragments into the pHD-Scarless-DsRed plasmid (#64703, Addgene) for HDR, vector and genomic DNA fragments were amplified using Phusion High-Fidelity DNA Polymerase (#M0530S, Invitrogen) and primers #9-16 (Table 1). Amplified products were incubated with NEBuilder HiFi DNA Assembly kit [#E2621, New England Biolabs (NEB)] at 50°C for one hour and transfected into *E.coli*. Plasmids were extracted through NucleoSpin Plasmid EasyPure (#U0727C, Takara) and the successful insertion of genomic DNA fragments were confirmed by restriction enzyme digestions and sequencing.

Then, plasmids were sent for microinjection (BestGene). *MGAT-1* gRNA vector was microinjected into *vas-cas9 (X)* embryos to generate *MGAT-1*^{KO}. *CG8839, MGAT-2*, and *MGAT-3* gRNA vectors together with HDR vectors were microinjected into *vas-cas9 (X)* embryos to generate *CG8839*^{KO}, *MGAT-2*^{KO} and *MGAT-3*^{KO}. Flies carrying mutations were

selected by sequencing the gRNA cleavage region (*MGAT-1*^{KO}) or tracking *DsRed* markers (*CG8839*^{KO}, *MGAT-2*^{KO} and *MGAT-3*^{KO}). Genotypes of knockout flies were confirmed by PCR using KOD One PCR Master Mix Blue (#KMM-201, TOYOBO) with genotyping primers (#25-32, Table 1).

2.3 Generation of *MGAT-2* and *MGAT-3* transgenic flies.

MGAT-2 and *MGAT-3* overexpression lines were generated using φC31 site-specific integration system.

To prepare cDNA templates, 5-6 whole-body larvae were collected and homogenized in ice-cold phosphate buffered saline (PBS) solution with a pestle. After removing PBS by centrifuge, total RNA was extracted with Sepasol-RNA I Super G (#0937984, nacalai tesque) following the manufacturer's standard protocol. Subsequently, extracted RNA was treated with Recombinant DNase I (#2270A, Takara) for 30 minutes, followed by Phenol: Chloroform: Isoamyl Alcohol Mix (#25970-14, nacalai tesque) denaturation. Then, RNA was precipitated with 100% ethanol (EtOH) and CH3COONa (300 mM, #06893-24, nacalai tesque) by incubating on ice for 30 minutes and washed with 70% EtOH. Total RNA was dissolved in RNase-free water and RT-PCR was conducted using extracted total RNA following the manufacturer's protocol. 13 µl reaction premix containing 50 µM Oligo(dT)$_{20}$, 10 mM dNTP mix, 5 mg of total RNA in DEPC-treated water was prepared in a 0.2-ml PCR tube. The premix was incubated at 65°C for 5 minutes and chilled on ice for over 1 minute. The incubated reaction premix was combined with 7 µl of mix containing 4 µl of 5X SuperScript IV RT buffer, 1 µl of 100 mM DTT, 1 µl of SuperScript™ IV Reverse Transcriptase (#18090010, Invitrogen), and 1 µl of RNaseOUT™ Recombinant Ribonuclease Inhibitor (#10777019, Invitrogen). The reaction mix was incubated at 55°C for 10 minutes followed by 80°C for 10 minutes. RT product was stored in -20°C until further use.

Coding sequences (CDSs) of *MGAT-2* and *MGAT-3* were PCR amplified from *w*^{1118} cDNA using KOD One PCR Master Mix Blue (#KMM-201, TOYOBO) and *MGAT-2* and *MGAT-3* subcloning primers (#33-36, Table 1). *MGAT-2* amplified product was subsequently digested with Xho I (#R1046s, NEB) and Spe I-HF (#R3113S, NEB), while *MGAT-3* amplified product and empty vector pJFRC7-20XUAS-IVS-mCD8::GFP (#26220, Addgene) were digested with Xho I (#R1046s, NEB) and Xba I (#R0145S, NEB). All restricted enzyme digestions were incubated in 37°C for 1 hour. PCR products of *MGAT-2* and *MGAT-3* were ligated with pJFRC7-20XUAS-IVS-mCD8::GFP (#26220, Addgene) by Ligation High Ver. 2 (#LGK-201, Toyobo) for 30 minutes and transformed into *E. coli*. Plasmids were extracted

through NucleoSpin Plasmid EasyPure (#U0727C, Takara), and the existence of *MGAT-2* and *MGAT-3* were confirmed by restriction enzyme digestions and sequencing.

Constructed vectors were microinjected into P{CaryP}55C4 (BDSC #8622) embryos to generate *UAS-MGAT-2* and *UAS-MGAT-3*. Flies carrying transgenic insertions were selected by tracking red-eye markers. Genotypes of transgenic flies were confirmed by PCR using KOD One PCR Master Mix Blue (#KMM-201, TOYOBO) with genotyping primers (#37-39, Table 1).

2.4 Quantitative PCR (qPCR)

Early or late 3rd instar larvae (8~10 whole bodies) or ~70 dissected anterior regions (Fig. 2) were collected and homogenized in ice-cold PBS solution with a pestle. After removing PBS by centrifuge, the total RNA was extracted with Sepasol-RNA I Super G (#0937984, Nacalai) following the manufacturer's standard protocol. Then, RNA was treated with Recombinant DNase I (#2270A, Takara) for 30 minutes, followed by Phenol: Chloroform: Isoamyl Alcohol 25:24:1 Mixed (#25970-14, Nacalai) denaturation. RNA was precipitated with 100% ethanol (EtOH) and CH3COONa (300 mM, #06893-24, Nacalai) by incubating in -20°C overnight and washed with 70% EtOH. Total RNA was dissolved in RNase-free water and RT-PCR was conducted using extracted total RNA. 2 mg of total RNA diluted in 8 µl DEPC-treated water in a 0.2-ml PCR tube was incubated at 65°C for 5 minutes and chilled on ice for over 1 minute. Then, the RNA was mixed with 2 µl ReverTra Ace qPCR RT Master Mix (#FSQ-201, Toyobo) and incubated at 50°C for 15 minutes followed by 98°C for 5 minutes. RT products were stored in -20°C until further use.

Primer sequences used for qPCR were described in Table 2. Ribosomal protein 49 (*rp49*) was used as a reference gene for the normalization of transcript levels. Quantitative PCR was performed using Applied Biosystems 7300 Real Time PCR System. The qPCR protocol consisted of an initial denaturation step at 98°C for 2 minutes, followed by 35 cycles of denaturation at 98°C for 10 seconds, annealing at 60°C for 10 seconds, and extension at 68°C for 30 seconds followed by a melt point measurement from the initial protocol of the qPCR machine.

Thunderbird Next SYBR qPCR Mix (#QPX-201, Toyobo) was used in reactions. ΔΔCt method was used for data analysis and the relative gene expression level of mutants was normalized by *rp49* and to positive control w^{1118} as a value of 100%.

2.5 Temperature gradient assays

Temperature gradient assays were conducted under two temperature conditions: 16°C - 26°C and 8°C -35°C.

To prepare synchronized larvae for temperature gradient assays, females were allowed to lay eggs in new food vials within a 3-6-hour time window. Then, larvae were raised in the same vial until they grow to test stages (2nd instar: 48 hours AEL; Early 3rd instar: 72 hours AEL; Late 3rd instar: 120 hours AEL). Control and mutants were examined on the same day.

Larvae were collected from the food into an 18% (72 and 120 hours AEL) or 22% (48 hours AEL) sucrose solution in 50 ml tubes (#1342-050S, Watson) to allow the larvae to float and the debris to sink. The top layer containing larvae were transferred to another 50 ml tube, which was filled with fresh 18% or 22% sucrose solution. The top layer with larvae was again transferred to a fresh 50 ml tube and the larvae were washed thoroughly with reverse osmosis (RO) water twice. The larvae were kept in a 35 mm dishes (#1000-035, Iwaki) at room temperature for 5-10 minutes to allow them to recover from the washing procedure, and subsequently used for the assays.

16°C -26°C temperature gradient assay was conducted following the previous studies (Sokabe et al., 2016; Liu et al., 2018) with modifications. Two aluminum plates (outer: 14 × 10.1 × 0.9 cm, inner 12.9 × 8.7 × 0.8 cm) was coated with 20 ml 2% agarose (Fig. 3a, d). The gel trays were placed on top of two aluminum blocks (5.1 cm wide, 25.5 cm long and 1.4 cm thick) separated by 10 cm and connected to two circulating water bathes (NCB-1210A, Eyela) to generate a continuous temperature gradient from 16°C -26°C (Fig. 3a-c). Agarose surfaces were gently scratched and sprayed water to prevent the gels from drying. To verify the 16°-26°C gradients, surface temperatures on the test plates in each center of six zone (2 cm wide) was measured by a digital thermometer (MC3000, Chino) (Fig. 3b-d).

To initiate the 16°C -26°C gradient assay, 40~65 larvae on each plate was released in a line at the border between the 22°C and 24°C zones (Fig. 3b). The whole surface of the gel was covered with a microplate lid to minimize escaping of larvae. The experiments were conducted under virtual darkness (<0.1 μW/cm^2) in an acrylic box. Larvae at the early (72 hours AEL) or late (120 hours AEL) 3rd instar stage were allowed to make temperature selection on plates in dark during testing time for 17 or 11 minutes. The distribution of larvae on each plate was captured by a digital camera (GR digital III, Ricoh). The center of each larva was determined as a distributed position recorded using Fiji (Schindelin et al., 2012) (Fig. 3d).

To draw the distribution of larvae in every 2-cm zone on plates, larvae were tabulated in the six temperature zones on each plate, represented by the center temperature (Fig. 3b). The proportion of larvae in each temperature zones was calculated as (number of larvae in a given 2-cm zone)/(total number of larvae in six zones) × 100%. I omitted from the tabulation larvae in the 0.45 cm borders between the gel and aluminum walls, larvae on the walls of the apparatus, larvae outside of the plates and immobile larvae in the release zone. The values from the upper and lower plates were averaged and treated as N=1. Plots of temperature distribution were made by Excel Office 365 (Microsoft) and Prism 9 (GraphPad).

8°C -35°C temperature gradient assay was described previously (Takeuchi et al., 2009; Suito et al., 2020), with modifications. The testing plate was assembled with an aluminum sheet (22.6 x 6.0 x 0.1 cm) and a rectangular acrylic ring structure (outer diameter 20.0 x 6.0 cm, inner diameter 19 x 5 cm, 0.5 cm height) which formed a shallow tray (Fig. 4a). The interior of this tray was covered with a black aluminum tape (#J3270, Nitto). On the backside of the aluminum plate, two acrylic rods (18 x 0.5 x 0.5 cm) were attached to the longer edges to facilitate the fixation of the testing plate between the water-bath-connected aluminum blocks (Fig. 4b). Two trays were covered with 20 ml 2% agarose. In each tray, two acrylic rods (18 x 0.5 x 0.5 cm) were placed at longer edges during agarose solidification to generate two gaps for preventing larval escaping (Fig. 4b). Agarose surfaces were gently scratched and sprayed water to prevent the gels from drying. Gel trays were placed on top of two aluminum blocks separated by 18 cm and and connected to two circulating water bathes (NCB-1210A, Eyela) to generate a continuous temperature gradient from 8°C -35°C (Fig. 4b-d). Surface temperatures were measured every 3 cm on the test plate 0.5 cm from the wall by a digital thermometer (#MC3000, Chino) (Fig. 4c, d).

To initiate the 8°C -35°C gradient assay, 40~65 larvae were released in a line at 23°C (48, 72 hours AEL) or 29°C (120 hours AEL) (Fig. 4c). Each tray was placed with a rectangular acrylic ring structure (outer diameter 20.0 x 6.0 cm, inner diameter 19 x 5 cm, 0.5 cm height) and a square glass (20.0 x 6.0 x0.1 cm) covered with hydrophobic film (MF-600, Fujifilm) at both sides to prevent larval escaping, heat loss and fog (Fig. 4b). The experiments were conducted under LED red light (>600 nm) in an acrylic box. Larvae at the 2nd (48 hours AEL) or early 3rd (72 hours AEL) instar stage were allowed to make temperature selection on plates during testing time for 15 minutes while larvae at the late 3rd (120 hours AEL) instar stage were tested for 10 minutes. The distribution of larvae on each plate was captured by a digital camera

(GR digital III, Ricoh). The center of each larva was determined as a distributed position recorded using Fiji (Schindelin et al., 2012) (Fig. 4e).

To draw the distribution of larvae in every 3 cm zone on plates started from 8°C, larvae were tabulated in the nine temperature zones on each plate (Fig. 4c). The proportion of larvae in each temperature zones was calculated as (number of larvae in a given 3 cm zone)/(total number of larvae in six zones) × 100%. I omitted from the tabulation larvae 0.5 cm from the aluminum walls, larvae outside of the plates and immobile larvae in the release zone. The values from the upper and lower plates were averaged and treated as N=1. Plots of temperature distribution were made by Excel Office 365 (Microsoft) and Prism 9 (GraphPad).

2.6 Thermal two-way choice assay

The two-way choice assay was based on a method previously described (http://www.natureprotocols.com/2008/07/28/assaying_thermotaxis_behavior.php), with modifications. Early 3rd instar larvae (72 hours AEL) were reared and collected as previously described in temperature gradient assays.

The assay was conducted on a test plate (outer: 14 × 10.1 × 0.9 cm and inner: 12.9 × 8.7 × 0.8 cm), which was coated with 25 ml of 2% agarose (Fig. 5a). It was placed on top of two adjacent aluminum blocks, which were separated using a plastic film as a spacer. The blocks were individually temperature controlled using a circulating water bath (NCB-1210A, Eyela). Agarose surfaces were gently scratched and sprayed water to prevent the gels from drying. Surface temperatures on the center of each side of the test plate were measured and confirmed using thermometers (#MC3000, Chino).

To initiate the assay, 40-65 larvae were released in a line at the border between the 24°C and other temperature areas (release zone) (Fig. 5a, b). Experiments were conducted under red LED light (>600 nm). The distribution of larvae on the plate was captured by a digital camera (#FL-CC1218-5MX, Ricon) after 15 minutes and the center of each larva was determined as a distributed position marked using Fiji (Schindelin et al., 2012) (Fig.5b). The preference index (PI) was calculated using the following formula: (Number of larvae on 24°C – Number of larvae on other temperatures) / (Total number of larvae on the test tray). Larvae within the release zone (1 cm wide) were not counted in either temperature zones or those outside the trays were not counted in the calculation.

2.7 Evaluation of developmental rate

In order to determine the timing of third-instar entry and pupation rate in *Drosophila* larvae, I followed the method described in previous report (Sokabe et al., 2016).

Larvae displayed club-like structure or branched-like spiracles were determined as 2nd or 3rd instar larvae (Poças et al., 2020) (Fig. 6). Larvae at the transition stage from 2nd to 3rd instar displayed two pairs of mouth hooks (Poças et al., 2020), they were treated as 3rd instar larvae when checking the timing of third-instar stage entry. To check the timing of third-instar stage entry, 15 larvae were collected 74 hours AEL and transferred to a glass slide. Larvae were then gently squashed between a glass slide and a cover glass, and their mouth hooks and spiracles were examined under a Nikon TE300 microscope to determine the proportion of third-instar larvae (Fig. 6).

The pupation timing was assessed by counting the number of larvae on the vial walls during light periods every 12 hours, starting from 108 hours AEL. The percentages of pupae were calculated based on the maximum number at 228 hours AEL. T50 and T80 were the times at which 50% and 80% of the pupae were produced, respectively.

2.8 Locomotion assay

To perform the larval locomotion assays, early 3rd instar larvae (72 hours AEL) were prepared in the same manner as described in temperature gradient assays.

The aluminum plate (outer: 14 × 10.1 × 0.9 cm and inner: 12.9 × 8.7 × 0.8 cm), coated with 25 ml 2% agarose was placed on two adjacent aluminum blocks maintaining 24°C or 18°C using the circulating water bath (NCB-1210A, Eyela) (Fig. 7a). The surface temperature was measured using thermometers (MC3000, Chino).

To initiate the assay, 10-12 larvae were sparsely released on the plate to prevent physical contact (Fig. 7b). I acclimated the larvae to the environment for 3 minutes and tracked their movements during the following 2 minutes. The movie was shot by a digital camera (FL-CC1218-5MX, Ricon) under red LED light (>600 nm) and the movie was imported into behavior tracking software Move-tr/2D to track and display the movement trajectory of each larva (Fig. 7c). The length of tracked distance in each individual was defined as “Moving distance”. The number of angels less than 150° displayed in the movement trajectory was tracked manually and defined as “No. of turning (# of turning)” (Fig. 7d).

2.9 *in vivo* GCaMP-imaging

in vivo GCaMP-imaging referred to the previous report with modifications (Klein et al., 2015). To measure the calcium responses of DOCCs and DOWCs, *UAS-GCaMP8m* was expressed with *R11F02-GAL4* and *Ir68a-GAL4*, respectively. To conduct this assay, early 3rd instar larvae (72 hours AEL) were prepared in the same manner as thermal behavioral assays described above. HL3 solution and calcium-free HL3 solution and were prepared with 70 mM NaCl, 5 mM KCl, 10 mM $NaHCO_3$, 20 mM $MgCl_2$, 5 mM HEPES, 115 mM sucrose and 5 mM trehalose (pH 7.2), with or without 1.8 mM $CaCl_2$. Anterior region of one larva was fixed on a silicone gel (Shin-Etsu, KE-1606) disc with 15 mm diameter, using insect dissection pins (Austerlitz 0.1 mm, Czech Republic). The silicone gel with the larva was fixed in the testing chamber in calcium-free HL3 bath solution (Fig. 8a, b). The fixed larva was placed under the Leica DM6 B upright microscope with the silicone gel in the test chamber (Fig. 8a, d). HL3 solution was filled to the chamber until it attached to the 25x/ 0.95 HC Fluotar water immerse lens (Leica) set on the microscope (Fig. 8c). HL3 solution was perfused at a 2.6 ml/minute speed by a peristaltic pump (PSM071AA, Advantec) connected to inline temperature controller (SC-20, Warner) and generated temperature fluctuation (Fig. 8c). During the recording, temperatures were first stabilized at 20°C for 1 minute, then went through two sinusoidal-like waves range from 18°C to 24°C within 4.5 minutes. Temperature close to the sample was recorded by a temperature controller (CL-100, Warner) with a thermistor probe (TA-29, Warmer) (Fig. 8c, d). Temperature fluctuations were recorded by AxoScope (Molecular Devices). GCaMP signals were captured with a 3-second interval for 5.5 minutes and tracked by DFC9000 sCMOS camera (Leica) connected to the microscope (Leica DM6 B upright, Leica) and recorded by Leica Application Suite X (Leica).

GCaMP-signal-recordings were treated with a computational clearing method (Thunderbird) and exported as multiple TIFF images and analyzed in ImageJ (Schneider et al., 2012). During analysis in ImageJ, StackReg plugin was used to optimize the alignment of cell images at a fixed position if a minor shake was observed during the recording. Temperature changes were analyzed by AxoScope (Molecular Devices) and Clampfit 11.2 (Molecular Devices).

Changes in fluorescence intensity ($\Delta F/F_{min}$) were used to assess the Ca^{2+} responses [[(Ft $-F_{MIN})/F_{MIN}$]. Ft corresponds to the value obtained every 3 s, while F0 indicated the minimum response recorded between 1-5 minutes. Average ratio of maximum/minimum GCaMP-fluorescence (F_{MAX}/F_{MIN}) were determined as the mean value of maximum/minimum GCaMP-

fluorescence between 60-162 seconds and 168-270 seconds in DOCCs and between 60-150 seconds and 174-264 seconds in DOWCs. The area under curve was computed using trapezoidal rule [(Ft + Ft +1)/2 × 3 (sampling interval)] in two cooling (1^{st}: 96-162 seconds; 2^{nd}: 204-270 seconds) or warming (1^{st}: 114-150 seconds and 2^{nd}: 219-264 seconds) periods in DOCCs or DOWCs. The calculations were normalized to the area under curve of the 1^{st} cooling process (96-162 seconds, DOCCs) or the 1^{st} warming process (114-150 seconds, DOWCs) in *MGAT-2^{KO}/+; R11F02-GAL4/+* or *MGAT-2^{KO}/+; Ir68a-GAL4/+* controls to a value of 1.The average activation duration was calculated as the average of the time duration (in seconds) from the minimum to the maximum GCaMP-fluorescence of 60-162 seconds and 168-270 seconds (DOCCs) or 60-150 seconds and 174-264 seconds (DOWCs).

2.10 Statistical analysis

All data were presented as means ± standard error of mean (SEM). The number of times each experiment was performed (*N*) is indicated in the figure legends. The normality of distributions was assessed by Kruskal-Wally's test ($p < 0.05$ rejected normal distribution). For pairwise comparisons, statistical analysis was tested by unpaired Student's t-test when normally distributed and by Mann-Whitney U test when not normally distributed. For multiple pairwise comparisons, one-way analysis of variance (ANOVA) with the Dunnett's or Tukey's post hoc analysis was used for the normal distribution cases and Kruskal-Wallis test with Steel test or Steel-Dwass test was performed for the not normally distributed sets. Statistical tests were performed using Prism 9 (GraphPad) or EZR (version 1.61; Saitama Medical Center, Jichi Medical University) (Kanda, 2013), which is a graphical user interface for R (The R Foundation for Statistical Computing). Statistical significance is indicated by asterisks, where $*P < 0.05$, $**P < 0.01$, and $***P < 0.001$. NS denotes not significant.

3 Results

3.1 FAAHs displayed potential involvements in warm avoidance of *Drosophila* larvae.

CG8839 was reported as a human FAAH2 ortholog in *Drosophila* (Jacobs and Sehgal, 2020). To explore the possible involvement of *CG8839* in *Drosophila* thermal preference, I performed temperature gradient assays using *CG8839* mutants, $CG8839^{EP}$ and $CG8839^{KO}$. $CG8839^{EP}$ is a P-element insertion mutant generated in the FlyBase distribution project, with an EP element (Bellen et al., 2004) inserted 1.3 kb upstream of the start codon (Fig. 9a). The expression of *CG8839* in this allele was significantly reduced to 68.38% ± 4.66% of the control (Fig. 9b). I generated $CG8839^{KO}$ by inserting a *DsRed* marker (~1.8 kb) 120 bp downstream from the start codon by CRISPR/Cas9 (Fig. 9a). *CG5112* was selected as a putative FAAH function annotated by FlyBase. To investigate its possible involvement in temperature sensation, I utilized a $CG5112^{PC}$, a P-element insertion mutant generated by the FlyBase distribution project (Häcker et al., 2003). Since a PC element (Bellen et al., 2004) with a length of ~8.2 kb is inserted into the 1st exon, 241 bp downstream from the start codon (Fig. 9c), this P-element allele was predicted as a null mutant.

I first tested early and late 3rd instar larvae under a 16°C -26°C thermal gradient (Fig. 10a, b). At the early stage, control and $CG8839^{EP}$ both accumulated in the 24°C zone (control: 23.40 ± 3.09%; $CG8839^{EP}$: 28.34 ± 3.11%) (Fig. 10a). At the late stage, although both control and $CG8839^{EP}$ migrated to the cool range, control accumulated toward the 16°C zone (35.83 ± 3.54%), while $CG8839^{EP}$ showed no obvious peak in 16°C-20°C zones (Fig. 10b). These results suggested that *CG8839* may be involved in warm avoidance at late 3rd instar stage.

Since 16-26°C did not cover the whole physiological temperature range for *Drosophila*, making it difficult to discuss beyond this temperature range, I extended the range to 8°C -35°C, which included the optimal temperature range and noxious temperatures for *Drosophila* (Barbagallo and Garrity, 2015).

On an 8°C -35°C temperature gradient, control at the early 3rd instar stage showed highest accumulation in the 23°C -26°C zone (31.27 ± 2.78%), which was consistent with the 16°C -26°C gradient condition above. $CG8839^{EP}$ larvae displayed a tendency of more accumulation in temperature zones between 8°C and 23°C, while $CG8839^{KO}$ showed a mild shift to the warm temperatures showing no obvious peak accumulation in 23°C -26°C and 26°C -29°C zones (23°C -26°C: 24.73 ± 2.70%; 26°C -29°C: 24.56 ± 2.82%) (Fig. 10c). At

the late 3rd instar stage, control and *CG8839*^{KO} larvae shifted towards cool temperature and showed no obvious peak from 11°C -23°C while *CG8839*^{EP} accumulated in the 20°C -23°C zone (28.58 ± 6.59%, 24.89 ± 3.29%) (Fig. 10d). *CG5112*^{PC} larvae exhibited the highest accumulation in the 23-26°C zone (34.71 ± 2.82%), which was comparable to the control (Fig. 10c), however, at the late 3rd instar stage, *CG5112*^{PC} still accumulated in the 20°C -23°C zone (28.58 ± 6.59%, 24.89 ± 3.29%) (Fig. 10d).

As for *CG8839*, the thermal preference results were not consistent between *CG8839*^{EP} and *CG8839*^{KO}, but given that the latter is a null mutant, *CG8839* might be involved in warm temperature avoidance especially at the early 3rd instar stage. On the other hand, *CG5112* could play a role in warm avoidance at the late 3rd instar stage. Taken together, FAAHs including *CG8839* and *CG5112* may be involved in promoting warm avoidance at 3rd instar stage.

3.2 DAGL (*inaE*) played a potential role in temperature gradient discrimination of *Drosophila larvae*.

inaE was identified as a DAGL coding gene in *Drosophila* (Leung et al., 2008). I utilized a hypomorphic *inaE* mutant (Leung et al., 2008), *inaE*^{N125}, to explore the possible involvement of DAGL in temperature preference by thermal gradient assays.

Under the 16-26°C temperature condition at the early 3rd instar stage, control larvae showed an equal distribution in all temperature zones with no clear preference or avoidance, whereas *inaE*^{N125} larvae exhibited the highest proportion in the 22°C zone (28.66 ± 1.67%) (Fig. 11a). At the late stage, control exhibited the highest proportion in the 16°C zone (31.76 ± 3.39%), whereas *inaE*^{N125} larvae stayed in 20°C and 22°C zones (20°C: 27.02 ± 2.03%; 22°C: 27.15 ± 2.08%) (Fig. 11b).

On a wider temperature gradient (8°C -35°C), control larvae at the early 3rd instar stage displayed a peak distribution in the 23°C -26°C zone (23.34 ± 0.92%), while the *inaE*^{N125} slightly shifted to cool temperatures and displayed more accumulation in the 20-23°C zone than the control (Control: 20.94 ± 5.30%; *inaE*^{N125}: 26.96 ± 3.62%) (Fig. 11c). At the late stage, both control and *inaE*^{N125} moved toward cool temperatures and displayed no obvious peak from 11°C -23°C (Fig. 11d).

Overall results suggested that *inaE* could be involved in temperature sensation, but the outcomes were complicated. The discrepancy between two different gradient conditions might be a resultant of a different temperature slope generated on plates: 16°C -26°C condition had a slope at 1°C/cm, while 8°C -35°C condition had a slope at 1.5°C/cm. If *inaE* is particularly important for temperature discrimination at high resolution, *inaE*^{N125} may fail to discriminate

small changes in temperature in the 16°C-26°C condition. Taken together, these results suggested a plausible involvement of DGAL (*inaE*) in temperature gradient discrimination.

3.3 *MGAT-2* and *MGAT-3* were involved in the cool avoidance of *Drosophila* larvae.

3.3.1 *Drosophila MGATs* were possible orthologs of human monoacylglycerol O-acyltransferase 2 (MOGATs).

Drosophila genes *MGAT-1* (*CG1941*, FBgn0033214), *MGAT-2* (*CG1942*, FBgn0033215) and *MGAT-3* (*CG1946*, FBgn0033216) were named after the putative molecular function annotation described as MAG/DAG acyltransferases by FlyBase, *Drosophila* Gene Ontology annotation (Tweedie et al., 2009), and following analysis. These genes tandemly aligned to form a cluster on the genome (Fig. 12a) with a high amino acid identity (MGAT-1 & MGAT-2: 69.60%; MGAT-1 & MGAT3: 65.91%; MGAT-2 & MGAT-3: 67.05%). They all have six exons, with a same number of amino acids (aa) in MGAT-1/-2 (353 aa), and 350 aa in MGAT-3. These facts imply that the MGATs may share similar molecular functions.

Enzymes function as MAG/DAG acyltransferases belonged to diacylglycerol acyltransferase 2 (DGAT2) family (Turchetto-Zolet et al., 2011). In case of human, six genes [DGAT2, DGAT2L6, MOGAT1/2/3, and Acyl-coA wax alcohol acyltransferase 1 (AWAT1)] are included in DGAT2 family (Turchetto-Zolet et al., 2011). When I compared the amino acid sequence between *Drosophila MGAT-1/-2/-3* and the six members in human DGAT2 family, *Drosophila MGAT-2* and *MGAT-3* displayed the highest identity to human MOGAT2 (*MGAT-2*: 39.52%, *MGAT-3*: 39.82%) (Ensembl). *Drosophila MGAT-1* showed the highest identity to DGAT2-like 6 (DGAT2L6) (39.47%) and the second highest identity to MOGAT3 (38.20%) (Ensembl). Therefore, *MGAT-1/-2/-3* in *Drosophila* displayed higher amino acid conservation to human MOGATs than other members in DGAT2 family, suggesting a possible conserved function as MGAT.

3.3.2 *MGAT-2*/*MGAT-3* supported the discrimination between optimal and lower temperatures.

To study the loss-of-function of *MGAT-1/-2/-3* in temperature sensation, I generated *MGAT* knockout lines using CRISPR/cas9 technique (Fig. 12b-d). *MGAT-1*^{KO} was generated by introducing 5 bp deletion in the 1st exon to induce a frameshift (Fig. 12b), while *MGAT-2*^{KO}

and *MGAT-3^{KO}* were generated by inserting a *DsRed* reporter 33 bp and 28 bp downstream of the start codon, respectively (Fig. 12c, d).

I tested mRNA levels of *MGAT-1/-2/-3* in *MGAT-KOs* to examine potential effects of expression levels within the *MGAT*-cluster. As a result, mRNA levels of *MGAT-1*, *MGAT-2* or *MGAT-3* was abolished in each targeted allele, which showed more than 95% reduction compared with the control (Fig. 13). Interestingly, *MGAT-2* mRNA level in *MGAT-1^{KO}* was significantly reduced compared to the control (*MGAT-2*: 47.30 ± 10.00%) (Fig. 13a), this reduction in neighboring-gene mRNA level was also observed in *MGAT-2^{KO}* (*MGAT-3*: 52.08 ± 5.73%) and *MGAT-3^{KO}* (*MGAT-2*: 33.28 ± 3.70%) compared to the control (Fig. 13b, c). These results indicated that targeted *MGAT-1/-2/-3* knockouts were null-mutants, and their reduced expression level possibly suppressed the expression of *MGATs* within the cluster at a transcriptional level.

To investigate the involvement of *MGAT-1/-2/-3* in thermal preference through larval developmental stages, I first tested *MGAT* knockouts on an 8°C -35°C temperature gradient (Fig. 14 and 15). At the early 3rd instar stage, control and *MGAT-1^{KO}* showed the highest accumulation in the 23°C -26°C zone (Control: 32.47 ± 3.84%; *MGAT-1^{KO}*: 38.53 ± 2.70%) (Fig. 14a, b and 15a). However, *MGAT-2^{KO}* displayed the highest distribution in the 20°C -23°C zone (31.65 ± 4.30%) (Fig. 14c and 15a). This cool tendency was rescued by a wild-type genomic transgene containing *MGAT-1, -2* and *-3* (*{MGAT-1/-2/-3}*) (Fig. 17a). This transgenic line showed a peak distribution in 23°C -26°C zone (34.48 ± 2.47%), which was a comparable pattern to the control (Fig. 15a). *MGAT-3^{KO}* displayed robust distribution in a cool range and a distribution peak was in the 20°C -23°C zone (24.17 ± 2.23%) (Fig. 14d and 15b). This loss of cool avoidance was also rescued by the *{MGAT-1/-2/-3}* genomic rescue. This transgenic line displayed a comparable pattern as the control and showed the highest distribution in the 23°C -26°C zone (32.34 ± 1.57%) (Fig. 15b). At the late 3rd instar stage, both control and *MGAT* mutants shifted to lower temperatures. Control showed a peak in the 17°C -20°C zone (26.45% ± 1.86%), while *MGAT* mutants showed shifts to cooler temperature zones (Fig. 15c). I also tested the distribution of *MGAT-2^{KO}* and *MGAT-3^{KO}* larvae at 2nd instar stage. Control showed a sharp peak with the highest accumulation in the 23°C -26°C zone (Control: 47.77 ± 1.78%) (Fig. 16). *MGAT-2^{KO}* also displayed the peak distribution in the 23°C -26°C zone (42.03 ± 7.09%), however, a higher distribution was observed in the 20°C -23°C zone and lower temperature zones compared to the control (Fig. 16). *MGAT-3^{KO}* also displayed an accumulation in lower temperature zones (Fig. 16). In all three larval stages, less than 5% of larvae stayed at 8°C -11°C or 32°C -35°C zone in control and mutants. As results suggest,

MGAT-2 and *MGAT-3* contributed to innocuous cool temperature avoidance towards optimal temperature in both 2nd and 3rd instar stages. Despite a clear alteration of *MGAT-2^{KO}* and *MGAT-3^{KO}* at the multiple stages, I determined to follow behavioral observations at early 3rd instar stage in the following studies due to easier handling of that stage of larvae.

Two-way choice assay allows *Drosophila* to select two distinct temperatures. I next introduced a two-way choice assay to investigate another aspect of thermotactic behaviors of *MGAT-KOs.* Larvae were released on a testing plate between two temperature sides, one side was kept at 24°C and another side was set with test temperatures. Larvae were allowed to freely decide and stay on either side. After a certain period, I counted the number of larvae on each side and calculated the preference index (PI). A lack of temperature bias results in a PI of 0, whereas a complete preference for 24°C or the alternative temperature results in a PI of +1.0 or –1.0, respectively.

In a two-way choice assay, control and *MGAT-1^{KO}* larvae selected 24°C over other testing temperatures (16°C, 18°C, 20°C, 22°C, 26°C and 28°C) (Fig. 17a). Aversion of 26°C and 28°C was observed in *MGAT-2^{KO}* and *MGAT-3^{KO}*, however, they failed to distinguish from 16°C, 18°C, 20°C and 22°C to 24°C (Fig. 17a and 18). Such impaired ability was rescued in *MGAT-2^{KO}*; *{MGAT-1/-2/-3}* and *MGAT-3^{KO}; {MGAT-1/-2/-3}* in a 20°C versus 24°C condition (Fig. 17b, c). Given the interaction of mRNA expression between *MGAT*s (Fig. 13), I tested trans-heterozygous of *MGAT-2^{KO}* and *MGAT-3^{KO}* (*MGAT-2^{KO}/ MGAT-3^{KO}*). The result showed a 20°C selection instead of 24°C (Fig. 17d), which further suggested the possible interaction between *MGAT-2* and *MGAT-3*.

Taken together, these results revealed the involvement of *MGAT-2*/*MGAT-3* in temperature discriminations between optimal temperature 24°C to lower temperatures.

3.3.3 Impaired cool avoidance in *MGAT-2/-3* were not due to the changes in development.

Temperature preference of larvae appeared to be development-dependent from the early to late 3rd instar stage (Fig. 15), a loss of cool avoidance in *MGAT* mutants may be due to developmental changes. Thus, I examined the entrance of 3rd instar stage at 74 h AEL in control and *MGAT* knockouts (Fig. 19a) and no significant difference were observed. Additionally, pupation speeds were indistinguishable between mutants and control (Fig. 19b, c). These findings suggested that the impaired cool avoidances in *MGAT-2^{KO}* and *MGAT-3^{KO}* were unlikely to be caused by changes in development.

3.3.4 Role of *MGAT-1/-2/-3* in temperature-dependent locomotion activities.

Drosophila larva determined the preferred temperature by reorientating the direction from a sequence of running and turning events, and the turning events requires the temperature discrimination (Luo et al., 2010). As a result, if cool avoidance was impaired in *MGAT-2/-3* knockouts, larvae may require more "moving" and "turnings" for thermal decision-making under a lower temperature. Therefore, I performed locomotion assays to observe the moving distance and the number of turning in control and *MGAT* knockouts on an optimal temperature 24°C and a lower temperature 18°C. Under 24°C, no significant difference in moving distance and the number of turnings were observed between control and *MGAT* knockout larvae (Fig. 20a, b). However, under 18°C, *MGAT-3*^{KO} showed a significantly longer moving distance (cm) (Control: 3.52 ± 1.80; *MGAT-3*^{KO}: 4.69 ± 0.35) and a higher number of turning than in the control (number) (Control: 5.83 ± 0.70; *MGAT-3*^{KO}: 9.04 ± 0.96) (Fig. 20c, d). This might support the impairment of cool avoidance in *MGAT-3*^{KO} from an alternative aspect.

3.3.5 *MGAT-2* and *MGAT-3* functioned in TRP channel expressing neurons.

To dissect the mechanism of *MGATs* in cool avoidance, it is necessary to address the cellular requirement of *MGAT-2* and *MGAT-3*. Given the fundamental role of the nervous system in detecting and responding to temperature stimuli (Xiao and Xu, 2021), I first utilized the GAL4/UAS system to perform RNAi-mediated knockdown of *MGAT-2* or *MGAT-3* using a *pan-neuronal* driver (*elav-GAL4*) (Fig. 21a). In a 20°C versus 24°C condition, significant reductions of 24°C selection in *elav-GAL4/+*-induced *MGAT-2* or *MGAT-3* knockdown (*elav > MGAT-2-RNAi; elav > MGAT-3-RNAi*) were observed compared to *elav/+* control (Fig. 21b). On an 8°C -35°C temperature gradient, while *elav/+*, *MGAT-2-RNAi/+* and *MGAT-3-RNAi/+* controls displayed a clear peak in the 23°C -26°C zone, *elav-GAL4/+*-induced *MGAT-2* and *MGAT-3* knockdown exhibited left shifts in the distribution (Fig. 21c). These results suggest that *MGAT-2* and *MGAT-3* functioned in neurons to regulate thermal preference of larvae.

It has been reported that *iav* (TRPV) and TRPL (TRPC) were involved in cool temperature avoidance of *Drosophila* larvae (Kwon et al., 2010; Rosenzweig et al., 2008). To evaluate the possible interaction of *MGAT-2* and/or *MGAT-3* with *iav* or TRPL, I performed RNAi-mediated knockdowns of *MGAT-2*/*-3* using the *iav*- and *TRPL-GAL4* drivers (Fig. 22). In a 20°C versus 24°C condition, a significant reduction of 24°C selection was observed when *MGAT-2* or *MGAT-3* was knocked down in *iav-expressing* neurons (*iav > MGAT-2-RNAi; iav > MGAT-3-RNAi*) compared to *iav*/+ control (Fig. 22a), while no such reduction was observed when *MGATs* were knocked down in *TRPL-expressing* neurons (*TRPL > MGAT-2-RNAi;*

TRPL > MGAT-3-RNAi) compared to *TRPL/+* control (Fig. 22b). Since Iav is expressed in chordotonal organs in the PNS (Kwon et al., 2010), I expected that both *MGAT-2* and *MGAT-3* interacted with Iav in chordotonal organs to mediate innocuous cool avoidance.

Previous studies have implicated TRPA1 as a key player in warm avoidance responses (Kwon et al., 2008; Shen et al., 2011; Sokabe et al., 2016). *trpA1* isoforms A and B were expressed in larval CNS (Hamada et al., 2008; Li and Montell, 2021), whereas isoforms C and D were expressed in the ventral nerve cord (VNC) and multidendritic (md) neurons (Zhong et al., 2012). Also, artificial increase of PUFA in TRPA1 neurons resulted in cool shift in temperature preference (Suito et al., 2020). To explore the possibility of *MGAT-2* and *MGAT-3* interaction with TRPA1, I performed RNAi-mediated knockdown of *MGAT-2* or *MGAT-3* using *trpA1-AB-GAL4* or *trpA1-CD-GAL4* expressing in distinctive neurons (Fig. 23). In a 20°C versus 24°C condition, *trpA1-AB*/+-induced *MGAT-3* RNAi knockdown (*trpA1-AB > MGAT-3-RNAi*) displayed defect in 24°C selection compared to *trpA1-AB*/+ and *MGAT-3-RNAi*/+ controls (Fig. 23a). In a 26°C versus 24°C condition, the defect in 24°C selection in this RNAi knockdown line (*trpA1-AB > MGAT-3-RNAi*) was also observed compared to *trpA1-AB*/+ control (Fig. 23b). *trpA1-CD-GAL4*/+-induced *MGAT-2* or *MGAT-3* RNAi knockdown displayed no significant difference in 24°C selection in a 20°C versus 24°C condition (Fig. 23c). On an 8°C -35°C temperature gradient, *trpA1-AB-GAL4*/+-induced *MGAT-3* RNAi knockdown (*trpA1-AB > MGAT-3-RNAi*) displayed an equivalent distribution in 20°C -32°C zones, while peak distribution in *trpA1-AB/+* and *MGAT-3-RNAi/+* control was clearly observed in 20°C -23°C zone (Fig. 23d). These results manifested that *MGAT-3* distinctively function in *trpA1-AB-expressing* neurons to mediate warm avoidance.

3.3.6 *MGAT-2* primarily functioned in DOCCs to mediate cool avoidance.

Dorsal organ cool cells (DOCCs) and dorsal organ warm cells (DOWCs) are located in the dorsal organ ganglion (DOG) of *Drosophila* larvae and have been reported as warm and cool temperature responding neurons (Hernandez-Nunez et al., 2021; Klein et al., 2015; Ni et al., 2016; Tyrrell et al., 2021). Thus, it is possible that *MGAT-2* and *MGAT-3* are involved in DOCCs or DOWCs to mediate cool avoidance. *Ir25a* is an IR co-receptor which broadly expressed in anterior sensory neurons including DOCCs and DOWCs and contribute to thermosensation (Hernandez-Nunez et al., 2021). Therefore, I first performed RNAi-mediated knockdown of *MGAT-2* or *MGAT-3* using an *Ir25a-GAL4* driver (*Ir25a > MGAT-2-RNAi*, *Ir25a > MGAT-3-RNAi*) (Fig. 24a-c). In a 20°C versus 24°C condition, RNAi knockdown of *MGAT-2* in *Ir25a-expressing* neurons displayed a less selection of 24°C compared with *Ir25a/+*

and *MGAT-2-RNAi/+* controls (Fig. 24a) and RNAi knockdown of *MGAT-3* in *Ir25a-expressing* neurons also displayed a less selection of 24°C, compared with *Ir25a/+* and *MGAT-3-RNAi/+* controls (Fig. 24b). The distribution on an 8°C -35°C temperature gradient in *Ir25a/+*, *MGAT-2-RNAi/+*, and *MGAT-3-RNAi/+* controls displayed the highest accumulation in the 23°C -26°C zone (Fig. 24c), while RNAi-mediated knockdown of *MGAT-2* or *MGAT-3* using *Ir25a-GAL4* driver (*Ir25a > MGAT-2-RNAi*, *Ir25a > MGAT-3-RNAi*) displayed a cool shift of overall distribution with a peak accumulation in 20°C -23°C rather than 23°C -26°C zone (Fig. 24c).

Ir21a and *Ir68a* were specifically expressed in DOCCs and DOWCs and mediate cool and warm avoidance, respectively (Hernandez-Nunez et al., 2021; Ni et al., 2016). To dissect the specific involvement of *MGAT-2* and *MGAT-3* in DOCCs and DOWCs, I performed RNAi knockdown of *MGAT-2* or *MGAT-3* using GAL4 lines specifically expressed in DOCCs (*R11F02-Gal4* and *Ir21a-Gal4*) and DOWCs (*Ir68a-GAL4*) (Fig. 24d-f). In a 20°C versus 24°C condition, RNAi knockdown of *MGAT-2* (*R11F02 > MGAT-2-RNAi*, in d; *Ir21a > MGAT-2-RNAi*, in e) but not *MGAT-3* (*R11F02 > MGAT-3-RNAi*, in d; *Ir21a > MGAT-3-RNAi*, in e), in DOCCs displayed a loss of 24°C selection compared to *R11F02/+* or *Ir21a/+* control (Fig. 24d, e). RNAi knockdown of *MGAT-2* in DOWCs showed a significantly less 24°C selection compared to *Ir68a/+* control (Fig. 24f).

To further confirm the involvement of *MGAT-2* and *MGAT-3* in DOCCs and DOWCs, I first overexpressed *MGAT-2* and *MGAT-3* using transgenic lines and expressed them in *Ir25a-expressing* neurons under a knockout background by an *Ir25a-GAL4* driver. In a 20°C versus 24°C condition, *MGAT-2* overexpression in *Ir25a-expressing* neurons (*Ir25a > MGAT-2*) rescued the defect of 24°C selection observed in *Ir25a/+* or *UAS-MGAT-2/+* carried *MGAT-2^{KO}* (Fig. 25a). Then, I expressed *MGAT-2* in DOCCs using *R11F02-GAL4* driver in *MGAT-2^{KO}* and it showed a rescued phenotype of 24°C selection in a 20°C versus 24°C condition, compared to *Ir25a/+* and *MGAT-2/+* carried *MGAT-2^{KO}* (Fig. 25a). Under the same condition, *MGAT-3* overexpression in *Ir25a-expressing* neurons (*Ir25a > MGAT-3*), *Ir25a/+,* and *MGAT-3/+* displayed loss of 24°C selection in *MGAT-3^{KO}* (Fig. 25b). On an 8°C -35°C temperature gradient, when *MGAT-2* was overexpressed in DOCCs using *R11F02-GAL4* driver in *MGAT-2^{KO}*, larvae showed peak accumulation in the 23°C -26°C zone (Fig. 25c). Meanwhile, *R11F02/+* and *UAS-MGAT-2/+* in *MGAT-2^{KO}* background displayed highest peak in the 20°C -23°C zone (Fig. 25c).

Collectively, these results revealed involvement of *MGAT-2* in both DOCCs and DOWCs in cool avoidance, while complex roles of *MGAT-3* in multiple neurons. Particularly, *MGAT-2* function in DOCCs may be sufficient for cool avoidance.

3.3.7 *MGAT-2* function in cool avoidance was compensated by human MOGAT2.

Drosophila MGAT-2 exhibited high identity to human MOGAT2. To investigate whether the molecular function is conserved between human MOGAT2 and *Drosophila MGAT-2*, I overexpressed human DGAT2 family members (MOGAT2, MOGAT3, and DGAT2) in DOCCs carried *MGAT-2^{KO}*, using a *R11F02-GAL4* driver. The rescued phenotype of 24°C preference in a 20°C versus 24°C condition was only observed when overexpressing human MOGAT2 in DOCCs (*R11F02 > hMOGAT2*) carried *MGAT-2^{KO}*, compared to *R11F02/+* and *hMOGAT2/+* carried *MGAT-2^{KO}* (Fig. 26). Overexpressing human *MOGAT3* or *DGAT2* (*R11F02 > hMOGAT3, R11F02 > hDGAT2*) did not rescue the phenotype from *R11F02/+*, *hMOGAT3/+* and *hDGAT2/+* carried *MGAT-2^{KO}* (Fig. 26).

These behavioral results suggested that human MOGAT2 was able to compensate the loss of *MGAT-2* function in *Drosophila*. This may imply a conservated molecular function between the human MOGAT2 and *Drosophila MGAT-2.*

3.3.8 Loss of *MGAT-2* caused the deterioration of cooling responses in DOCCs and warming responses in DOWCs.

Results showed above suggested the primary role of *MGAT-2* in DOCCs, however, the underline mechanism in these neurons needs further investigation. DOCCs responded to temperature cooling process which attributed to cool avoidance of *Drosophila* larvae (Klein et al., 2015; Ni et al., 2016). Therefore, *MGAT-2* may be involved in mediating the cool response of DOCCs. To assess whether *MGAT-2* contributes to cooling sensation of DOCCs, I used a genetically encoded calcium sensor GCaMP8m to perform *in vivo*-GCaMP imaging. *R11F02 > GCaMP8m* was used to monitor cooling responses in DOCCs. As for the result, DOCCs exhibited reduced responses to cooling in *MGAT-2^{KO}*, and this defect was partially rescued by the expression of an *MGAT-2* transcript in the DOCCs using *R11F02-GAL4* (Fig. 27a-c). Average ratio of maximum/minimum GCaMP fluorescent response (F_{MAX}/F_{MIN}) from 24°C to 18°C was significantly reduced in *MGAT-2^{KO}* compared to *MGAT-2^{KO}/+* control (*MGAT-2^{KO}/+*: 2.53 ± 0.14; *MGAT-2^{KO}*: 1.70 ± 0.17) (Fig. 27d). The area under curve during cooling from 24°C to 18°C also suggested the significant reduction of accumulated GCaMP8m fluorescent response in *MGAT-2^{KO}* during 1st (*MGAT-2^{KO}/+*: 1 ± 0.09; *MGAT-2^{KO}*: 0.67 ± 0.06) and 2nd

(*MGAT-2^{KO}*/+: 0.90 ± 0.08; *MGAT-2^{KO}*: 0.58 ± 0.06) cooling processes compared to *MGAT-2^{KO}*/+ control (Fig. 27e).

The previous report suggested the cross-inhibition of DOCCs and DOWCs during the cooling or warming process (Hernandez-Nunez et al., 2021). Therefore, I further investigated the warm responsiveness of DOWCs in *MGAT-2^{KO}*. *Ir68a > GCaMP8m* was used to monitor DOWCs responses. DOWCs exhibited reduced responses to warming in *MGAT-2^{KO}* compared to *MGAT-2^{KO}*/+ (Fig. 28a-c). Average ratio of F_{MAX}/F_{MIN} from 18°C to 24°C was approximately 40% reduced in *MGAT-2^{KO}* compared to *MGAT-2^{KO}*/+ (*MGAT-2KO*/+: 1.09 ± 0.22; *MGAT-2^{KO}*: 0.62 ± 0.12) (Fig. 28d). The area under curve during warming from 18°C to 24°C suggested the reduction of accumulated GCaMP8m fluorescent response in *MGAT-2^{KO}* during the 1st (*MGAT-2^{KO}*/+: 1 ± 0.09; *MGAT-2^{KO}*: 0.62 ± 0.15) warming process compared to *MGAT-2^{KO}*/+ control (Fig. 28e).

In summary, these results suggest that the loss of *MGAT-2* caused the deterioration of cooling and warming responses in DOCCs and DOWCs, respectively.

3.3.9 *MGAT-2* maintained *Ir25a* and *Ir21a* mRNA levels.

Ir25a, *Ir93a*, and *Ir21a* played critical roles in cool responsiveness of DOCCs while *Ir25a*, *Ir93a*, and *Ir68a* play critical roles in warm-responsiveness of DOWCs (Ni et al., 2016; Hernandez-Nunez et al., 2021; Tyrrell et al., 2021). Therefore, loss of cool avoidance in *MGAT-2^{KO}* and *MGAT-3^{KO}* and deterioration showed in DOCCs and DOWCs in *MGAT-2^{KO}* may be caused by the defects in indicated *Irs*.

At the early 3rd instar stage, compared with the control, mRNA expression level of *Ir25a* and *Ir21a* in *MGAT-2^{KO}* (*Ir25a*: 42.36% ± 12.74%; *Ir21a*: 59.21% ± 9.09%) and *MGAT-3^{KO}* (*Ir25a*: 0.39 ± 0.07; *Ir21a*: 30.08% ± 10.28%) displayed significant reduction (Fig. 29a, b), while no significant difference was observed in the expression level of *Ir93a* and *Ir68a* (Fig. 29c, d). In addition, no significant difference was observed in *MGAT-1/-2/-3* knockouts in *Ir21a*, *Ir93a*, *Ir25a* and *Ir68a* at the late 3rd instar stage compared with the control (Fig. 30).

These results suggested that *MGAT-2* and *MGAT-3* maintained the *Ir21a* and *Ir25a* expression at the transcription level at the early 3rd instar stage.

3.3.10 mRNA level of *broad* was affected by *MGAT-2.*

Many transcription factors are involved in regulating transcription levels of target genes, thereby influencing their mRNA expression. The effect of *MGAT-2* and *MGAT-3* mutation on the mRNA levels of *Ir25a* and *Ir21a* may be attributed to their ability to modulate the

transcription activities. A recent study presented that the expression level of *Ir21a* may rely on the *Ir25a* expression in the *Drosophila* adult antenna (Vulpe et al., 2021), this raised the possibility that the reduction of *Ir21a* in *MGAT-2^{KO}* and *MGAT-3^{KO}* could be consequence of *Ir25a* reduction.

Therefore, I sought for predicted *Ir25a* transcriptional factors in just another s-axis pipeline for annotation of regulatory motifs 2022 (JASPAR 2022) (Castro-Mondragon et al., 2022) using University of California, Santa Cruz (UCSC) genome browser. Candidates of transcription factor were selected utilizing transcription factor binding sites (TFBSs) predictions in *Drosophila melanogaster* (genome: dm6) for all profiles in the JASPAR CORE insect's collection. Predicted binding site of transcription factors was limited in the upstream of *Ir25a* coding region, from the *Ir25a* upstream gene *tank* to the start codon of *Ir25a,* 653 bp in total. 6 candidate transcription factors were selected (Fig. 31). Among these transcription factors, a binding motif of *GATA-d* was predicted in upstream of *MGAT-2, MGAT-3, Ir25a,* and *Ir21a*; the binding motif of *broad* was predicted in both *MGAT-2* and *Ir25a;* the binding motif of *pan* was estimated both *Ir25a* and *Ir21a*, and the binding motives of *Abd-B, Dr* and *exd* were only observed in *Ir25a* among *Ir25a*, *Ir21a* and *MGAT-2* (Fig. 31a). *Ubx* and *Vsx2* binding motives were observed upstream of *Ir93a* start codon but not in *MGAT-s, Ir25a,* or *Ir21a* (Fig. 31). Since no significant difference observed in the *Ir93a* mRNA level among control, *MGAT-2^{KO}* and *MGAT-3^{KO}* (Fig. 29c), *Ubx* and *Vsx2* were selected as negative controls. In addition, a recent report suggested the MLX-family transcriptional factor could be modulated by the lipid droplet (Mejhert et al., 2020). Considering the *MGAT-2* involvement in lipid droplet formation (Wilfling et al., 2013), I also selected *Drosophila* MLX transcriptional factor *mondo* (Mattila et al., 2015) to confirm its possible regulation by the *MGAT-2* or *MGAT-3*.

I tested the mRNA level of these predicted transcriptional factors (Fig, 31) in whole-body and the anterior region at the early 3rd instar stage (72 hours AEL) in control, *MGAT-2^{KO}* and *MGAT-3^{KO}* (Fig. 32 and 33). mRNA level in the whole body showed no significant changes in all candidates (Fig. 32), however, *broad* showed a tendency (P=0.19) of reduction in *MGAT-2^{KO}* (68.37 ± 11.64%) (Fig. 32b). Indeed, reductions of *broad* mRNA level in anterior regions were observed in *MGAT-2^{KO}* (59.86 ± 9.27%) and *MGAT-3^{KO}* (53.20 ± 19.17%) (Fig. 33b), while *GATA-d* (49.04 ± 10.87%), *Dr* (63.62 ± 13.04%), *Ubx* (70.74 ± 11.40%), *Vsx2* (54.26 ± 24.65%), and *mondo* (62.93 ± 8.15%) showed a tendency of reduction in *MGAT-3^{KO}* (Fig. 33a, e, g-i).

These results suggested that *MGAT-2* and *MGAT-3* are important for maintaining the expression level of *broad*, which regulates the expression level of *Ir25a* and *Ir21a* at a transcriptional level.

4 Discussion

Thermal sensation of *Drosophila* relies on thermo-receptors including TRP channels, a GR, and IRs (Barbagallo and Garrity, 2015). Their expression level, activation properties and distribution are regulated by various mechanisms. My study provided first evidence of the involvement of fatty acid-related enzymes including FAAH, DAGL, and MGAT families in sensory systems and thermotactic behaviors. *MGATs*, particularly *MGAT-2*, mediates cool temperature sensing processes by maintaining the transcriptional level of *Irs*.

In the process of the behavioral screening of multiple fatty acid-related enzymes, when testing the early 3rd instar larvae of the control, a different distribution was observed in two temperature conditions. Control on a 16°C-26°C condition showed no clear peak on the gradient, while on an 8°C-35°C condition showed a clear peak around 24°C. Currently, there are no clear mechanisms for the different distribution, but there are several possibilities. First, on a thermal gradient, larvae determine their movement direction by discerning small temperature changes. 16°C-26°C condition was set up under a 1°C/cm temperature slope when 8°C-35°C condition was under a 1.5°C/cm slope. A lower slope, on the 16°C-26°C condition, implied smaller temperature differences which could induce more challenge in decision-making and ended up with less accumulation in a specific zone. Second, I observed a few larvae distributed in the 11°C-17°C zones on an 8°C-35°C condition. This indicates that the distribution in the 16°C zone on the 16°C-26°C condition displayed the accumulation of all larvae staying at lower temperatures. As a result, 16°C-26°C condition cannot show the full figure of larval thermal preference. And this is the reason I determined to observe temperature preference on a wider gradient from 8°C to 35°C.

I observed warm accumulations on two thermotaxis conditions in FAAH mutants. This suggested a potential involvement of FAAHs in warm avoidance (Fig. 10). One of the FAAH coding genes I tested, *CG8839*, is involved in seizure recovery through activation of a TRPA channel *water witch* (Jacobs and Sehgal, 2020). I found that *water witch* displayed a preference to higher temperatures on an 8°C-35°C temperature gradient at the late 3rd instar stage (unpublished), which is plausible to suggest that FAAH mediates the function of *water witch* in warm avoidance behavior. The co-function of FAAHs and *water witch* require further investigation.

DAGL (*inaE*) mutants displayed differential thermal preferences between two different slopes of thermal gradients (Fig. 11). DAGL mutant exhibited an accumulation closer to the release zone compared to the control group in a shallower temperature slope, this possibly

indicated a loss of sensitivity in small temperature discrimination. TRPA1 was reported to contribute to heat avoidance and a Rhodopsin/PLC signaling cascade activated TRPA1 to regulate thermal preference in an optimal temperature range between 18°C and 24°C (Shen et al., 2011; Sokabe et al., 2016). Previous reports also elucidated the role of DAGL (*inaE*) in phototransduction signaling pathway by releasing 2-LG to activate TRP channels (Sokabe et al., 2022). Considered the analogous rhodopsin/PLC/TRP signaling cascade between phototransduction and thermosensation (Montell, 2021), DAGL may also be involved in the signaling pathway of TRPA1-medaited temperature sensation. Then, one possibility of the *inaE* results is that the DAGL mutation suppresses the activation of TRPA1, leading to the inability to discriminating small temperature changes. To prove this assumption, the functional interaction of DAGL and TRPA1 under multiple temperature slopes should be tested. Another possibility for the cool tendency of $inaE^{N125}$ mutant on an 8°C-35°C condition was technical issue on rearing condition. I observed that the control on Fig. 11c showed accumulation in the 11°C -17°C zone compared with other controls under the same condition. This result was obtained when I first set up the gradient assay and such a cold temperature accumulation is rarely observed in control in previous reports and in current examines. It is possible that the experimental setup contains unknown issue and the cool trend showed in the mutant requires further confirmation.

MGAT-1/-2/-3 form a gene cluster (Fig. 12) and displayed high amino acid identity to human MOGAT2. Human MOGAT2 presents as a single copy in the genome (Yang and Nickels, 2015). On the other hand, limited *Drosophila* species within the *Drosophila melanogaster group* display this triplication of *MGATs*, while other species such as *D. mojavensis* contain a single copy (Stark et al., 2007). This possibly indicates that multiplication events occurred specifically in the branch of *Drosophila melanogaster group* during the evolution. Duplications may possess a “two-fold hypothesis”, which induces an enhanced expression beyond the gene copy number (Loehlin et al., 2022; Loehlin and Carroll, 2016). This property might explain the suppression of the transcriptional level of the neighboring genes in single *MGAT* knockouts (Fig. 13).

The involvement of *MGAT-2* and *MGAT-3* in cool temperature avoidance was initially demonstrated at the behavioral level in *MGAT* knockouts (Fig. 14-18). The cross-inhibition of *MGAT-2/-3* at a transcriptional level (Fig. 13b, c) in *MGAT-2/-3* knockouts was partially supported by the loss of cool avoidance observed in their trans-heterozygous mutants (Fig. 17d). However, this cross-inhibition alone does not fully explain the behavioral phenotype, as $MGAT\text{-}1^{KO}$ resulted in a transcriptional reduction of *MGAT-2* without affecting cool avoidance

behaviors (Fig. 13, 15a and 17a). *MGAT-2* and *MGAT-3* also mediate larval cool avoidance independently. Investigations of the roles of *MGAT-2* and *MGAT-3* in sensory neurons revealed partially overlapping yet distinct functional patterns of these genes (Fig. 22-24). *MGAT-3* was involved in cool avoidance in multiple sensory neurons (Fig. 22 and 24) but also contributed to warm avoidance in *trpA1-AB-expressing* neurons (Fig. 23), suggesting the wide and complicated involvement of this gene in temperature preference. In contrast, *MGAT-2* primary functions in DOCCs (Fig. 24 and 25), suggesting more specific roles in this set of neurons. These results imply the possible interaction of *MGAT-2* and *MGAT-3* in the neurons expressing both of them.

Interestingly, reduced responses were observed in DOCCs during multiple cooling events in *MGAT-2*^{KO} (Fig. 27). This indicated the role of *MGAT-2* in mediating neuronal responses to cooling in DOCCs. One possibility is that the total number of temperature-responsible molecules in DOCCs such as *Irs*, were reduced. This interpretation was supported by a significant reduction of *Ir25a* and *Ir21a* transcripts in DOCC-containing tissues in *MGAT-2*^{KO} (Fig. 29a, b). The reduction of *Ir25a* and *Ir21a* in *MGAT-3*^{KO} may be caused by the functional interaction between *MGAT-2/-3* (Fig. 29a, b). Additionally, the inadequate rescue of the cooling response was observed upon overexpression of *MGAT-2* in DOCCs (Fig. 27c-e). This suggested the function of *MGAT-2* in additional sensory neurons interacted with DOCC cooling responses, such as DOWCs. A previous report suggests cross-inhibition between DOCCs and DOWCs in cooling/warming responses (Hernandez-Nunez et al., 2021). I first expected that an enhanced DOWCs warming response affected by *MGAT-2* suppressed cooling responses of DOCCs in *MGAT-2*^{KO}. However, the response of DOWCs to warming stimuli in *MGAT-2*^{KO} was reduced, meanwhile, overexpression of *MGAT-2* in DOWCs failed to recover the warming response (Fig. 28). This suggests that the cross-inhibition between DOCCs and DOWCs may not be a dominant mechanism for the reduced responses in these two types of neurons in the absence of *MGAT-2*. *Ir25a* is expressed in both DOCCs and DOWCs in DOG (Ni et al., 2016; Sánchez-Alcañiz et al., 2018; Hernandez-Nunez et al., 2021), the reduction of *Ir25a* in the anterior region should affect the functionality of all these neurons (Fig. 29a). This suggests that the reduced *Ir25a* expression in *MGAT-2* mutant could be the cause of deteriorated warming response in DOWCs. Furthermore, considering the potential co-expression of *MGAT-2* in multiple *Ir25a-expressing* neurons, temperature responses of DOCCs and DOWCs could also be influenced by other *Ir25a-expressing* neurons in the DOG. Findings in this study suggest that *MGAT-2* maintains the temperature responsiveness of DOCCs and DOWCs by maintaining the transcriptional level of *Ir25a*, thereby supporting cool avoidance

at a behavioral level. However, the direct evidence of co-expression in *MGAT-2* and *Ir25a-expressing* neurons requires further confirmation.

At the behavioral level, specific knockdown of *MGAT-2* in DOWCs resulted in indiscrimination between 20°C and optimal temperature 24°C (Fig. 24f). Considering the suppression of warming response in DOWCs due to the absence of *MGAT-2* (Fig. 28), this loss of optimal temperature selection from 24°C to 20°C may be attributed to the inability of warm temperature differentiation from 24°C to other temperatures, in addition to the DOCC-mediated loss of cool temperature avoidance. It is necessary to clarify the warm avoidance phenotype of this specific knockdown in different thermal behavior assays.

Human MOGAT2 is a possible ortholog of *Drosophila MGAT-2*, since the human MOGAT2, but not human DGAT2, was able to compensate the loss of the cool avoidance in *MGAT-2*^{KO} (Fig. 26). These results challenged the previous name "*Dgat2*" given to this gene (Wilfling et al., 2013), and supported the new given name "*MGAT-2*" based on the predicted molecular function in this study. In humans, MOGATs are primarily known as intermediate proteins involved in TAG synthesis by producing DAG from MAG substrates, followed by additional DGATs responsible for TAG synthesis by synthesizing TAG from DAG substrates (Yang and Nickels, 2015). Both human MOGAT2 and MOGAT3 exhibit DGAT activity, however, MOGAT3 exhibits significantly higher DGAT activity than MOGAT2 when MAGs or DAGs are used as substrates (Cao et al., 2007). This evidence suggests that *Drosophila MGAT-2* could predominantly contribute to mediating cool avoidance behavior by its MOGAT activity rather than both MOGAT and DGAT activities. *Drosophila MGAT-2* displays conflicting effects in TAG accumulation under *in vitro* conditions (Wilfling et al., 2013; Wang et al., 2019), this is a possible clue that *MGAT-2* relays on DGATs to synthesize TAG. Thus, if this DAG-TAG axis plays a role in the regulation of *Irs*, additional DGATs are possibly required in the DOCCs/DOWCs. *Drosophila* DGAT1 coding gene *midway* was reported in TAG synthesis in oogenesis (Buszczak et al., 2002), however, there is currently no evidence indicating its expression in sensory system. It requires further studies to identify possible DGATs in *Drosophila* sensory neurons function with *MGAT-2*.

broad was preliminarily identified as a transcriptional factor (Fig. 31-33) for *Ir25a* expression. It has been reported to be expressed in both CNS and PNS at multiple stages, including the 3rd instar stage (Scott et al., 2011; Zhou et al., 2009, 2019). This implies a possible role of *broad* in maintaining the expression level of *Ir25a* within sensory neurons including DOCCs/DOWCs. Reduced *broad* expression level is observed in adults or larvae when they are exposed to harmful stimuli such as low oxygen stress (Zhou et al., 2007) or a toxic drug

treatment (Stern et al., 2012). This indicates a possible association between *broad* expression level and cellular damage. Meanwhile, the accumulation of TAG in lipid droplets have been shown to have protective role to oxidative stress (Circu and Aw, 2010) and prevent cellular damage. *MGAT-2* is known to be involved in lipid droplet formation through TAG synthesis (Wilfling et al., 2013). Therefore, the decreased expression of *broad* in *MGAT-2*^{KO} (Fig. 33b) might be attributed to the oxidative stress resulting from the reduction of protective TAG and lipid droplets.

broad is known as an early ecdysone response transcriptional factor and plays a key role in ecdysone signaling pathway (Karim et al., 1993; Von Kalm et al., 1994). Although *broad* and the ecdysone signaling pathway are widely reported in regulating larval development and metamorphosis (Belles and Piulachs, 2015), the developmental time scale of *MGAT-2* mutant larvae was not changed (Fig. 21). This possibly indicates that *MGAT-2* and *broad* does not co-function in tissues determining developmental stage changes. In addition, ecdysone signaling mediates TAG accumulation and the expression level of TAG-related enzymes in fat body at the 3rd instar stage (Kamoshida et al., 2012; Wang et al., 2010). If this interaction exists in sensory neurons, the reduction of *broad* expression level in *MGAT-2*^{KO} (Fig. 33b) could be explained by defects of TAG synthesis in the negative feedback to ecdysone signaling. Additionally, AMPK signaling pathway functions as the upstream of ecdysone in sensory neurons and the upstream of *MGAT-2* in skeletal muscle (Livelo et al., 2023; Marzano et al., 2021). This indicates a possible involvement of AMPK in the interaction between *MGAT-2* and *broad*. These assumptions require further exploration of *MGAT-2* and *broad* interactions at a physiological level.

The main roles of *board* in the nervous system are development and pruning of neurons (Marzano et al., 2021; Scott et al., 2011; Zhou et al., 2009). In addition to the potential effects on *Ir25a*, *board* may also influence the neural response to temperature by affecting neural maturation. Changes in fatty acid compositions also impact neural development (Ziegler et al., 2017), thus, *MGAT*-2 may also influence on neural responsiveness independently of its effects on *Ir25a*. Therefore, temperature sensation could be impaired by neurodevelopmental disorders with the absent of *MGAT-2*. However, more evidence is required to support developmental changes of DOCCs and DOWCs under *MGAT-2* and *broad* mutation.

Taken together, findings in this study underscore the important role of fatty acid-related enzymes in temperature perception and the underlying mechanism, particularly in the case of *MGAT-2*. This provides a novel perspective on how fatty acid metabolism regulates sensory receptors in the sensory system.

5 References

Barbagallo, B., Garrity, P.A., 2015. Temperature sensation in *Drosophila*: current opinion in neurobiology 34, 8–13. https://doi.org/10.1016/j.conb.2015.01.002

Bellen, H.J., Levis, R.W., Liao, G., He, Y., Carlson, J.W., Tsang, G., Evans-Holm, M., Hiesinger, P.R., Schulze, K.L., Rubin, G.M., Hoskins, R.A., Spradling, A.C., 2004. The BDGP Gene Disruption Project. Genetics 167, 761–781. https://doi.org/10.1534/genetics.104.026427

Belles, X., Piulachs, M.-D., 2015. Ecdysone signalling and ovarian development in insects: from stem cells to ovarian follicle formation. Biochimica et Biophysica Acta (BBA)-Gene Regulatory Mechanisms 1849, 181–186. https://doi.org/10.1016/j.bbagrm.2014.05.025

Benton, R., Vannice, K.S., Gomez-Diaz, C., Vosshall, L.B., 2009. Variant ionotropic glutamate receptors as chemosensory receptors in *Drosophila*. Cell 136, 149–162. https://doi.org/10.1016/j.cell.2008.12.001

Bhatt-Wessel, B., Jordan, T.W., Miller, J.H., Peng, L., 2018. Role of DGAT enzymes in triacylglycerol metabolism. Archives of Biochemistry and Biophysics 655, 1–11. https://doi.org/10.1016/j.abb.2018.08.001

Brankatschk, M., Gutmann, T., Knittelfelder, O., Palladini, A., Prince, E., Grzybek, M., Brankatschk, B., Shevchenko, A., Coskun, Ü., Eaton, S., 2018. A temperature-dependent switch in feeding preference improves *Drosophila* development and survival in the cold. Developmental Cell 46, 781-793.e4. https://doi.org/10.1016/j.devcel.2018.05.028

Budelli, G., Ni, L., Berciu, C., Van Giesen, L., Knecht, Z.A., Chang, E.C., Kaminski, B., Silbering, A.F., Samuel, A., Klein, M., Benton, R., Nicastro, D., Garrity, P.A., 2019. Ionotropic receptors specify the morphogenesis of phasic sensors controlling rapid thermal preference in *Drosophila*. neuron 101, 738-747.e3. https://doi.org/10.1016/j.neuron.2018.12.022

Buszczak, M., Lu, X., Segraves, W.A., Chang, T.Y., Cooley, L., 2002. Mutations in the *midway* gene disrupt a *Drosophila* acyl coenzyme A: Diacylglycerol acyltransferase. Genetics 160, 1511–1518. https://doi.org/10.1093/genetics/160.4.1511

Cabezas-Bratesco, D., Mcgee, F.A., Colenso, C.K., Zavala, K., Granata, D., Carnevale, V., Opazo, J.C., Brauchi, S.E., 2022. Sequence and structural conservation reveal

fingerprint residues in TRP channels. eLife 11, e73645. https://doi.org/10.7554/eLife.73645

Cao, J., Cheng, L., Shi, Y., 2007. Catalytic properties of MGAT3, a putative triacylglycerol synthase. Journal of Lipid Research 48, 583–591. https://doi.org/10.1194/jlr.M600331-JLR200

Castro-Mondragon, J.A., Riudavets-Puig, R., Rauluseviciute, I., Berhanu Lemma, R., Turchi, L., Blanc-Mathieu, R., Lucas, J., Boddie, P., Khan, A., Manosalva Pérez, N., Fornes, O., Leung, T.Y., Aguirre, A., Hammal, F., Schmelter, D., Baranasic, D., Ballester, B., Sandelin, A., Lenhard, B., Vandepoele, K., Wasserman, W.W., Parcy, F., Mathelier, A., 2022. JASPAR 2022: the 9th release of the open-access database of transcription factor binding profiles. Nucleic Acids Research 50, D165–D173. https://doi.org/10.1093/nar/gkab1113

Circu, M.L., Aw, T.Y., 2010. Reactive oxygen species, cellular redox systems, and apoptosis. Free Radical Biology and Medicine 48, 749–762. https://doi.org/10.1016/j.freeradbiomed.2009.12.022

Dec, K., Alsaqati, M., Morgan, J., Deshpande, S., Wood, J., Hall, J., Harwood, A.J., 2023. A high ratio of linoleic acid (n-6 PUFA) to alpha-linolenic acid (n-3 PUFA) adversely affects early stage of human neuronal differentiation and electrophysiological activity of glutamatergic neurons in vitro. Front. Cell Dev. Biol. 11, 1166808. https://doi.org/10.3389/fcell.2023.1166808

Dillon, M.E., Wang, G., Huey, R.B., 2010. Global metabolic impacts of recent climate warming. Nature 467, 704–706. https://doi.org/10.1038/nature09407

Ensembl 2022 | Nucleic Acids Research | Oxford Academic [WWW Document], n.d. URL https://academic.oup.com/nar/article/50/D1/D988/6430486?login=true (accessed 6.23.23).

Falomir-Lockhart, L.J., Cavazzutti, G.F., Giménez, E., Toscani, A.M., 2019. fatty acid signaling mechanisms in neural cells: fatty acid receptors. Front. Cell. Neurosci. 13, 162. https://doi.org/10.3389/fncel.2019.00162

Fowler, M.A., Montell, C., 2013. *Drosophila* TRP channels and animal behavior. Life Sciences 92, 394–403. https://doi.org/10.1016/j.lfs.2012.07.029

Gallio, M., Ofstad, T.A., Macpherson, L.J., Wang, J.W., Zuker, C.S., 2011. the coding of temperature in the *Drosophila* brain. Cell 144, 614–624. https://doi.org/10.1016/j.cell.2011.01.028

Garrity, P.A., Goodman, M.B., Samuel, A.D., Sengupta, P., 2010. Running hot and cold: behavioral strategies, neural circuits, and the molecular machinery for thermotaxis in *C. elegans* and *Drosophila*. Genes Dev. 24, 2365–2382. https://doi.org/10.1101/gad.1953710

Gu, P., Gong, J., Shang, Y., Wang, F., Ruppell, K.T., Ma, Z., Sheehan, A.E., Freeman, M.R., Xiang, Y., 2019. Polymodal nociception in *Drosophila* requires alternative splicing of TrpA1. Current Biology 29, 3961-3973.e6. https://doi.org/10.1016/j.cub.2019.09.070

Häcker, U., Nystedt, S., Barmchi, M.P., Horn, C., Wimmer, E.A., 2003. *piggyBac* -based insertional mutagenesis in the presence of stably integrated *P*-elements in *Drosophila*. Proc. Natl. Acad. Sci. U.S.A. 100, 7720–7725. https://doi.org/10.1073/pnas.1230526100

Hamada, F.N., Rosenzweig, M., Kang, K., Pulver, S.R., Ghezzi, A., Jegla, T.J., Garrity, P.A., 2008. An internal thermal sensor controlling temperature preference in *Drosophila*. Nature 454, 217–220. https://doi.org/10.1038/nature07001

Hernandez-Nunez, L., Chen, A., Budelli, G., Berck, M.E., Richter, V., Rist, A., Thum, A.S., Cardona, A., Klein, M., Garrity, P., Samuel, A.D.T., 2021a. Synchronous and opponent thermosensors use flexible cross-inhibition to orchestrate thermal homeostasis. Sci. Adv. 7, eabg6707. https://doi.org/10.1126/sciadv.abg6707

Hernandez-Nunez, L., Chen, A., Budelli, G., Berck, M.E., Richter, V., Rist, A., Thum, A.S., Cardona, A., Klein, M., Garrity, P., Samuel, A.D.T., 2021b. Synchronous and opponent thermosensors use flexible cross-inhibition to orchestrate thermal homeostasis. Sci. Adv. 7, eabg6707. https://doi.org/10.1126/sciadv.abg6707

Housden, B.E., Hu, Y., Perrimon, N., 2016. Design and generation of *Drosophila* single guide RNA expression constructs. Cold Spring Harb Protoc 2016, pdb.prot090779. https://doi.org/10.1101/pdb.prot090779

Jacobs, J.A., Sehgal, A., 2020. Anandamide metabolites protect against seizures through the trp channel water witch in *Drosophila* melanogaster. Cell Reports 31, 107710. https://doi.org/10.1016/j.celrep.2020.107710

Jiang, L.-H., Yao, X., Çiğ, B., 2023. TRP channels in oxidative stress signalling. Cells 12, 1251. https://doi.org/10.3390/cells12091251

Kamoshida, Y., Fujiyama-Nakamura, S., Kimura, S., Suzuki, E., Lim, J., Shiozaki-Sato, Y., Kato, S., Takeyama, K., 2012. Ecdysone receptor (EcR) suppresses lipid accumulation in the *Drosophila* fat body via transcription control. Biochemical and Biophysical Research Communications 421, 203–207. https://doi.org/10.1016/j.bbrc.2012.03.135

Kanda, Y., 2013. Investigation of the freely available easy-to-use software 'EZR' for medical statistics. Bone Marrow Transplant 48, 452–458. https://doi.org/10.1038/bmt.2012.244

Karim, F.D., Guild, G.M., Thummel, C.S., 1993. The *Drosophila* Broad-Complex plays a key role in controlling ecdysone-regulated gene expression at the onset of metamorphosis. Development 118, 977–988. https://doi.org/10.1242/dev.118.3.977

Kashio, M., Tominaga, M., 2022. TRP channels in thermosensation. Current Opinion in Neurobiology 75, 102591. https://doi.org/10.1016/j.conb.2022.102591

Khuong, T.M., Wang, Q.-P., Manion, J., Oyston, L.J., Lau, M.-T., Towler, H., Lin, Y.Q., Neely, G.G., 2019. Nerve injury drives a heightened state of vigilance and neuropathic sensitization in *Drosophila*. Sci. Adv. 5, eaaw4099. https://doi.org/10.1126/sciadv.aaw4099

Klein, M., Afonso, B., Vonner, A.J., Hernandez-Nunez, L., Berck, M., Tabone, C.J., Kane, E.A., Pieribone, V.A., Nitabach, M.N., Cardona, A., Zlatic, M., Sprecher, S.G., Gershow, M., Garrity, P.A., Samuel, A.D.T., 2015. Sensory determinants of behavioral dynamics in *Drosophila* thermotaxis. Proc. Natl. Acad. Sci. U.S.A. 112. https://doi.org/10.1073/pnas.1416212112

Knecht, Z.A., Silbering, A.F., Ni, L., Klein, M., Budelli, G., Bell, R., Abuin, L., Ferrer, A.J., Samuel, A.D., Benton, R., Garrity, P.A., 2016. Distinct combinations of variant ionotropic glutamate receptors mediate thermosensation and hygrosensation in *Drosophila*. eLife 5, e17879. https://doi.org/10.7554/eLife.17879

Koh, T.-W., He, Z., Gorur-Shandilya, S., Menuz, K., Larter, N.K., Stewart, S., Carlson, J.R., 2014. The *Drosophila* IR20a Clade of Ionotropic Receptors Are Candidate Taste and Pheromone Receptors. Neuron 83, 850–865. https://doi.org/10.1016/j.neuron.2014.07.012

Kozai, D., Ogawa, N., Mori, Y., 2014. Redox Regulation of Transient Receptor Potential Channels. Antioxidants & Redox Signaling 21, 971–986. https://doi.org/10.1089/ars.2013.5616

Kwon, Y., Shen, W.L., Shim, H.-S., Montell, C., 2010. Fine Thermotactic Discrimination between the Optimal and Slightly Cooler Temperatures via a TRPV Channel in Chordotonal Neurons. J. Neurosci. 30, 10465–10471. https://doi.org/10.1523/JNEUROSCI.1631-10.2010

Kwon, Y., Shim, H.-S., Wang, X., Montell, C., 2008. Control of thermotactic behavior via coupling of a TRP channel to a phospholipase C signaling cascade. Nat Neurosci 11, 871–873. https://doi.org/10.1038/nn.2170

Lee, Youngseok, Lee, Yong, Lee, J., Bang, S., Hyun, S., Kang, J., Hong, S.-T., Bae, E., Kaang, B.-K., Kim, J., 2005. Pyrexia is a new thermal transient receptor potential channel endowing tolerance to high temperatures in *Drosophila* melanogaster. Nat Genet 37, 305–310. https://doi.org/10.1038/ng1513

Leung, H.-T., Tseng-Crank, J., Kim, E., Mahapatra, C., Shino, S., Zhou, Y., An, L., Doerge, R.W., Pak, W.L., 2008. DAG Lipase Activity Is Necessary for TRP Channel Regulation in *Drosophila* Photoreceptors. Neuron 58, 884–896. https://doi.org/10.1016/j.neuron.2008.05.001

Li, K., Gong, Z., 2017. Feeling Hot and Cold: Thermal Sensation in *Drosophila*. Neurosci. Bull. 33, 317–322. https://doi.org/10.1007/s12264-016-0087-9

Li, Q., Montell, C., 2021. Mechanism for food texture preference based on grittiness. Current Biology 31, 1850-1861.e6. https://doi.org/10.1016/j.cub.2021.02.007

Liu, J., Sokabe, T., Montell, C., 2018. A temperature gradient assay to determine thermal preferences of *Drosophila* larvae. Journal of Visualized Experiments 2018, 1–10. https://doi.org/10.3791/57963

Liu, Q., Siloto, R.M.P., Snyder, C.L., Weselake, R.J., 2011. Functional and Topological Analysis of Yeast Acyl-CoA:Diacylglycerol Acyltransferase 2, an Endoplasmic Reticulum Enzyme Essential for Triacylglycerol Biosynthesis. Journal of Biological Chemistry 286, 13115–13126. https://doi.org/10.1074/jbc.M110.204412

Livelo, C., Guo, Y., Abou Daya, F., Rajasekaran, V., Varshney, S., Le, H.D., Barnes, S., Panda, S., Melkani, G.C., 2023. Time-restricted feeding promotes muscle function through purine cycle and AMPK signaling in *Drosophila* obesity models. Nat Commun 14, 949. https://doi.org/10.1038/s41467-023-36474-4

Loehlin, D.W., Carroll, S.B., 2016. Expression of tandem gene duplicates is often greater than twofold. Proc. Natl. Acad. Sci. U.S.A. 113, 5988–5992. https://doi.org/10.1073/pnas.1605886113

Loehlin, D.W., Kim, J.Y., Paster, C.O., 2022. A tandem duplication in *Drosophila melanogaster* shows enhanced expression beyond the gene copy number. Genetics 220, iyab231. https://doi.org/10.1093/genetics/iyab231

Luo, L., Gershow, M., Rosenzweig, M., Kang, K., Fang-Yen, C., Garrity, P.A., Samuel, A.D.T., 2010. Navigational decision making in *Drosophila* thermotaxis. J. Neurosci. 30, 4261–4272. https://doi.org/10.1523/JNEUROSCI.4090-09.2010

Luo, M., Wang, Z., Zhang, H., Arens, E., Filingeri, D., Jin, L., Ghahramani, A., Chen, W., He, Y., Si, B., 2020. High-density thermal sensitivity maps of the human body. Building and Environment 167, 106435. https://doi.org/10.1016/j.buildenv.2019.106435

Marzano, M., Herzmann, S., Elsbroek, L., Sanal, N., Tarbashevich, K., Raz, E., Krahn, M.P., Rumpf, S., 2021. AMPK adapts metabolism to developmental energy requirement during dendrite pruning in *Drosophila*. Cell Reports 37, 110024. https://doi.org/10.1016/j.celrep.2021.110024

Mattila, J., Havula, E., Suominen, E., Teesalu, M., Surakka, I., Hynynen, R., Kilpinen, H., Väänänen, J., Hovatta, I., Käkelä, R., Ripatti, S., Sandmann, T., Hietakangas, V., 2015. Mondo-Mlx mediates organismal sugar sensing through the Gli-similar transcription Factor Sugarbabe. Cell Reports 13, 350–364. https://doi.org/10.1016/j.celrep.2015.08.081

Mejhert, N., Kuruvilla, L., Gabriel, K.R., Elliott, S.D., Guie, M.-A., Wang, H., Lai, Z.W., Lane, E.A., Christiano, R., Danial, N.N., Farese, R.V., Walther, T.C., 2020. Partitioning of MLX-Family transcription factors to lipid droplets regulates metabolic gene expression. Molecular Cell 77, 1251-1264.e9. https://doi.org/10.1016/j.molcel.2020.01.014

Montell, C., 2021. *Drosophila* sensory receptors—a set of molecular swiss army knives. Genetics 217, 1–34. https://doi.org/10.1093/genetics/iyaa011

Montell, C., 2011. The history of TRP channels, a commentary and reflection. Pflugers Arch– - Eur J Physiol 461, 499–506. https://doi.org/10.1007/s00424-010-0920-3

Neely, G.G., Keene, A.C., Duchek, P., Chang, E.C., Wang, Q.-P., Aksoy, Y.A., Rosenzweig, M., Costigan, M., Woolf, C.J., Garrity, P.A., Penninger, J.M., 2011. TrpA1 regulates thermal nociception in *Drosophila*. pLoS ONE 6, e24343. https://doi.org/10.1371/journal.pone.0024343

Ni, L., 2021. The structure and function of ionotropic receptors in *Drosophila*. Front. Mol. Neurosci. 13, 638839. https://doi.org/10.3389/fnmol.2020.638839

Ni, L., Bronk, P., Chang, E.C., Lowell, A.M., Flam, J.O., Panzano, V.C., Theobald, D.L., Griffith, L.C., Garrity, P.A., 2013. A gustatory receptor paralogue controls rapid warmth avoidance in *Drosophila*. Nature 500, 580–584. https://doi.org/10.1038/nature12390

Ni, L., Klein, M., Svec, K.V., Budelli, G., Chang, E.C., Ferrer, A.J., Benton, R., Samuel, A.D., Garrity, P.A., 2016. The ionotropic receptors IR21a and IR25a mediate cool sensing in *Drosophila*. eLife 5, e13254. https://doi.org/10.7554/eLife.13254

Poças, G.M., Domingos, P.M., Mirth, C.K., 2020. quantification of macronutrients intake in a thermogenetic neuronal screen using *Drosophila* larvae. JoVE 61323. https://doi.org/10.3791/61323

Porcelli, D., Gaston, K.J., Butlin, R.K., Snook, R.R., 2017. Local adaptation of reproductive performance during thermal stress. J. Evol. Biol. 30, 422–429. https://doi.org/10.1111/jeb.13018

Rosenzweig, M., Kang, K., Garrity, P.A., 2008. Distinct TRP channels are required for warm and cool avoidance in *Drosophila melanogaster*. Proc. Natl. Acad. Sci. U.S.A. 105, 14668–14673. https://doi.org/10.1073/pnas.0805041105

Sánchez-Alcañiz, J.A., Silbering, A.F., Croset, V., Zappia, G., Sivasubramaniam, A.K., Abuin, L., Sahai, S.Y., Münch, D., Steck, K., Auer, T.O., Cruchet, S., Neagu-Maier, G.L., Sprecher, S.G., Ribeiro, C., Yapici, N., Benton, R., 2018. An expression atlas of variant ionotropic glutamate receptors identifies a molecular basis of carbonation sensing. Nat Commun 9, 4252. https://doi.org/10.1038/s41467-018-06453-1

Schindelin, J., Arganda-Carreras, I., Frise, E., Kaynig, V., Longair, M., Pietzsch, T., et al. (2012). Fiji: an open-source platform for biological-image analysis. Nat Methods 9(7), 676-682. doi: 10.1038/nmeth.2019.

Schneider, C. A., Rasband, W. S., & Eliceiri, K. W. (2012). NIH Image to ImageJ: 25 years of image analysis. Nature Methods, 9(7), 671–675. doi:10.1038/nmeth.2089

Scott, J.A., Williams, D.W., Truman, J.W., 2011. The BTB/POZ zinc finger protein Broad-Z3 promotes dendritic outgrowth during metamorphic remodeling of the peripheral stretch receptor dbd. Neural Dev 6, 39. https://doi.org/10.1186/1749-8104-6-39

Shen, W.L., Kwon, Y., Adegbola, A.A., Luo, J., Chess, A., Montell, C., 2011. Function of Rhodopsin in temperature discrimination in *Drosophila*. Science 331, 1333–1336. https://doi.org/10.1126/science.1198904

Sokabe, T., Chen, H.-C., Luo, J., Montell, C., 2016a. A switch in thermal preference in *Drosophila* larvae depends on multiple rhodopsins. Cell Reports 17, 336–344. https://doi.org/10.1016/j.celrep.2016.09.028

Sokabe, T., Tsujiuchi, S., Kadowaki, T., Tominaga, M., 2008. *Drosophila* painless is a Ca^{2+}-requiring channel activated by noxious heat. J. Neurosci. 28, 9929–9938. https://doi.org/10.1523/JNEUROSCI.2757-08.2008

Stark, A., Lin, M.F., Kheradpour, P., Pedersen, J.S., Parts, L., Carlson, J.W., Crosby, M.A., Rasmussen, M.D., Roy, S., Deoras, A.N., Ruby, J.G., Brennecke, J., Harvard FlyBase curators, Crosby, M.A., Matthews, B.B., Schroeder, A.J., Sian Gramates, L., St Pierre,

S.E., Roark, M., Wiley Jr, K.L., Kulathinal, R.J., Zhang, P., Myrick, K.V., Antone, J.V., Gelbart, W.M., Berkeley *Drosophila* Genome Project, Carlson, J.W., Yu, C., Park, S., Wan, K.H., Celniker, S.E., Hodges, E., Hinrichs, A.S., Caspi, A., Paten, B., Park, S.-W., Han, M.V., Maeder, M.L., Polansky, B.J., Robson, B.E., Aerts, S., Van Helden, J., Hassan, B., Gilbert, D.G., Eastman, D.A., Rice, M., Weir, M., Hahn, M.W., Park, Y., Dewey, C.N., Pachter, L., Kent, W.J., Haussler, D., Lai, E.C., Bartel, D.P., Hannon, G.J., Kaufman, T.C., Eisen, M.B., Clark, A.G., Smith, D., Celniker, S.E., Gelbart, W.M., Kellis, M., 2007. Discovery of functional elements in 12 *Drosophila* genomes using evolutionary signatures. Nature 450, 219–232. https://doi.org/10.1038/nature06340

Stern, S., Fridmann-Sirkis, Y., Braun, E., Soen, Y., 2012. Epigenetically heritable alteration of fly development in response to toxic challenge. Cell Reports 1, 528–542. https://doi.org/10.1016/j.celrep.2012.03.012

Suito, T., Nagao, K., Takeuchi, K., Juni, N., Hara, Y., Umeda, M., 2020a. Functional expression of Δ12 fatty acid desaturase modulates thermoregulatory behaviour in *Drosophila*. Sci Rep 10, 11798. https://doi.org/10.1038/s41598-020-68601-2

Takeuchi, K.I., Nakano, Y., Kato, U., Kaneda, M., Aizu, M., Awano, W., Yonemura, S., Kiyonaka, S., Mori, Y., Yamamoto, D., Umeda, M., 2009. Changes in temperature preferences and energy homeostasis in dystroglycan mutants. Science 323, 1740–1743. https://doi.org/10.1126/science.1165712

Turchetto-Zolet, A.C., Maraschin, F.S., De Morais, G.L., Cagliari, A., Andrade, C.M., Margis-Pinheiro, M., Margis, R., 2011. Evolutionary view of acyl-CoA diacylglycerol acyltransferase (DGAT), a key enzyme in neutral lipid biosynthesis. BMC Evol Biol 11, 263. https://doi.org/10.1186/1471-2148-11-263

Turner, H.N., Armengol, K., Patel, A.A., Himmel, N.J., Sullivan, L., Iyer, S.C., Bhattacharya, S., Iyer, E.P.R., Landry, C., Galko, M.J., Cox, D.N., 2016. The TRP Channels Pkd2, NompC, and Trpm act in cold-sensing neurons to mediate unique aversive behaviors to noxious cold in *Drosophila*. Current Biology 26, 3116–3128. https://doi.org/10.1016/j.cub.2016.09.038

Tweedie, S., Ashburner, M., Falls, K., Leyland, P., McQuilton, P., Marygold, S., Millburn, G., Osumi-Sutherland, D., Schroeder, A., Seal, R., Zhang, H., The FlyBase Consortium, 2009. FlyBase: enhancing *Drosophila* Gene Ontology annotations. Nucleic Acids Research 37, D555–D559. https://doi.org/10.1093/nar/gkn788

Tyrrell, J.J., Wilbourne, J.T., Omelchenko, A.A., Yoon, J., Ni, L., 2021. Ionotropic receptor-dependent cool cells control the transition of temperature preference in *Drosophila* larvae. PLoS Genet 17, e1009499. https://doi.org/10.1371/journal.pgen.1009499

Van Giesen, L., Garrity, P.A., 2017. More than meets the IR: the expanding roles of variant Ionotropic Glutamate Receptors in sensing odor, taste, temperature and moisture. F1000Res 6, 1753. https://doi.org/10.12688/f1000research.12013.1

Von Kalm, L., Crossgrove, K., Von Seggern, D., Guild, G.M., Beckendorf, S.K., 1994. The Broad-Complex directly controls a tissue-specific response to the steroid hormone ecdysone at the onset of *Drosophila* metamorphosis. The EMBO Journal 13, 3505–3516. https://doi.org/10.1002/j.1460-2075.1994.tb06657.x

Vulpe, A., Mohapatra, P., Menuz, K., 2021. Functional characterization of odor responses and gene expression changes in olfactory co-receptor mutants in *Drosophila* (preprint). Neuroscience. https://doi.org/10.1101/2021.06.18.449017

Wang, S., Liu, S., Liu, H., Wang, J., Zhou, S., Jiang, R.-J., Bendena, W.G., Li, S., 2010. 20-hydroxyecdysone Reduces Insect Food Consumption Resulting in Fat Body Lipolysis During Molting and Pupation. Journal of Molecular Cell Biology 2, 128–138. https://doi.org/10.1093/jmcb/mjq006

Wang, W., Xin, J., Yang, X., Lam, S.M., Shui, G., Wang, Y., Huang, X., 2019. Lipid-gene regulatory network reveals coregulations of triacylglycerol with phosphatidylinositol/lysophosphatidylinositol and with hexosyl-ceramide. Biochimica et Biophysica Acta (BBA) - Molecular and Cell Biology of Lipids 1864, 168–180. https://doi.org/10.1016/j.bbalip.2018.11.010

Wat, L.W., Chao, C., Bartlett, R., Buchanan, J.L., Millington, J.W., Chih, H.J., Chowdhury, Z.S., Biswas, P., Huang, V., Shin, L.J., Wang, L.C., Gauthier, M.-P.L., Barone, M.C., Montooth, K.L., Welte, M.A., Rideout, E.J., 2020. A role for triglyceride lipase brummer in the regulation of sex differences in *Drosophila* fat storage and breakdown. PLoS Biol 18, e3000595. https://doi.org/10.1371/journal.pbio.3000595

Wilfling, F., Wang, H., Haas, J.T., Krahmer, N., Gould, T.J., Uchida, A., Cheng, J.-X., Graham, M., Christiano, R., Fröhlich, F., Liu, X., Buhman, K.K., Coleman, R.A., Bewersdorf, J., Farese, R.V., Walther, T.C., 2013. Triacylglycerol synthesis enzymes mediate lipid droplet growth by relocalizing from the er to lipid droplets. Developmental Cell 24, 384–399. https://doi.org/10.1016/j.devcel.2013.01.013

Xiao, R., Xu, X.Z.S., 2021. Temperature sensation: from molecular thermosensors to neural circuits and coding principles. Annu. Rev. Physiol. 83, 205–230. https://doi.org/10.1146/annurev-physiol-031220-095215

Xu, N., Zhang, S.O., Cole, R.A., McKinney, S.A., Guo, F., Haas, J.T., Bobba, S., Farese, R.V., Mak, H.Y., 2012. The FATP1–DGAT2 complex facilitates lipid droplet expansion at the ER–lipid droplet interface. Journal of Cell Biology 198, 895–911. https://doi.org/10.1083/jcb.201201139

Yang, M., Nickels, J., 2015. MOGAT2: A new therapeutic target for metabolic syndrome. Diseases 3, 176–192. https://doi.org/10.3390/diseases3030176

Yoo, S., Lim, J., Hwang, S., 2014. Sensory TRP Channel interactions with endogenous lipids and their biological outcomes. Molecules 19, 4708–4744. https://doi.org/10.3390/molecules19044708

Zhong, L., Bellemer, A., Yan, H., Honjo, K., Robertson, J., Hwang, R.Y., Pitt, G.S., Tracey, W.D., 2012. Thermosensory and nonthermosensory isoforms of *Drosophila* melanogaster TRPA1 reveal heat-sensor domains of a thermo-TRP channel. Cell Reports 1, 43–55. https://doi.org/10.1016/j.celrep.2011.11.002

Zhou, B., Williams, D.W., Altman, J., Riddiford, L.M., Truman, J.W., 2009. Temporal patterns of broad isoform expression during the development of neuronal lineages in *Drosophila*. Neural Dev 4, 39. https://doi.org/10.1186/1749-8104-4-39

Zhou, D., Xue, J., Chen, J., Morcillo, P., Lambert, J.D., White, K.P., Haddad, G.G., 2007. Experimental selection for *Drosophila* survival in extremely low O2 environment. PLoS ONE 2, e490. https://doi.org/10.1371/journal.pone.0000490

Zhou, Y., Yang, Y., Huang, Y., Wang, H., Wang, S., Luo, H., 2019. broad promotes neuroepithelial stem cell differentiation in the *Drosophila* optic lobe. Genetics 213, 941–951. https://doi.org/10.1534/genetics.119.302421

Ziegler, A.B., Thiele, C., Tenedini, F., Richard, M., Leyendecker, P., Hoermann, A., Soba, P., Tavosanis, G., 2017. Cell-autonomous control of neuronal dendrite expansion via the fatty acid synthesis regulator SREBP. Cell Reports 21, 3346–3353. https://doi.org/10.1016/j.celrep.2017.11.069

6 Figures

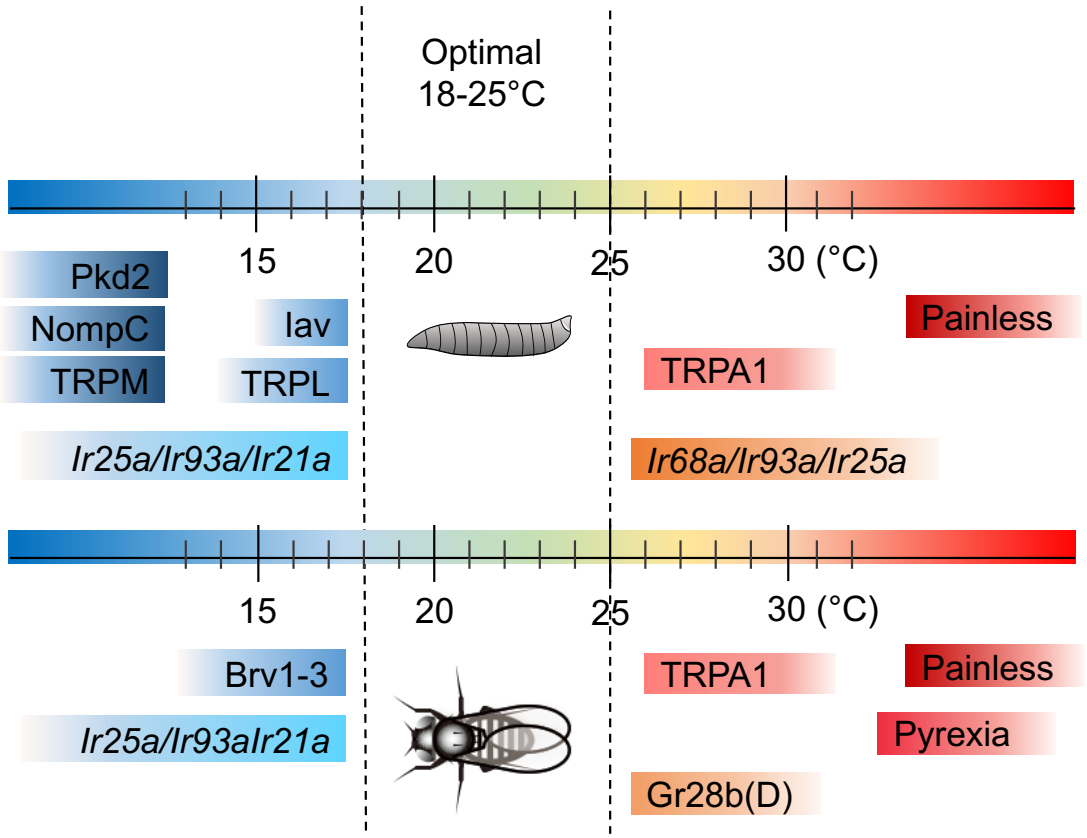

Figure 1. A schematic of reported TRP channels and IRs in the thermosensation of *Drosophila* larvae and adults.

In larvae (upper), TRPA1 is reported as a heat sensor, and *Ir68a/Ir93a/Ir25a* contribute to the neuronal heat response. Inactive (Iav, TRPV), TRPL, and *Ir25a/Ir93a/Ir21a* are required for cool avoidance. Painless is identified for sensing noxious heat temperatures, whereas Polycystic kidney disease 2 (Pkd2, TRPP), no mechanoreceptor potential C (NompC, TRPN) and TRPM are suggested as noxious cold-associated receptors.

In adults (lower), TRPA1 is reported as a heat sensor. Gr28b(D) is involved in warn avoidance, while Brivido 1-3 (Brv1-3, TRPPs) and *Ir25a/Ir93a/Ir21a* are required for cool avoidance. Painless and Pyrexia are reported for noxious heat sensation.

Figure 2. Dissection of *Drosophila* larval anterior region for RNA extraction.

The anterior region of a larva (indicated by a red rectangle) was dissected to collect thermal sensory neurons, including DOCCs/DOWCs. Microdissection scissors were used to incise along a red dash line shown in the middle panel and processed ~70 anterior regions for each genotype were collected for RNA extraction. The right panel represents a piece of dissected anterior region of the larva.

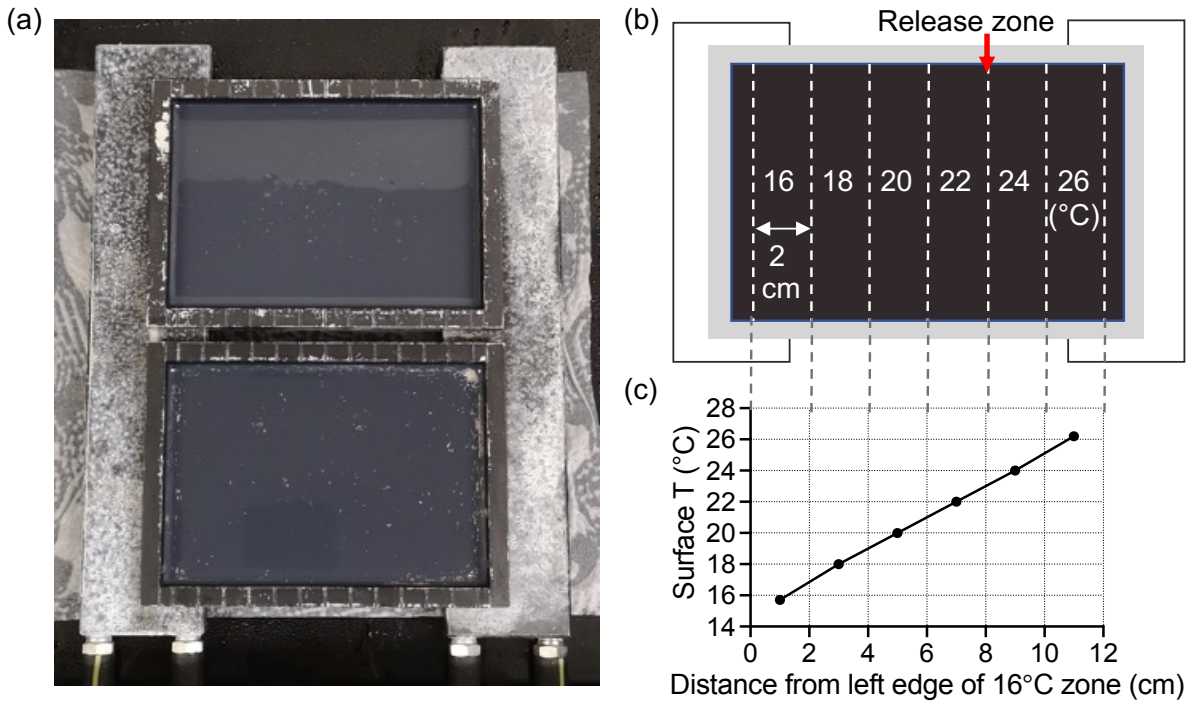
(a)
(b)
Release zone
16
18
20
22
24
26
(°C)
2
cm
(c)
Surface T (°C)
28
26
24
22
20
18
16
14
0
2
4
6
8
10
12
Distance from left edge of 16°C zone (cm)

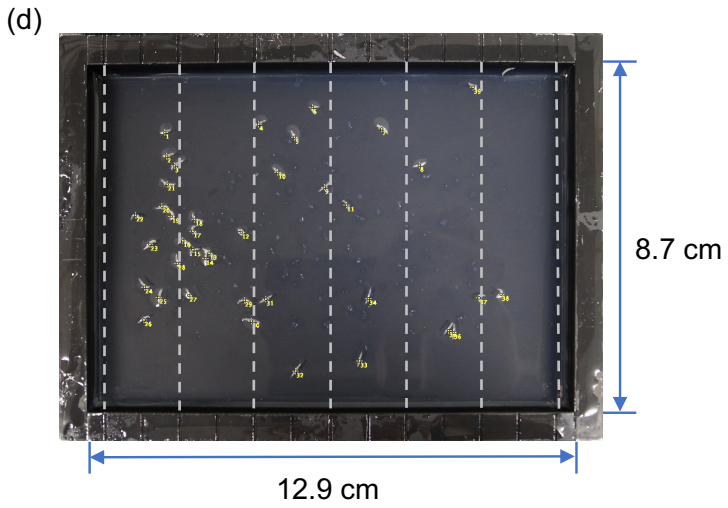
(d)
8.7 cm
12.9 cm

Figure 3. The experimental setup for 16ºC -26°C temperature gradient assay.

(a) The top view of the apparatus for the temperature gradient assay. Two aluminum plates were coated with agarose and placed on top of two aluminum blocks, each of which was set at a distinct temperature using circulating water from a water bath.

(b) Schematic diagram of a test plate divided into 2-cm wide zones. Larvae were released between 22°C and 24°C zones and the number of larvae in each of the six zones was tabulated.

(c) Actual temperatures measured in the center of the zones. Data represent mean ± SD, n = 3. Surface T: surface temperature.

(d) Representative image of control (w^{1118}) late 3rd instar larvae on the plate at 11 min on a 16 ºC -26°C gradient. Dashed lines divided the test plate into six temperature zones and inner sizes of the plate were indicated. Yellow spots mark the positions of larvae.

(a)

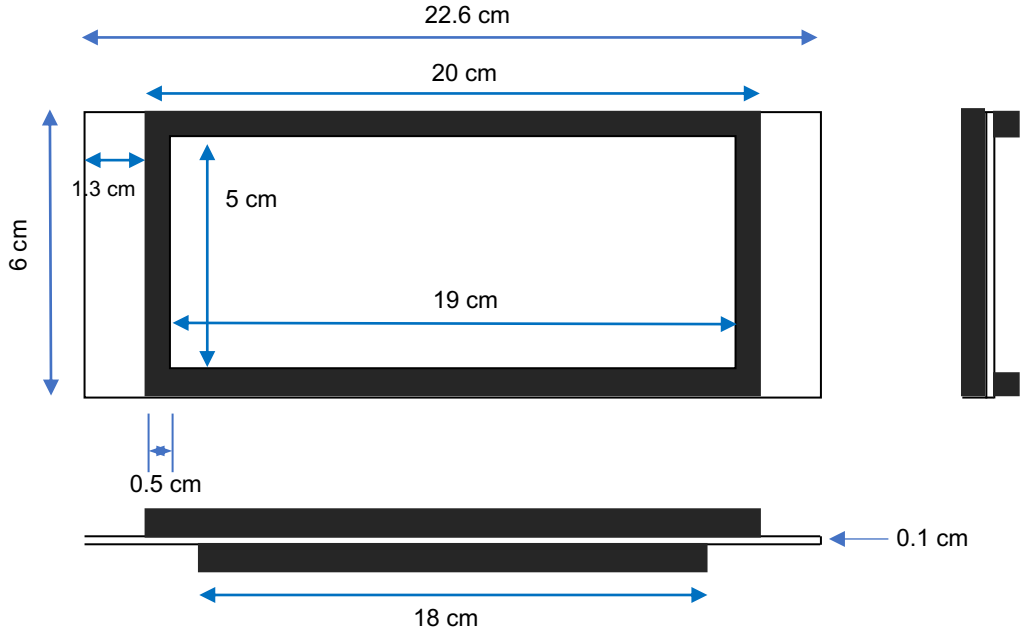

(b)

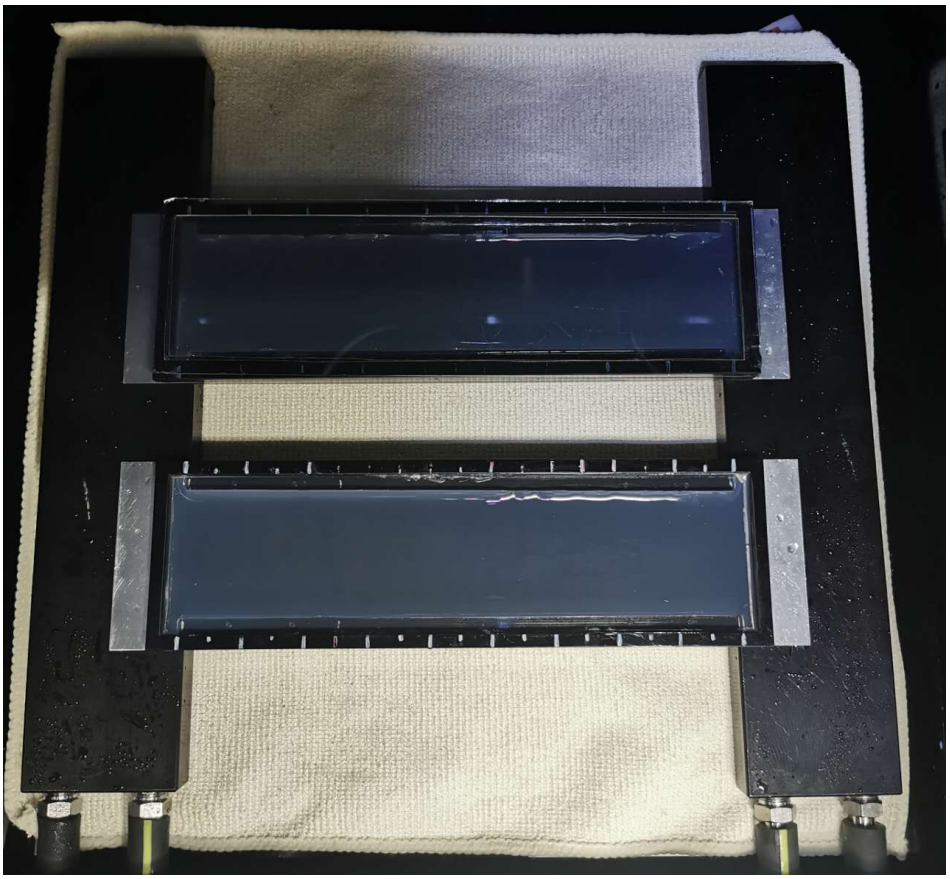

Figure is continued to the next page.

(c)

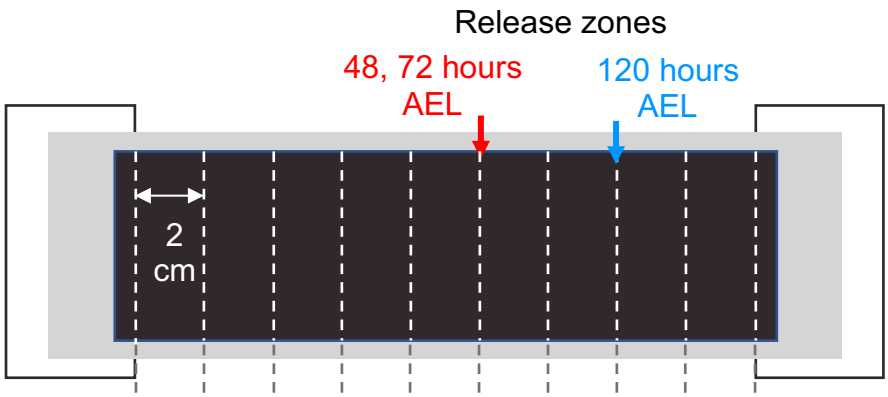
Release zones
48, 72 hours AEL
120 hours AEL
2 cm

(d)

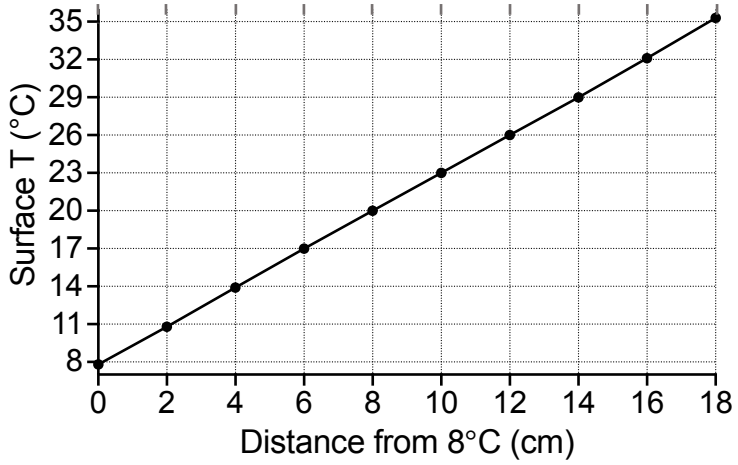
Surface T (°C)
35
32
29
26
23
20
17
14
11
8
0
2
4
6
8
10
12
14
16
18
Distance from 8°C (cm)

(e)

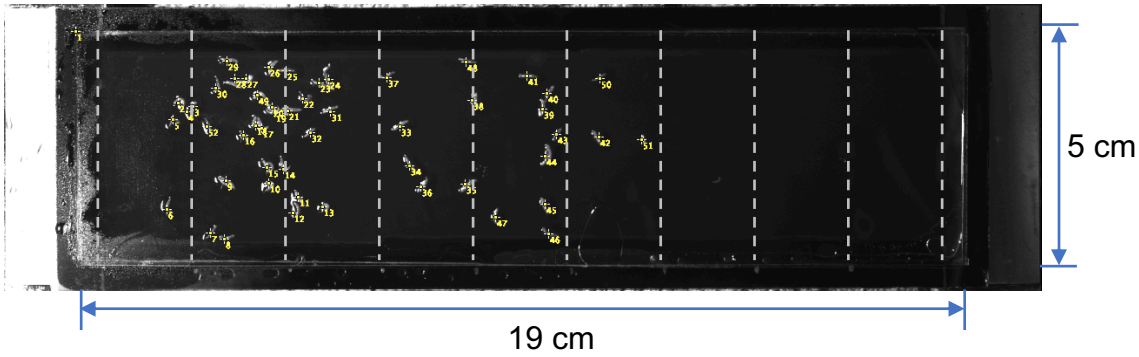
5 cm
19 cm

Figure 4. The experimental setup for 8ºC -35°C temperature gradient assay.

(a) Schematic three-view drawing of the testing plate. It was assembled with an aluminum sheet (white) and a rectangular acrylic ring (black) on top. Two acrylic rods were attached to the longer edges.

(b) The top view of the apparatus for the temperature gradient assay. Two testing plates were coated with agarose and were placed on top of two aluminum blocks, each of which was set at a distinct temperature using circulating water from a water bath. Two gaps between the gel and the longer edge were generated. A rectangular acrylic ring structure and a square cover glass were placed at the top of the plate during testing time, they were shown on the top plate.

(c) Schematic diagram of a test plate divided into 3-cm wide zones. 2nd and early 3rd instar larvae (48, 72 hours AEL) were released at 23°C (red arrow), while late 3rd instar (120 hours AEL) was released at 29°C (blue arrow). The number of larvae in each of the nine zones was tabulated.

(d) Actual temperatures measured on temperature zones. Data represent mean ± SD, n = 3. Surface T: surface temperature

(d) Representative image of control (w^{1118}) late 3rd instar larvae on the plate at 10 min on an 8 ºC -35°C gradient. Dashed lines divided the test plate into nine temperature zones and inner sizes of the plate were indicated. Yellow spots mark the positions of larvae.

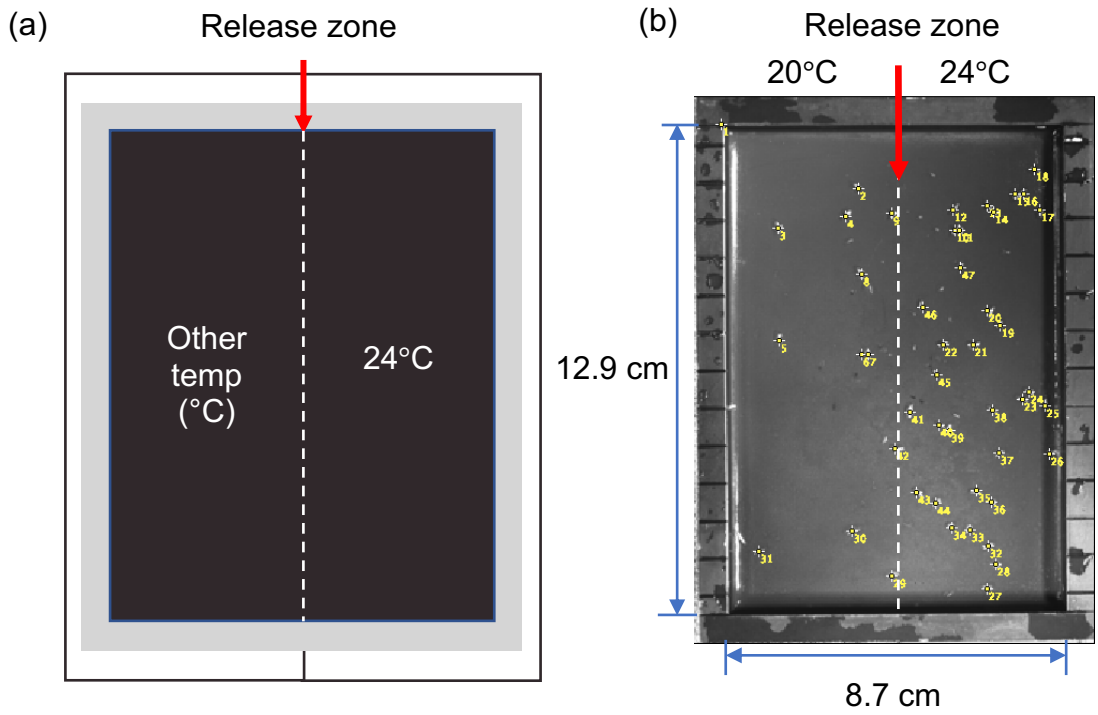

Figure 5. The experimental set-up for temperature two-way choice assay.

(a) Schematic diagram of a test plate divided into 2 sides. The aluminum plate was coated with agarose and was placed on top of two adjacent aluminum blocks, each of which was set at a distinct temperature using circulating water from a water bath. Larvae were released at the center zone of the plate (red arrow), the number of larvae one each side was recorded to calculate the PI.

(b) Representative image of control (w^{1118}) early 3rd instar larvae (72 hours AEL) on the plate at 15 minutes of temperature two-way choice assay. Yellow spots marked the positions of larvae. Inner sizes of the plate were indicated.

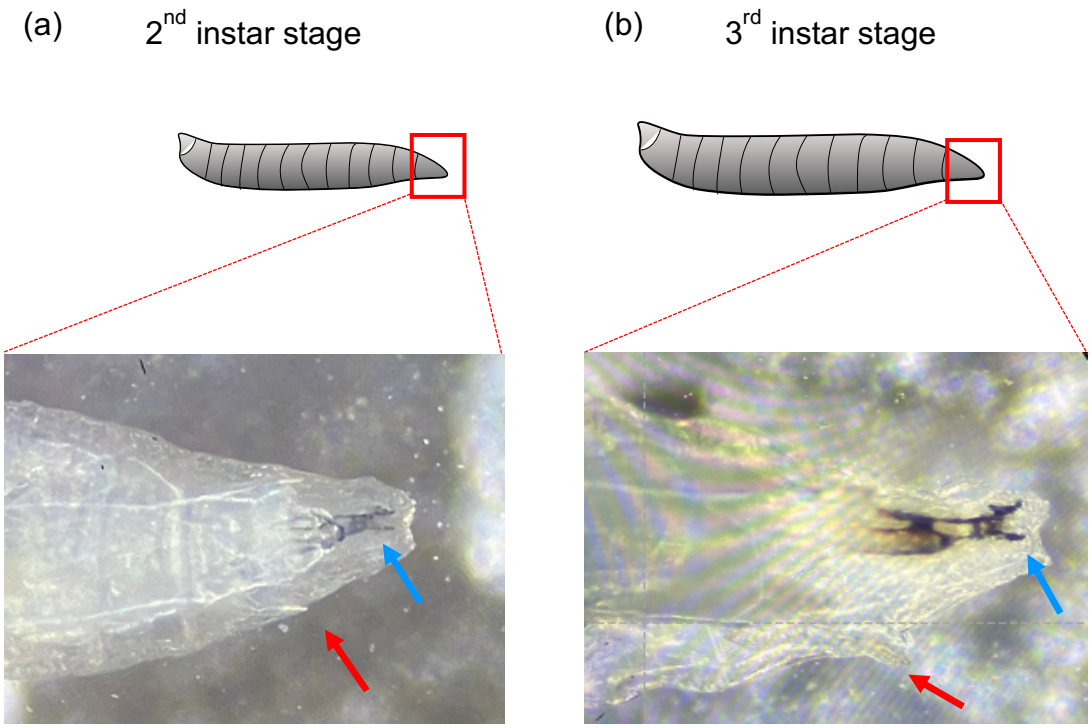

Figure 6. Morphology of anterior spiacles and mouth hooks in 2nd and 3rd instar *Drosophila* larvae.

(a, b) 2nd and 3rd instar displayed different body size (grey larvae cartoon) and distinctive morphology of anterior spiracles. The club-like (a, red arrow) and branched-like (b, red arrow) structures of anterior spiracles were observed in 2nd and 3rd instar larvae, respectively. Both stages exhibit one pair of mouth hooks (blue), a relatively larger size of the month hooks were observed in 3rd (a, blue arrow) instar larvae than 2nd instar larvae (b, blue arrow).

(a)

(b)

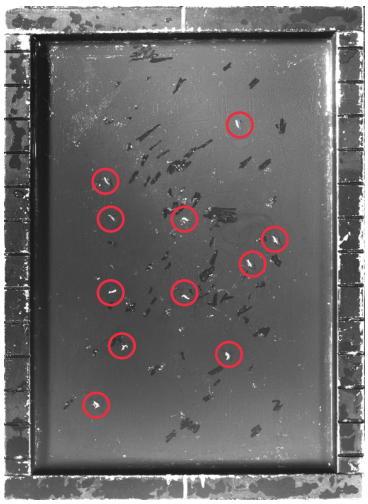

(c)

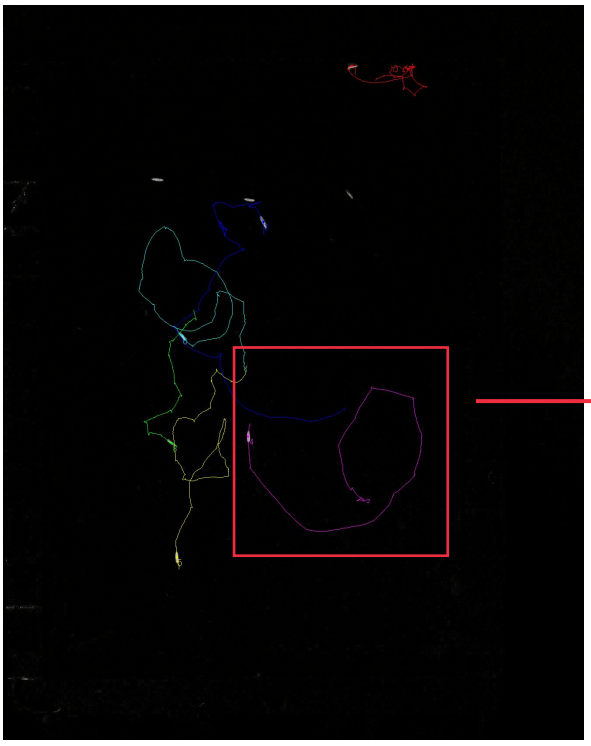

(d)

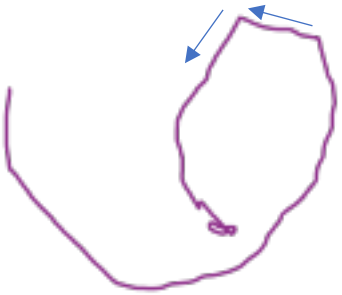

Figure 7. The experimental set-up for locomotion assay.

(a) Schematic diagram of the test plate put on two aluminum blocks. The aluminum plate was coated with agarose and placed on top of two adjacent aluminum blocks, both were set at 18°C or 24°C using circulating water from water bathes.

(b) 10-12 early 3rd instar larvae were separately released on the test plate; red cycles indicate the position of larval individuals at 0 minute.

(c) A representative image showing the movement trajectory of control (w^{1118}) at the early 3rd instar stage, colored traces indicate the movement trajectory of individuals in 2 minutes. The Purple trace cycled by a red rectangle was showed in (d).

(d) Quantification of “number of turning (# of turning)” based on the number of angels less than 150° displayed manually counted in the movement trajectory. Purple trace indicated a representative movement trajectory and blue arrows depict a 'turning' event.

(a)

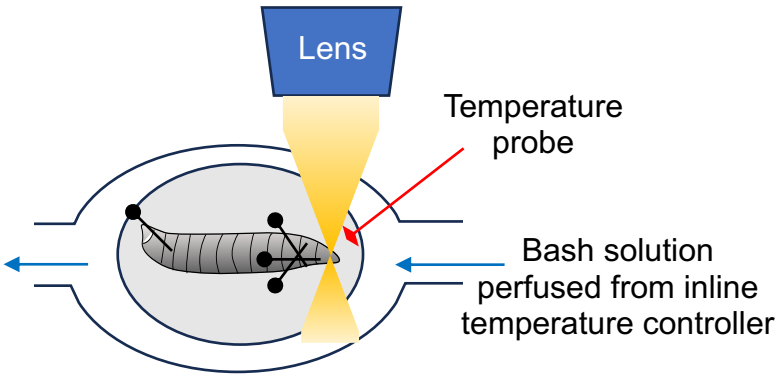
Lens
Temperature probe
Bash solution perfused from inline temperature controller

(b)

(c)

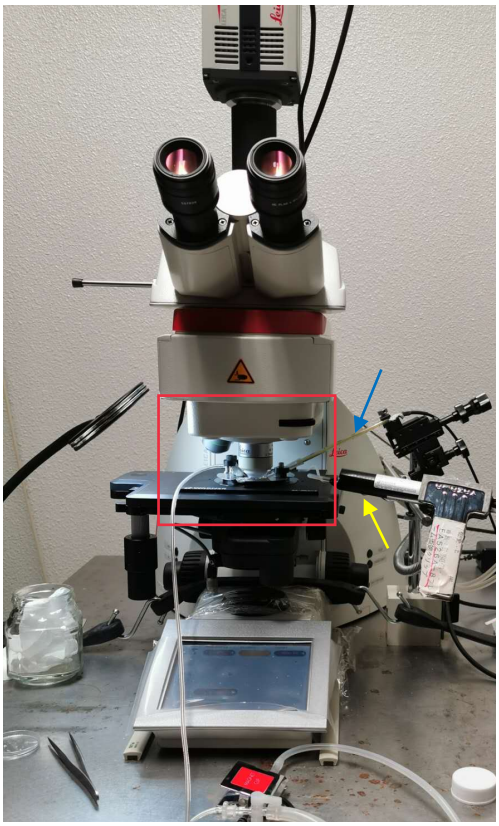

(d)

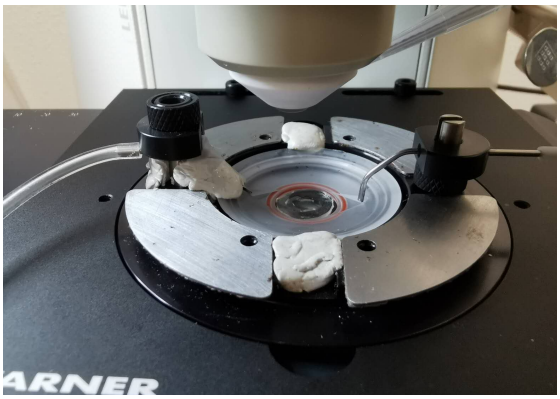

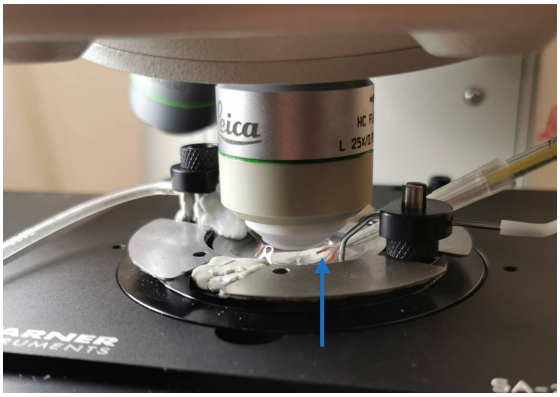

Figure 8. The experimental setup of *in vivo* GCaMP-imaging.

(a) Schematic diagram of larval DOCCs or DOWCs recording under the microscope. An early 3rd instar larva was fixed on a silicone gel (grey) by dissection pins (black sticks with round ends) and put in the test chamber perfusing bath solution from a temperature controller. DOCCs or DOWCs located in the anterior region were tracked by microscope from the lens (blue trapezoid). The temperature during recording was measured and recorded from a temperature probe (red stick with a bland end) close to the larval anterior region.

(b) Image of the fixed larva by dissection pins (upper). The amplified image of the anterior region (lower) was cycled by a red rectangle in the upper image.

(c) Image of Ca^{2+}-imaging setup under the microscopy. The yellow arrow indicates the inline temperature controller connected to the bath solution perfusion tube, and the blue arrow indicates the temperature probe. The red rectangular cycle indicates the position of the test chamber and lens and was amplified in (d).

(d) Upper image shows the silicone gel placed in the test chamber with a larval sample. The lower image shows the bath solution from the chamber with the sample attached to the lens. This is required during recording. A temperature probe (blue arrow) was sunk into the solution and located close to the larval anterior region during the recording.

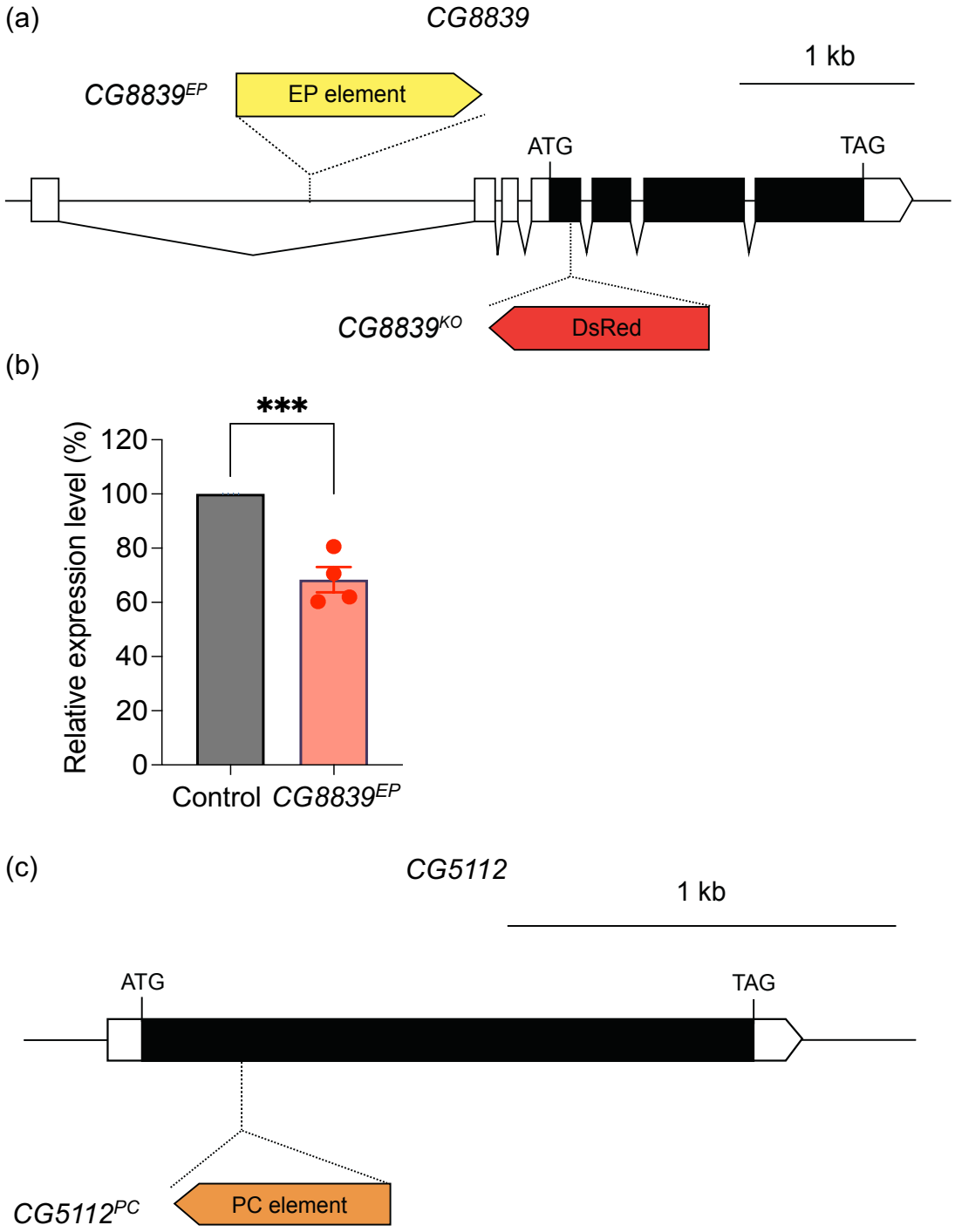
(a)
CG8839
1 kb
CG8839EP
EP element
ATG
TAG
CG8839KO
DsRed
(b)
***
Relative expression level (%)
120
100
80
60
40
20
0
Control
CG8839EP
(c)
CG5112
1 kb
ATG
TAG
CG5112PC
PC element

Figure 9. Mutation designs of *CG8839* and *CG5112.*

(a) Mutation design of $CG8839^{EP}$ and $CG8839^{KO}$. $CG8839^{EP}$ was generated by inserting an EP element (~7.8 kb, indicated in yellow) approximately 1.3 kb upstream of the start codon, while $CG8839^{KO}$ was generated by inserting a DsRed marker (~1.8 kb, indicated in red) 120 bp downstream from the start codon.

(b) Relative expression level of *CG8839* in $CG8839^{EP}$. (N=4). The expression level was normalized control (w^{1118}) into 100%. A statistical analysis was performed by Student's t test: ***P<0.001. The data are presented as mean ± SEM.

(c) Mutation design of $CG5112^{EP}$. $CG5112^{EP}$ was generated by inserting a PC element (~8.2 kb, showed in orange) 241 bp downstream from the start codon.

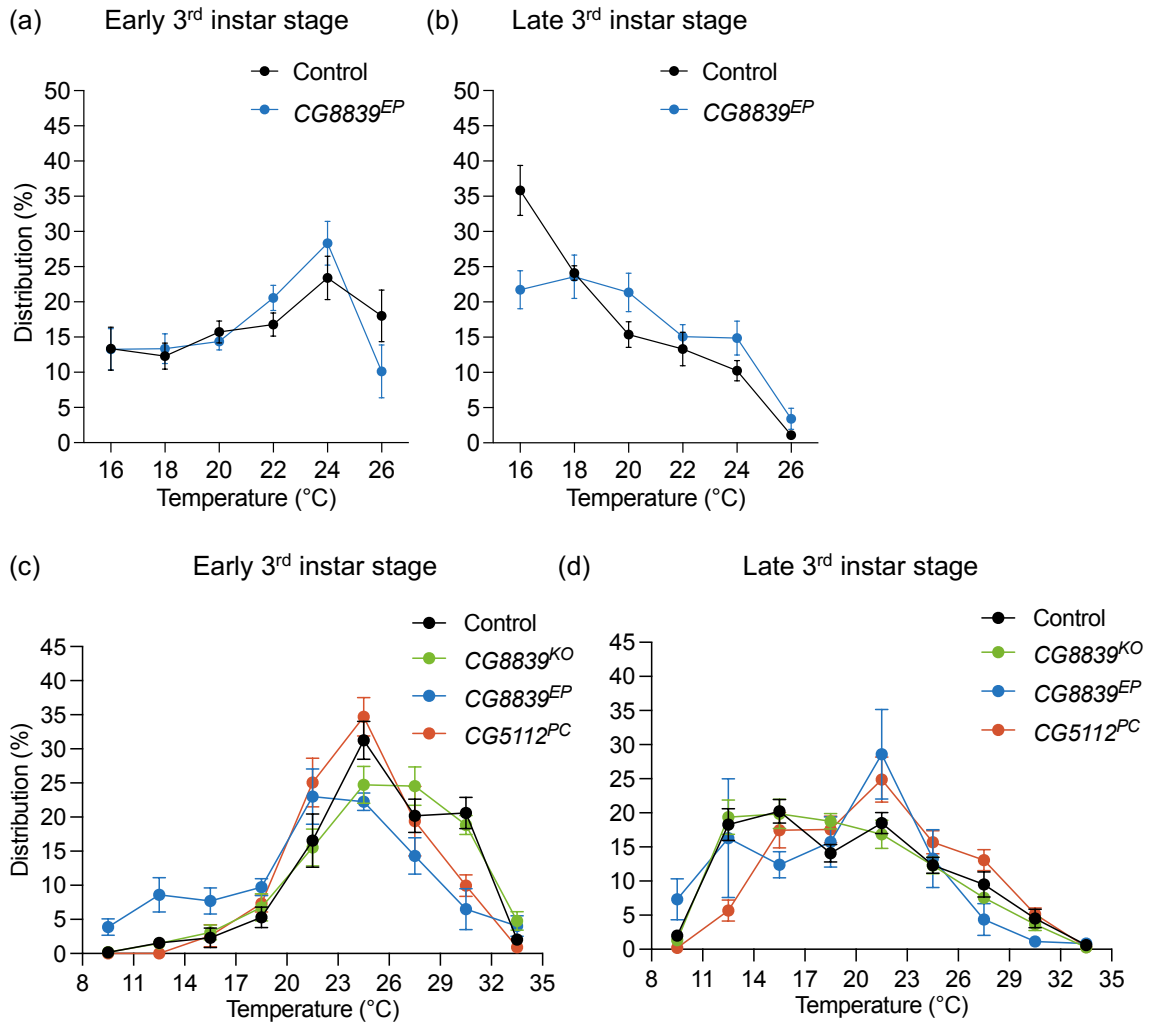

Figure 10. FAAHs (*CG8839* and *CG5112*) displayed potential involvements in warm avoidance in 3rd instar stage.

(a, b) Distribution of early (a) and late (b) 3rd instar larvae (72 and 120 hours AEL) on a 16ºC -26ºC thermal gradient. Control (w^{1118}, black) and $CG8839^{EP}$ (blue) were examined, N=6.

(c, d) Distribution of early (c) and late (d) 3rd instar larvae (72 and 120 hours AEL) on an 8ºC -35ºC thermal gradient. Control (w^{1118}, black) and $CG8839^{KO}$ (green), $CG8839^{EP}$ (blue) and $CG5112^{PC}$ (red) were examined, N=3-9.

The data are presented as mean ± SEM.

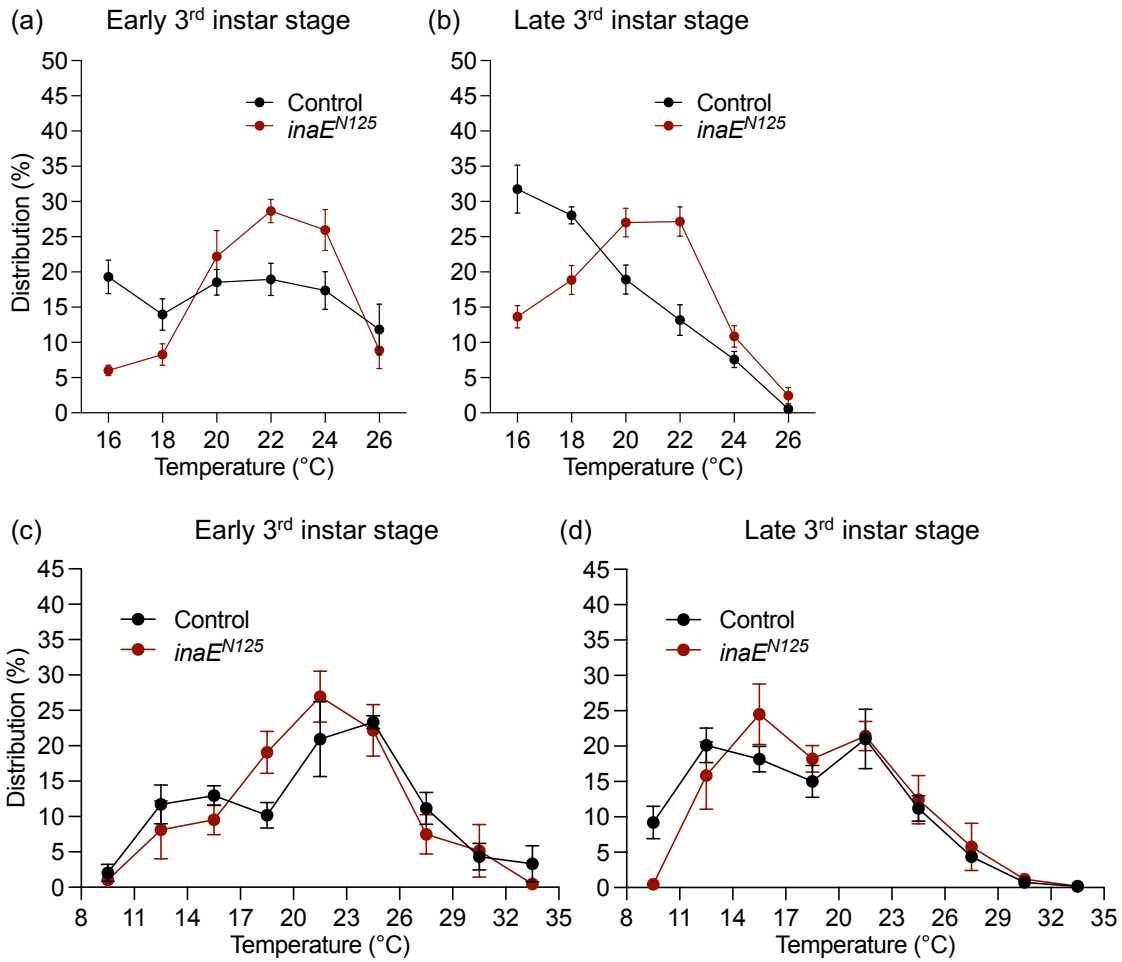

Figure 11. DAGL (*inaE*) played a potential role in temperature gradient discrimination.
(a, b) Distribution of early (a) and late (b) 3rd instar larvae (72 and 120 hours AEL) on a 16ºC -26ºC thermal gradient. Control (w^{1118}, black) and $inaE^{N125}$ (red) were examined, N=6-7.
(c, d) Distribution of early (c) and late (d) 3rd instar larvae (72 and 120 hours AEL) on an 8ºC -35ºC thermal gradient. Control (w^{1118}, black) and $inaE^{N125}$ (red) were examined, N=4-7.
The data are presented as mean ± SEM.

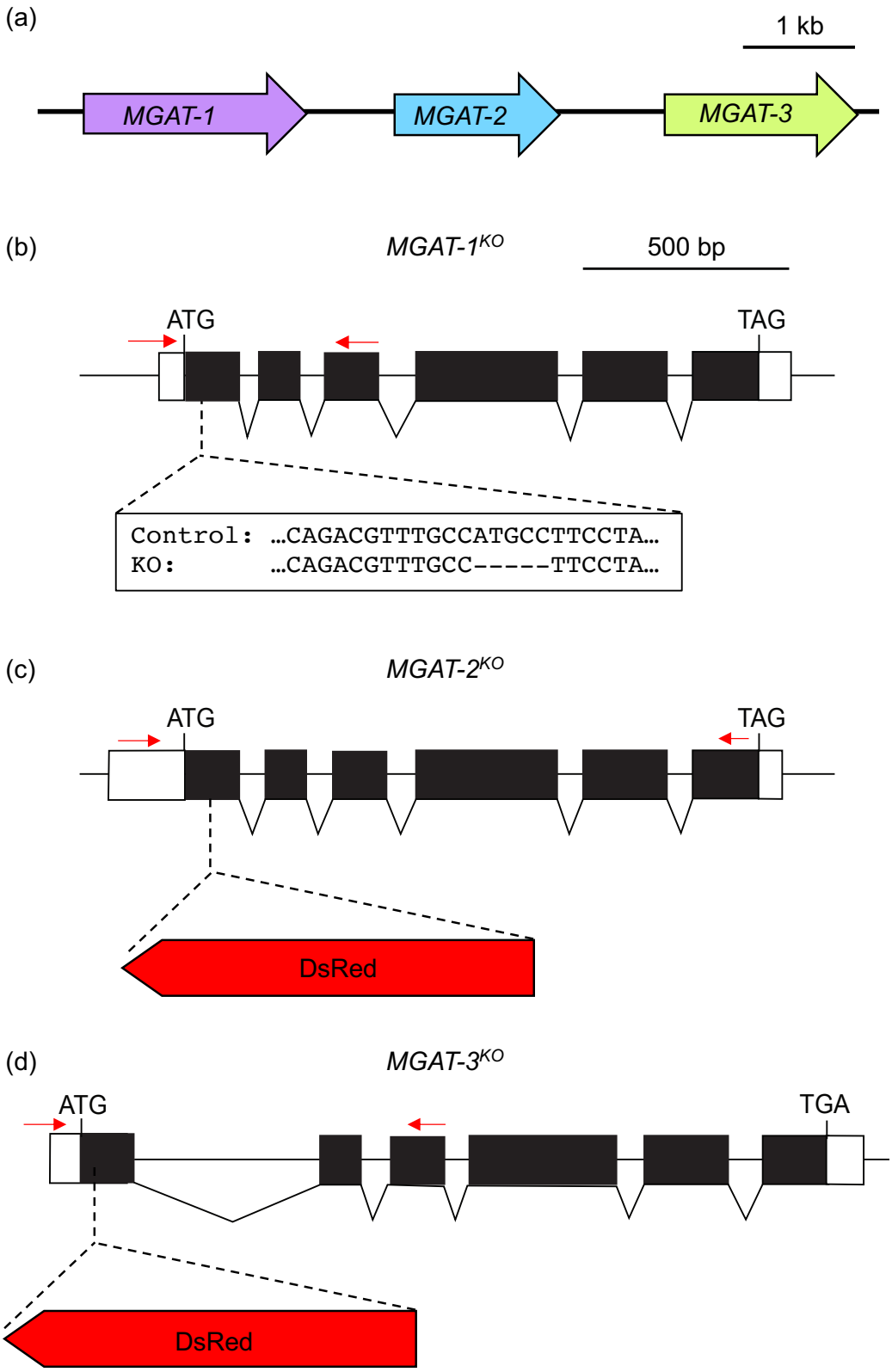
(a)
1 kb
MGAT-1
MGAT-2
MGAT-3
(b)
MGAT-1KO
500 bp
ATG
TAG
Control: …CAGACGTTTGCCATGCCTTCCTA…
KO: …CAGACGTTTGCC-----TTCCTA…
(c)
MGAT-2KO
ATG
TAG
DsRed
(d)
MGAT-3KO
ATG
TGA
DsRed

Figure 12. Genes structures and knockout designs of *MGATs*.

(a) Relative gene position of *MGAT-1* (purple), *MGAT-2* (blue) and *MGAT-3* (green) on the genome. Arrows indicate transcriptional direction.

(b-d) Gene structures and mutation designs of *MGAT-1*^{KO} (b), *MGAT-2*^{KO} (c) and *MGAT-3*^{KO} (d). Broken lines indicate introns, black boxes indicate CDS and white boxes indicate UTRs. "ATG" indicates the start codon and "TAG" and "TGA" indicate stop codons. Red arrow boxes indicate DsRed elements (~1.8 kb) and arrow directions are transcriptional directions. *MGAT-1*^{KO} (b) contains 5 bp deletion 55 bp downstream from the start codon, *MGAT-2*^{KO}(c) and *MGAT-3*^{KO} (d) were designed with the insertion of ~1.8 kb DsRed marker into 33 bp and 28 bp downstream of the start codon, respectively. Red arrows in (b-d) indicated the position of genotyping primers.

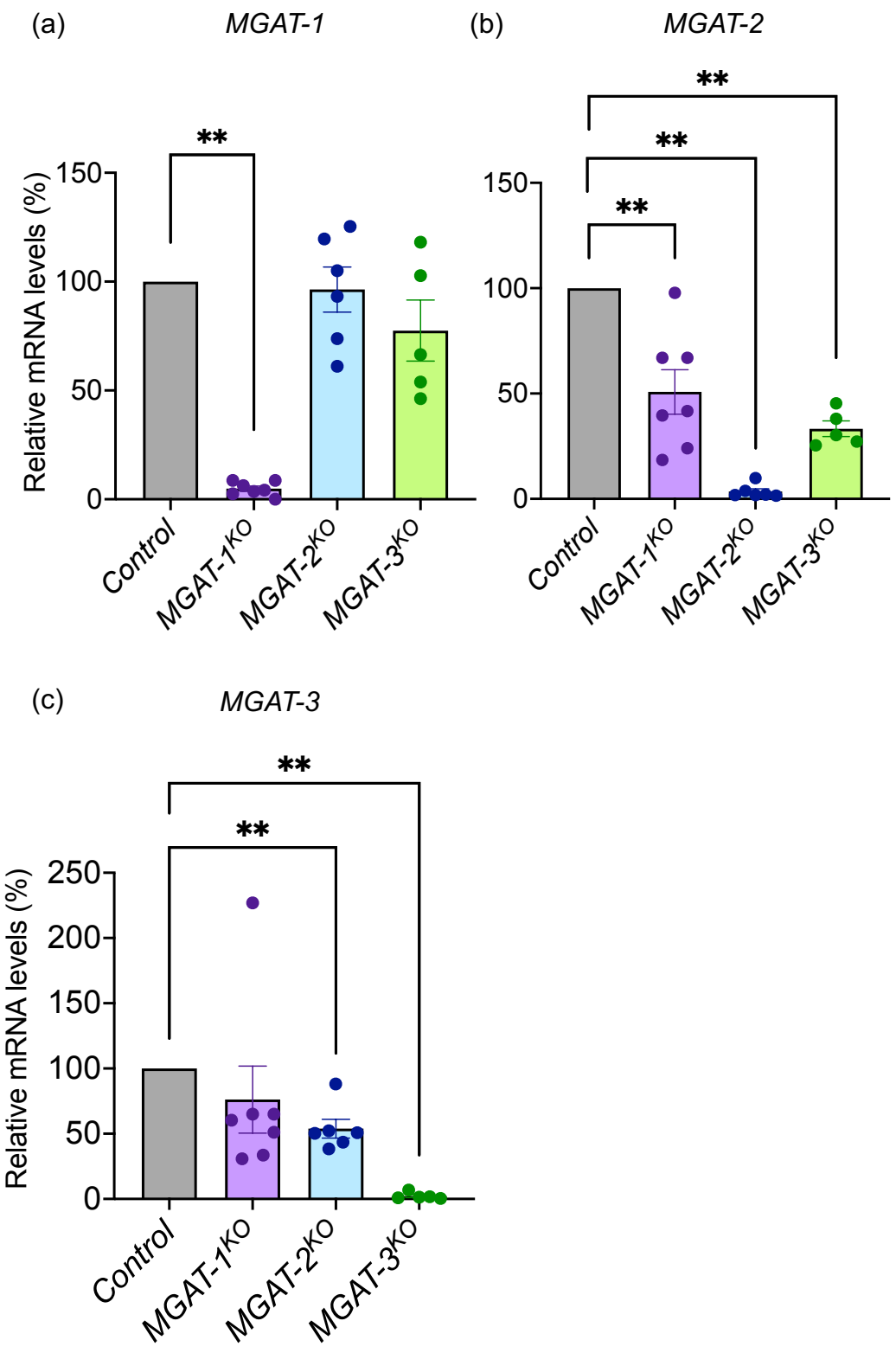
(a)
MGAT-1
(b)
MGAT-2
(c)
MGAT-3
Relative mRNA levels (%)
**
Control
MGAT-1KO
MGAT-2KO
MGAT-3KO

Figure 13. *MGAT* knockouts affected the mRNA levels of both target and neighboring *MGAT* genes.

(a-c) Relative mRNA levels in the whole body of early 3rd instar larvae (72 hours AEL) were examined in control (w^{1118}, black), $MGAT\text{-}1^{KO}$ (purple), $MGAT\text{-}2^{KO}$ (blue) and $MGAT\text{-}3^{KO}$ (purple). mRNA levels in mutants were normalized to control into 100%. Relative mRNA levels of *MGAT-1* (a), *MGAT-2* (a) and *MGAT-3* (a) were examined, N=5-7. Statistical analyzes were performed by Kruskal-Wallis test with Steel multiple comparison: *P<0.05, **P<0.01, no asterisk indicates no significant difference.

(a) Control

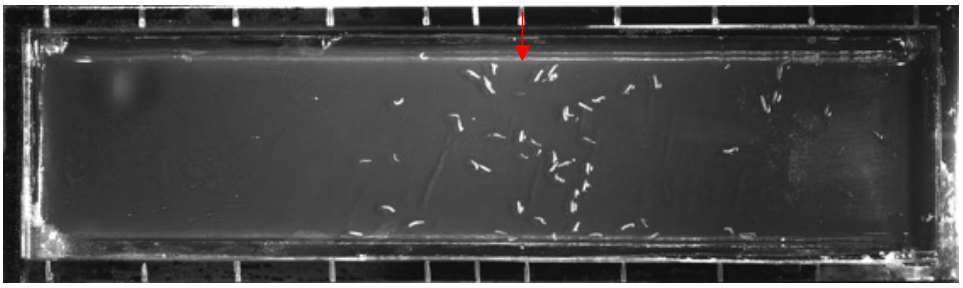

(b) *MGAT-1*^{KO}

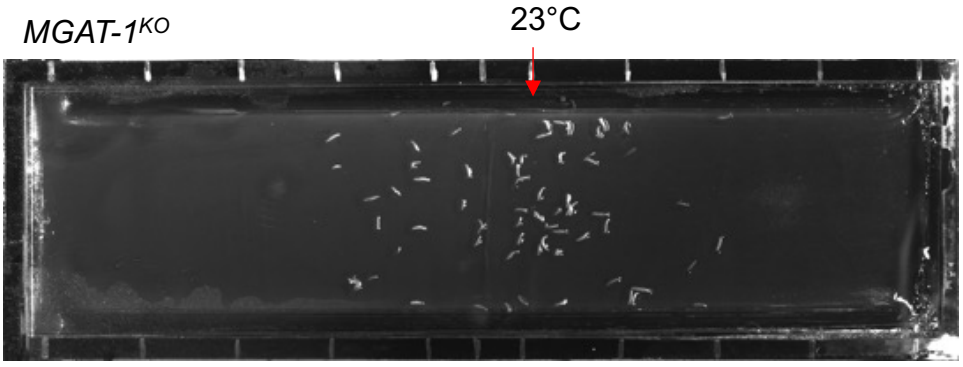

(c) *MGAT-2*^{KO}

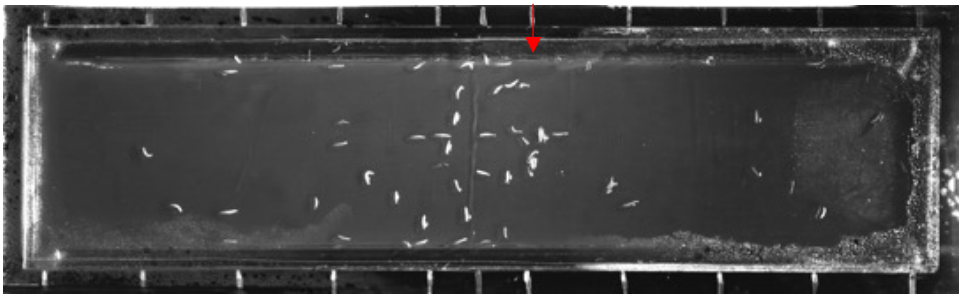

(d) *MGAT-3*^{KO}

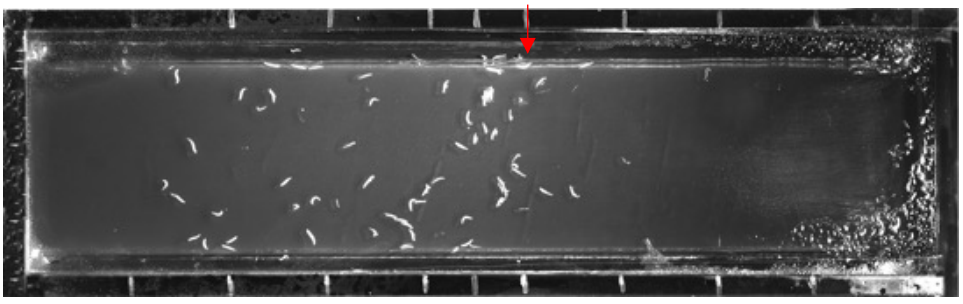

Figure 14. Representative images of control (w^{1118}, a), *MGAT-1*^{KO} (b), *MGAT-2*^{KO} (c) and *MGAT-3*^{KO} (d) early 3rd instar larvae (72 hours AEL) on an 8ºC -35ºC thermal gradient. White spots represent individual larvae. Red arrows in each image indicated the 23ºC releasing zone. Images were captured 15 minutes after larvae from each genotype moved under dark lights.

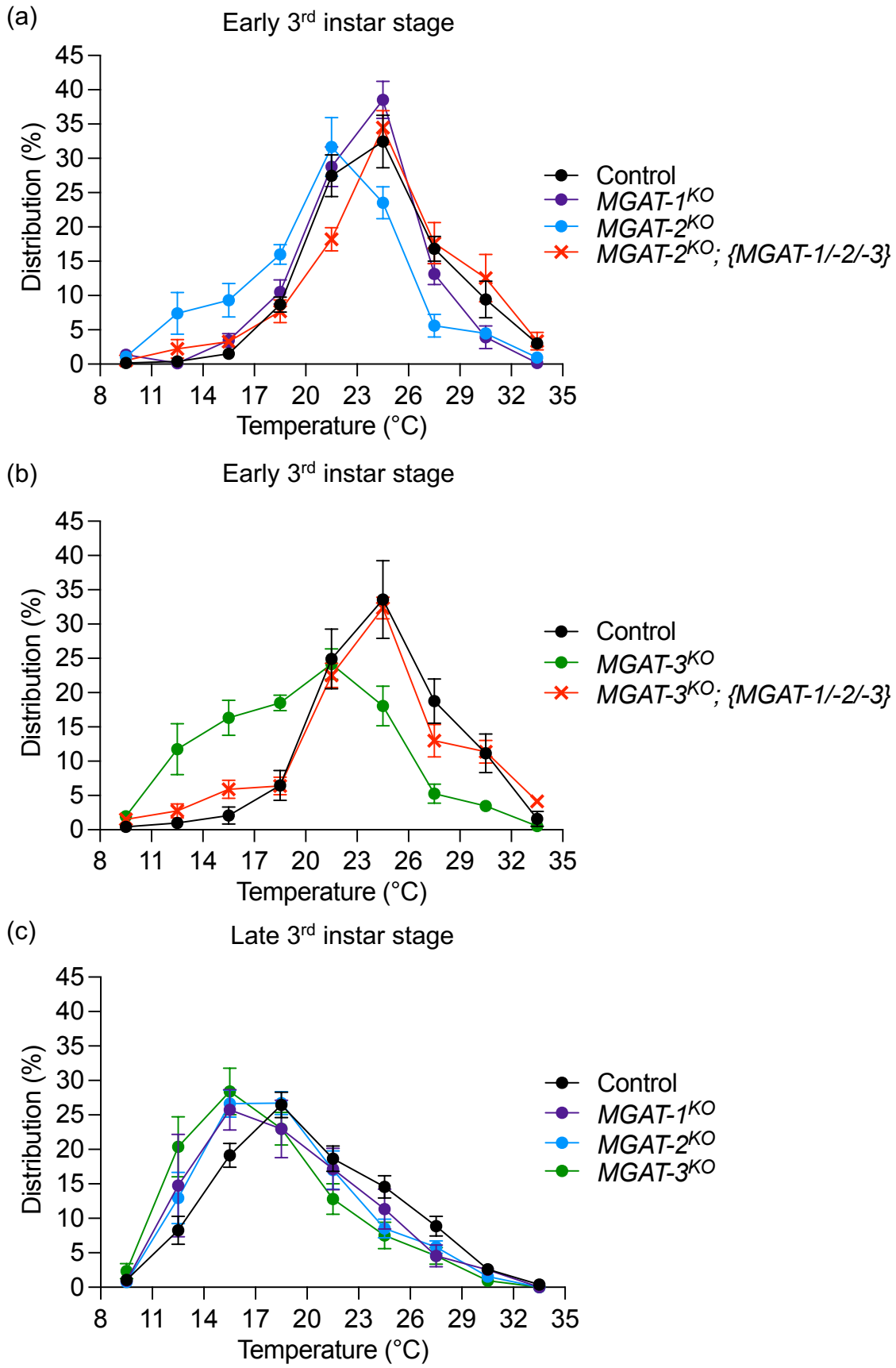
(a)
Early 3rd instar stage
Distribution (%)
Temperature (°C)
Control
MGAT-1KO
MGAT-2KO
MGAT-2KO; {MGAT-1/-2/-3}
(b)
Early 3rd instar stage
Distribution (%)
Temperature (°C)
Control
MGAT-3KO
MGAT-3KO; {MGAT-1/-2/-3}
(c)
Late 3rd instar stage
Distribution (%)
Temperature (°C)
Control
MGAT-1KO
MGAT-2KO
MGAT-3KO

Figure 15. *MGAT-2/MGAT-3* contributed to innocuous cold avoidance at early and late 3rd instar stages.

(a, b) Distribution of early 3rd instar larvae (72 hours AEL) on an 8ºC -35ºC thermal gradient. {*MGAT-1/-2/-3*} denoted wild type genomic transgenes including *MGAT-1*, *MGAT-2* and *MGAT-3*. The data are presented as mean ± SEM.

(a) Distribution of control (w^{1118}, black, round marker), $MGAT\text{-}1^{KO}$ (purple, round marker), $MGAT\text{-}2^{KO}$ (blue, round marker) and $MGAT\text{-}2^{KO}$; {*MGAT-1/-2/-3*} (red, "X" marker).

(b) Distribution of control (w^{1118}, black, round marker), $MGAT\text{-}3^{KO}$ (green, round marker) and $MGAT\text{-}3^{KO}$; {*MGAT-1/-2/-3*} (red, "X" marker).

(d) Distribution of late 3rd instar larvae (120 hours AEL) on an 8ºC -35ºC thermal gradient. Control (w^{1118}, black), $MGAT\text{-}1^{KO}$ (purple), $MGAT\text{-}2^{KO}$ (blue) and $MGAT\text{-}3^{KO}$ (green) were examined. The data are presented as mean ± SEM.

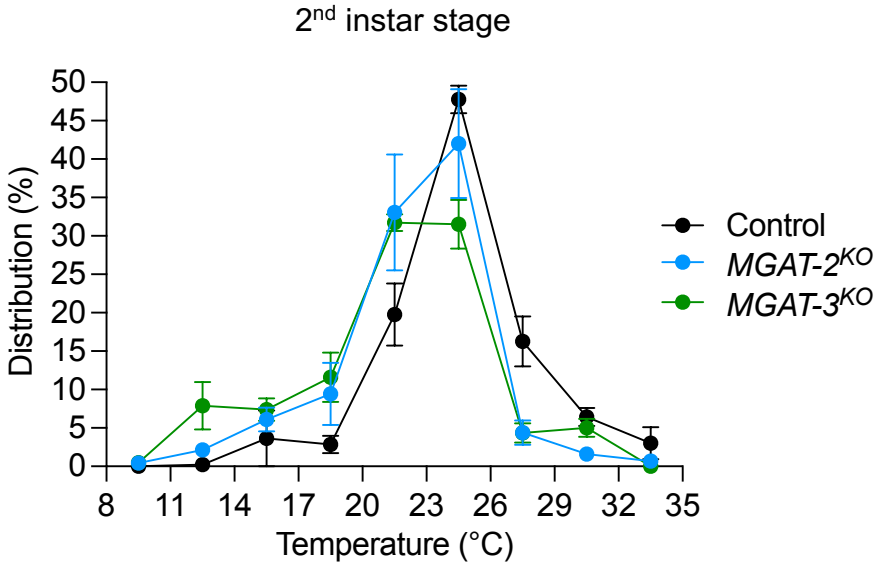

Figure 16. *MGAT-2/MGAT-3* contributed to cool avoidance at 2nd instar stage.

Distribution of 2nd instar larvae (48 hours AEL) on an 8ºC -35ºC thermal gradient. Control (w^{1118}, grey), *MGAT-2*^{KO} (blue) and *MGAT-3*^{KO} (green) were examined, N=3-5. The data are presented as mean ± SEM.

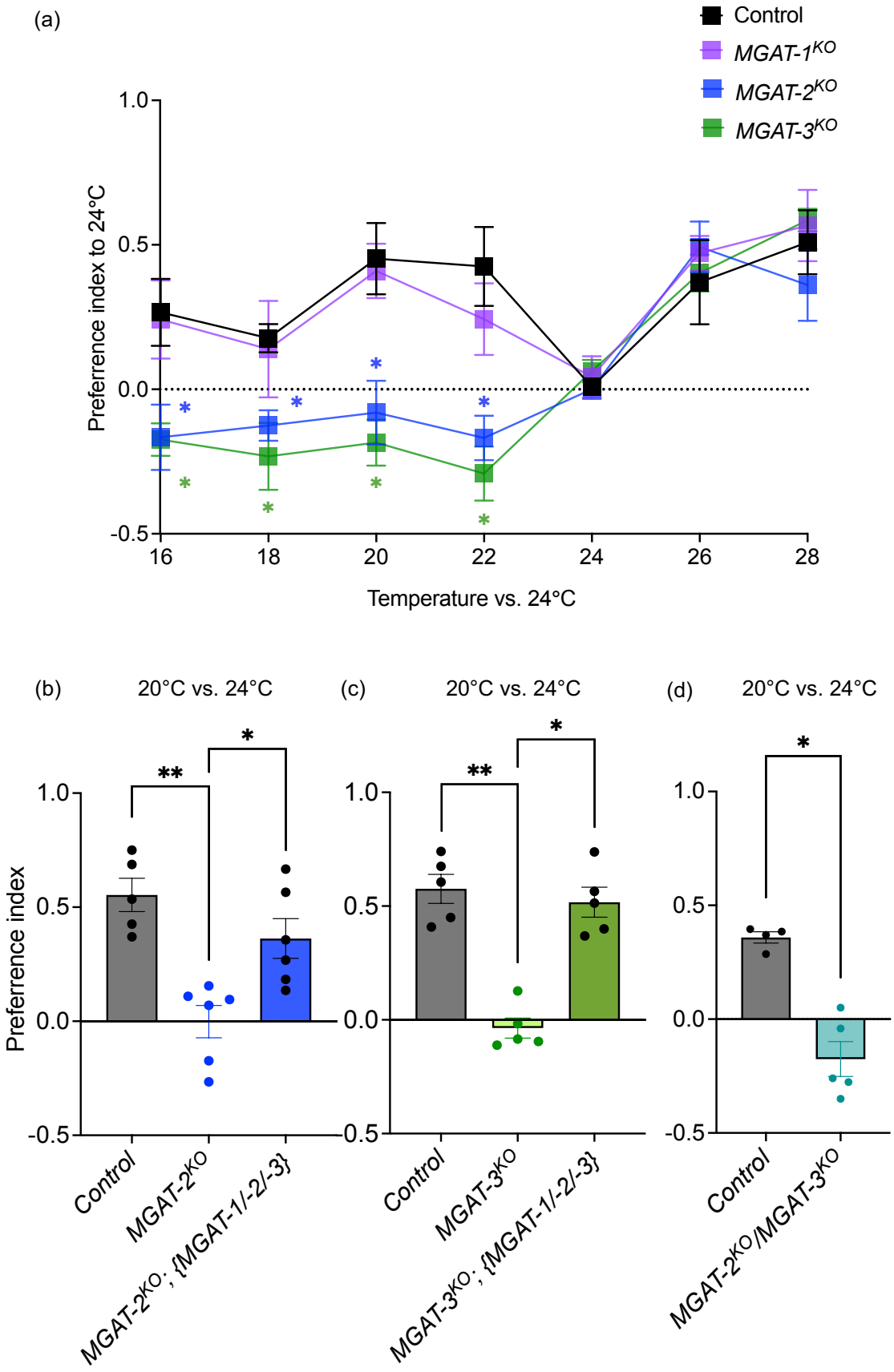
(a)
Control
MGAT-1KO
MGAT-2KO
MGAT-3KO
Preferrence index to 24°C
1.0
0.5
0.0
-0.5
16
18
20
22
24
26
28
Temperature vs. 24°C
(b)
20°C vs. 24°C
(c)
20°C vs. 24°C
(d)
20°C vs. 24°C
Preferrence index
Control
MGAT-2KO
MGAT-2KO; {MGAT-1/-2/-3}
MGAT-3KO
MGAT-3KO; {MGAT-1/-2/-3}
MGAT-2KO/MGAT-3KO

Figure 17. *MGAT-2*/*MGAT-3* supported discriminations between optimal temperature and lower temperatures.

(a) PIs of two-way choice assays with control (w^{1118}, grey), $MGAT\text{-}1^{KO}$ (purple), $MGAT\text{-}2^{KO}$ (blue) and $MGAT\text{-}3^{KO}$ (green) at the early 3rd instar larvae (72 hours AEL). Larvae of each genotype was given a choice between 24°C and other temperatures (16°C, 18°C, 20°C, 22°C, 24°C, 26°C, 28°C) and the PI under each temperature condition was calculated and plotted. Statistical tests were performed by Kruskal-Wallis test with Steel multiple comparison: *P<0.05. The data are presented as mean ± SEM.

(b-d) PIs of 20°C versus 24°C condition two-way choice assay with indicated genotypes using early 3rd instar larvae (72 hours AEL). The data are presented as mean ± SEM.

(b) PIs were calculated using control (w^{1118}, black dots, grey bars), $MGAT\text{-}2^{KO}$ (blue dots, blue bars) and $MGAT\text{-}2^{KO}$; {*MGAT-1/-2/-3*} (blue dots, grey bars) lines, N=5-6. A statistical analysis was performed by Kruskal-Wallis test with Steel-Dwass multiple comparison: *P<0.05, **P<0.01.

(c) PIs were calculated using control (w^{1118}, black dots, grey bars), $MGAT\text{-}3^{KO}$ (green dots, green bars) and $MGAT\text{-}3^{KO}$; {*MGAT-1/-2/-3*} (green dots, grey bars) lines, N=5. A statistical analysis was performed by Kruskal-Wallis test with Steel-Dwass multiple comparison: *P<0.05, **P<0.01.

(d) PIs were calculated using control (w^{1118}, black) and $MGAT\text{-}2^{KO}$/$MGAT\text{-}3^{KO}$ (aquamarine). A statistical analysis was performed by Mann-Whitney U test, *P<0.05.

(a) Control

20°C 24°C

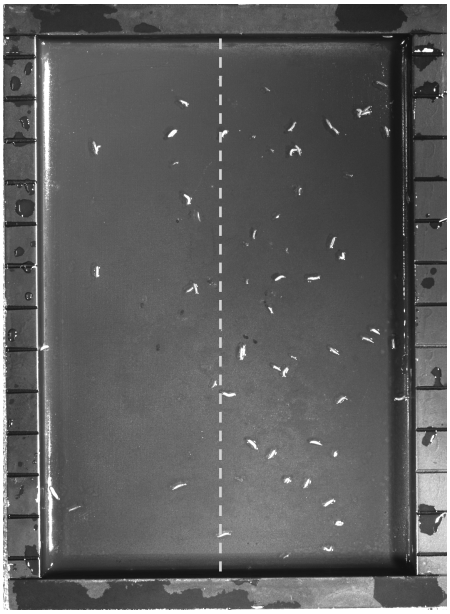

(b) *MGAT-1*^{KO}

20°C 24°C

(c) *MGAT-2*^{KO}

20°C 24°C

(d) *MGAT-3*^{KO}

20°C 24°C

Figure 18. Representative images of control (w^{1118}, a), *MGAT-1*^{KO} (b), *MGAT-2*^{KO} (c) and *MGAT-3*^{KO} (d) early 3rd instar larvae (72 hours AEL) in 20°C versus 24°C two-way choice assays. White spots represent individual larvae. The white dashed line in each image indicated the release zone. Surface temperatures left side of the release zones were 20°C and the right sides were 24°C. larvae were released at the release zone and the images were captured after 15 minutes each genotype moved under dark red lights (<600 nm).

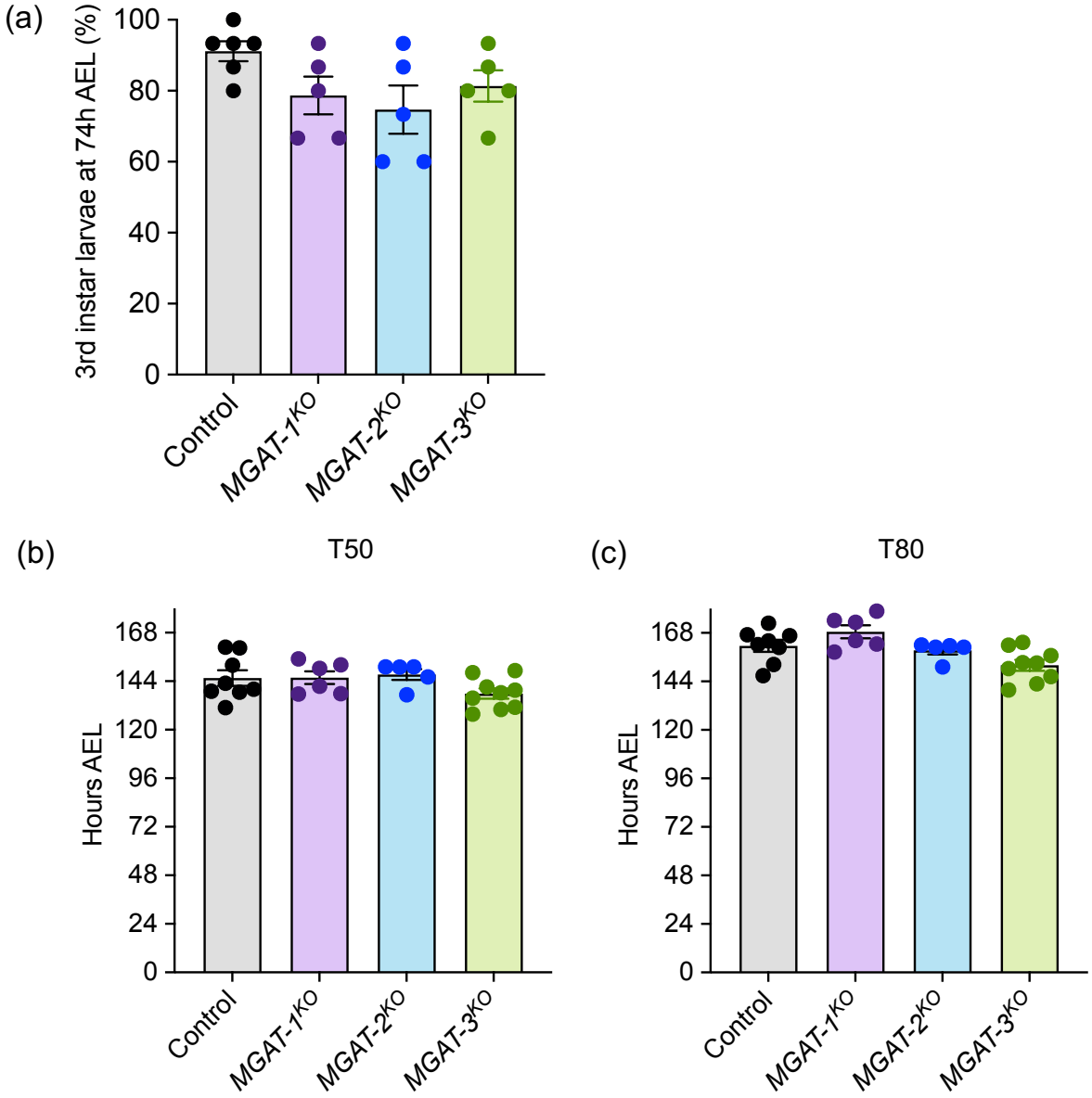

Figure 19. Developmental speed was not changed in *MGAT*-knockouts.

(a)The percentage of larvae entering the 3rd instar stage at 74 hours AEL based on the morphology of mouth hooks and spiracles in control (w^{1118}, black), *MGAT-1*^{KO} (purple), *MGAT-2*^{KO} (blue) and *MGAT-3*^{KO} (green), N=5-6.

(b, c) The time to pupation in control (w^{1118}, black), *MGAT-1*^{KO} (purple), *MGAT-2*^{KO} (blue) and *MGAT-3*^{KO} (green). T50 (b) and T80 (c) denote the times required for 50% (b) and 80% (c) of larvae to become pupae (N=5–8).

The data are presented as mean ± SEM. No significant difference based on one-way ANOVA with Dennett's multiple comparison.

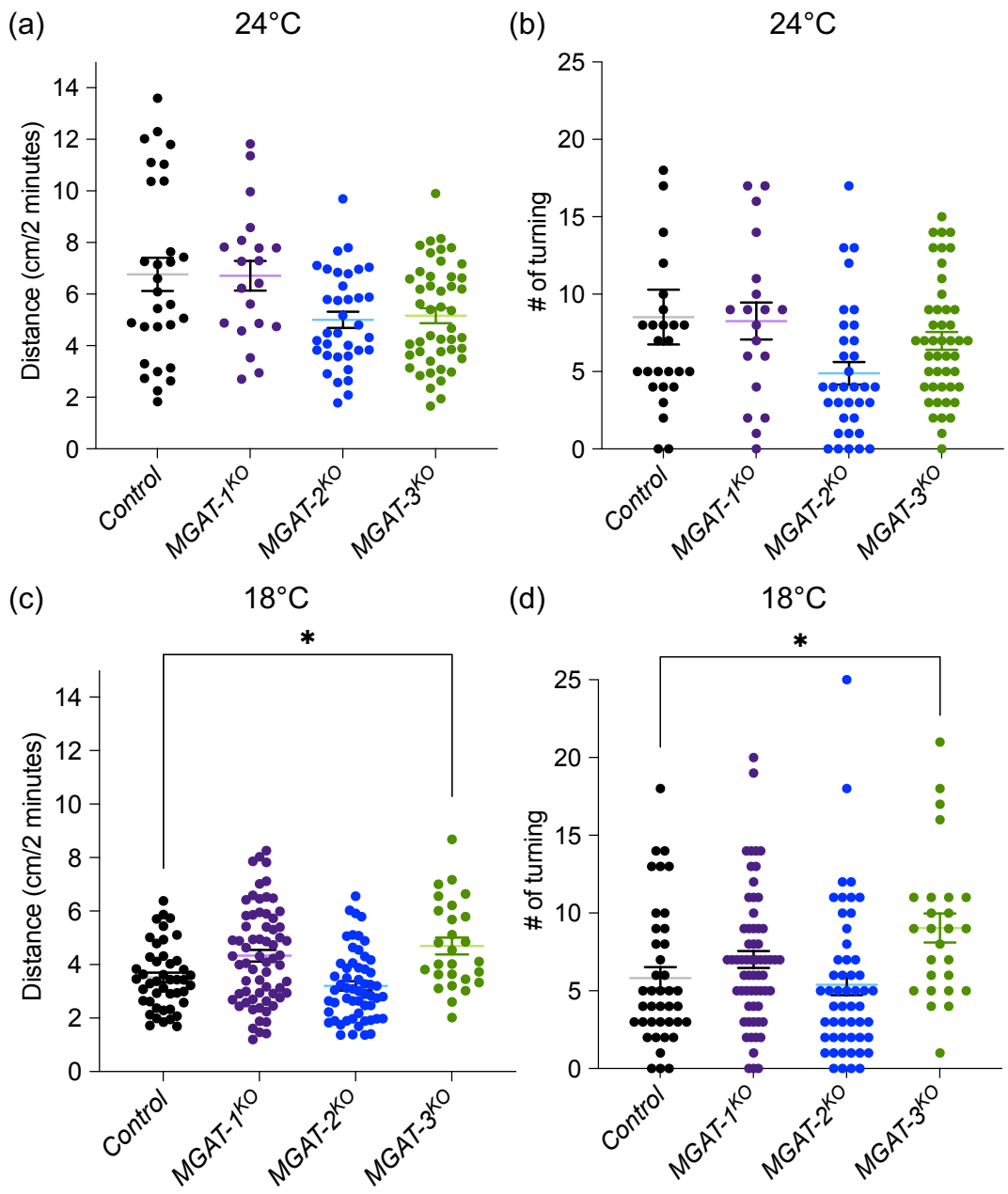
(a)
24°C
Distance (cm/2 minutes)
0
2
4
6
8
10
12
14
Control
MGAT-1KO
MGAT-2KO
MGAT-3KO
(b)
24°C
# of turning
0
5
10
15
20
25
Control
MGAT-1KO
MGAT-2KO
MGAT-3KO
(c)
18°C
*
Distance (cm/2 minutes)
0
2
4
6
8
10
12
14
Control
MGAT-1KO
MGAT-2KO
MGAT-3KO
(d)
18°C
*
# of turning
0
5
10
15
20
25
Control
MGAT-1KO
MGAT-2KO
MGAT-3KO

Figure 20. Role of *MGAT-1/-2/-3* in temperature-dependent locomotion activates.
Experiments were conducted using control (w^{1118}, black), *MGAT-1*^{KO} (purple), *MGAT-2*^{KO} (blue) and *MGAT-3*^{KO} (green) at the early 3rd instar stage (72 hours AEL). The data are presented as mean ± SEM.
(a) Moving distance (cm) of control, *MGAT-1*^{KO}, *MGAT-2*^{KO} and *MGAT-3*^{KO} under 24ºC for 2 minutes, N= 29-46. No significant difference based on one-way ANOVA with Dennett's multiple comparison.
(b) The number of turning (# of turning) in control, *MGAT-1*^{KO}, *MGAT-2*^{KO} and *MGAT-3*^{KO} under 24ºC for 2 minutes, N=27-66. No significant difference based on one-way ANOVA with Dennett's multiple comparison.
(c, d) Moving distance (cm) and the number of turning (# of turning) in control, *MGAT-1*^{KO}, *MGAT-2*^{KO} and *MGAT-3*^{KO} under 18ºC for 2 minutes. Statistical analyzes were performed by Kruskal-Wallis test with Steel multiple comparison: *P<0.05.

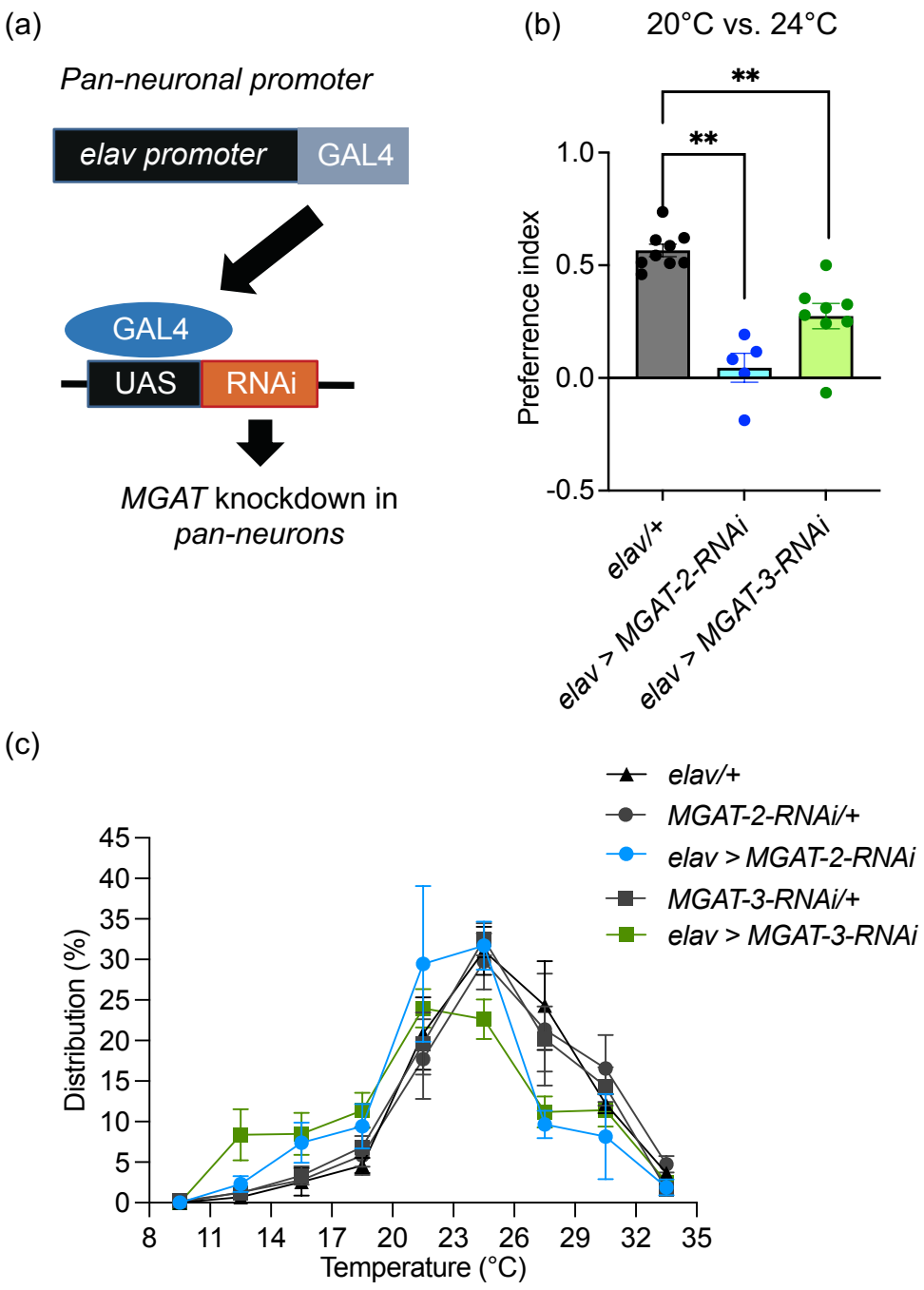
(a)
Pan-neuronal promoter
elav promoter
GAL4
GAL4
UAS
RNAi
MGAT knockdown in
pan-neurons
(b)
20°C vs. 24°C
**
**
Preferrence index
1.0
0.5
0.0
-0.5
elav/+
elav > MGAT-2-RNAi
elav > MGAT-3-RNAi
(c)
elav/+
MGAT-2-RNAi/+
elav > MGAT-2-RNAi
MGAT-3-RNAi/+
elav > MGAT-3-RNAi
Distribution (%)
45
40
35
30
25
20
15
10
5
0
8
11
14
17
20
23
26
29
32
35
Temperature (°C)

Figure 21. *MGAT-2* and *MGAT-3* contributed to cool avoidance in nervous system.

(a) A schematic of *MGAT-RNAi* knockdown in *pan-neurons* using *elav-GAL4* by GAL4/UAS system. *elav-promoter* (*pan-neuronal* promoter) specifically expressed GAL4 proteins in *elav-expressing* tissues, this protein combined with upstream activating sequence (UAS) to express double-stranded RNAs and induce RNA interference (RNAi) to target transcripts**.**

(b) PIs of 20°C versus 24°C condition two-way choice assay with indicated genotypes using early 3rd instar larvae (72 hours AEL). PIs were calculated using *UAS-dicer-2/+, elav-GAL4/+* (*elav/+,* black)*, UAS-dicer-2/UAS-MGAT-2-RNAi; elav-GAL4/+* (*elav > MGAT-2-RNAi,* blue) and *UAS-dicer-2/UAS-MGAT-3-RNAi; elav-GAL4/+* (*elav > MGAT-3-RNAi,* green) lines, N=5-9. A statistical analysis was performed by Kruskal-Wallis test with Steel multiple comparison: **P<0.01. The data are presented as mean ± SEM.

(c) Distribution of early 3rd instar larvae (72 hours AEL) on an 8ºC -35ºC thermal gradient. Lines carry *UAS-dicer-2/+, elav-GAL4/+* (*elav/+*, black, triangle marker)*, UAS-MGAT-2-RNAi/+* (*MGAT-2-RNAi/+*, grey, round marker), *UAS-dicer-2/UAS-MGAT-2-RNAi; elav-GAL4/+* (*elav > MGAT-2-RNAi,* blue, round marker), *UAS-MGAT-3-RNAi/+* (*MGAT-3-RNAi*/+, grey, square marker) and *UAS-dicer-2/UAS-MGAT-3-RNAi; elav-GAL4/+* (*elav > MGAT-b-RNAi,* green, square marker) were examined, N=4-5. The data are presented as mean ± SEM.

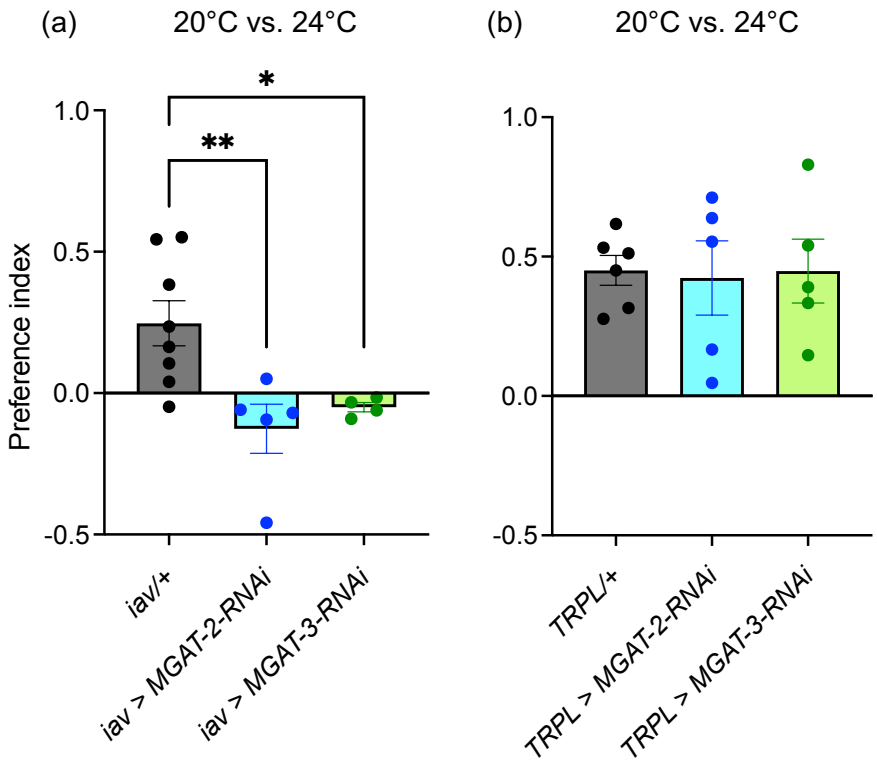

Figure 22. *MGAT-2* and *MGAT-3* functioned in cool avoidance in *iav-expressing* neruons.
(a-b) PIs of 20°C versus 24°C condition two-way choice assay with indicated genotypes using early 3rd instar larvae (72 hours AEL). The data are presented as mean ± SEM.
(a) PIs were calculated using *UAS-dicer-2, iav-GAL4/+* (*iav/+*, black), *UAS-dicer-2/UAS-MGAT-2-RNAi; iav-GAL4/+* (*iav > MGAT-2-RNAi,* blue) and *UAS-dicer-2/UAS-MGAT-3-RNAi; iav-GAL4/+* (*iav > MGAT-3-RNAi,* green) lines, N=4-8. A statistical analysis was performed by one-way ANOVA with Dennett's multiple comparison: *P<0.05, **P<0.01.
(b) PIs were calculated using *UAS-dicer-2, TRPL-GAL4/+* (*TRPL/+*, black), *UAS-dicer-2/UAS-MGAT-2-RNAi; TRPL-GAL4/+* (*TRPL > MGAT-2-RNAi,* blue) and *UAS-dicer-2/UAS-MGAT-3-RNAi; TRPL-GAL4/+* (*TRPL > MGAT-3-RNAi,* green) lines, N=5-6. No significant difference based on one-way ANOVA with Dennett's multiple comparison.

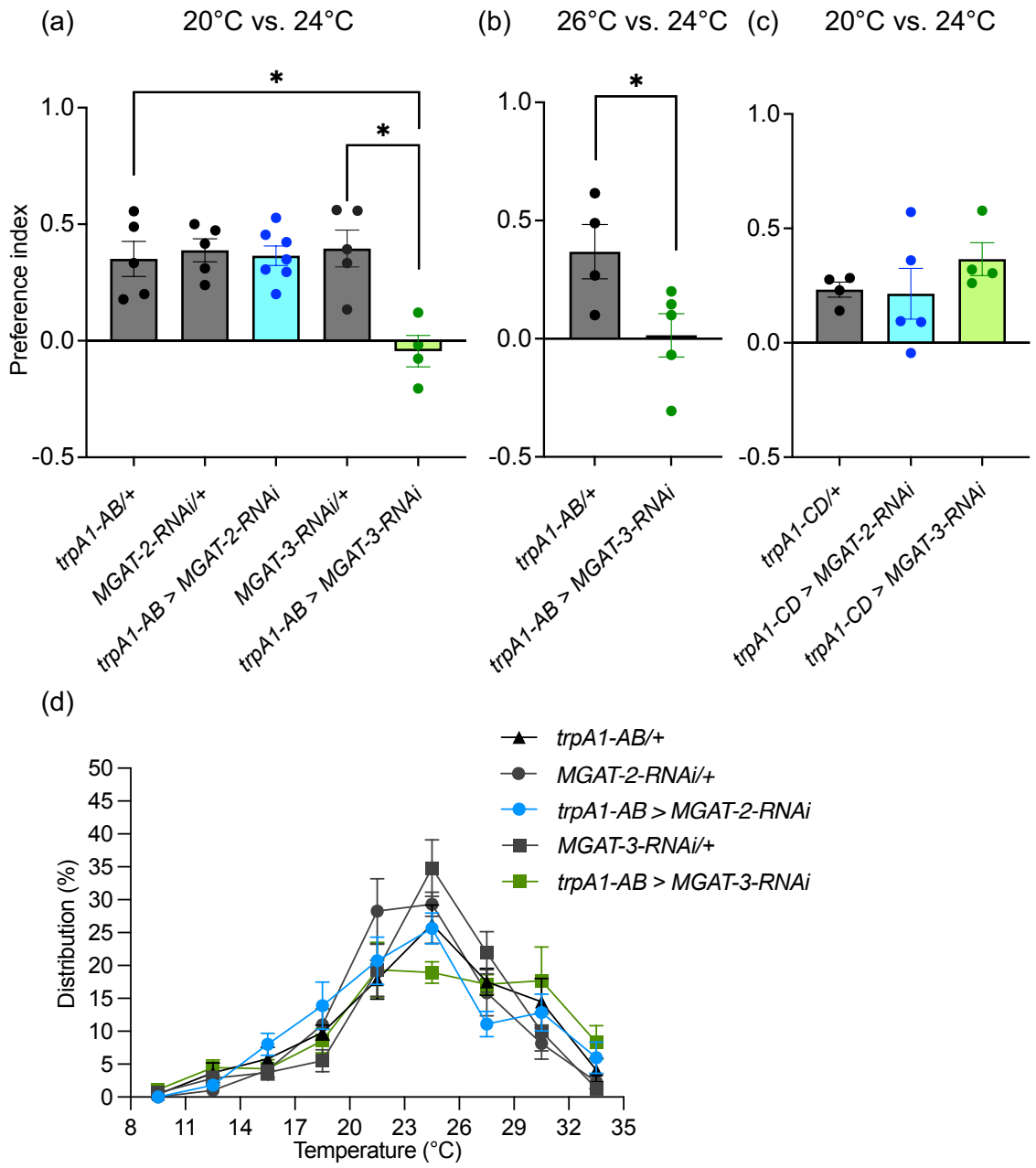
(a)
20°C vs. 24°C
(b)
26°C vs. 24°C
(c)
20°C vs. 24°C
Preference index
1.0
0.5
0.0
-0.5
*
*
*
trpA1-AB/+
MGAT-2-RNAi/+
trpA1-AB > MGAT-2-RNAi
MGAT-3-RNAi/+
trpA1-AB > MGAT-3-RNAi
trpA1-AB/+
trpA1-AB > MGAT-3-RNAi
trpA1-CD/+
trpA1-CD > MGAT-2-RNAi
trpA1-CD > MGAT-3-RNAi

(d)
trpA1-AB/+
MGAT-2-RNAi/+
trpA1-AB > MGAT-2-RNAi
MGAT-3-RNAi/+
trpA1-AB > MGAT-3-RNAi
Distribution (%)
50
45
40
35
30
25
20
15
10
5
0
8
11
14
17
20
23
26
29
32
35
Temperature (°C)

Figure 23. *MGAT-3* functioned in *trpA1-AB-expressing* neruons to mediate warm avoidance.
(a-c) PIs of 20°C (a, c) or 26°C (b) versus 24°C condition two-way choice assay with indicated genotypes using early 3rd instar larvae (72 hours AEL). The data are presented as mean ± SEM.
(a) PIs were calculated using *UAS-dicer-2, trpA1-AB-GAL4/+* (*trpA1-AB/+*, black), *UAS-MGAT-2-RNAi/+* (*MGAT-2-RNAi/+*, grey), *UAS-dicer-2/UAS-MGAT-2-RNAi; trpA1-AB-GAL4/+* (*trpA1-AB > MGAT-2-RNAi,* blue), *UAS-MGAT-3-RNAi/+* (*MGAT-3-RNAi/+*, grey), and *UAS-dicer-2/UAS-MGAT-3-RNAi; trpA1-AB-GAL4/+* (*trpA1-AB > MGAT-3-RNAi,* green) lines, N=4-7. A statistical analysis was performed by one-way ANOVA with Dennett's multiple comparison: *P<0.05.
(b) PIs were calculated using *UAS-dicer-2, trpA1-AB-GAL4/+* (*trpA1-AB/+*, black) and *UAS-dicer-2/UAS-MGAT-3-RNAi; trpA1-AB-GAL4/+* (*trpA1-AB > MGAT-3-RNAi,* green) lines, N=4-5. A statistical analysis was performed by Student's t-test: *P<0.05.
(c) PIs were calculated using *UAS-dicer-2, trpA1-AB-GAL4/+* (*trpA1-AB/+*, black), *UAS-dicer-2/UAS-MGAT-2-RNAi; trpA1-AB-GAL4/+* (*trpA1-AB > MGAT-2-RNAi,* blue), and *UAS-dicer-2/UAS-MGAT-3-RNAi; trpA1-AB-GAL4/+* (*trpA1-AB > MGAT-3-RNAi,* green) lines, N=3-6. No significant difference based on one-way ANOVA with Dennett's multiple comparison.
(d) Distribution of early 3rd instar larvae (72 hours AEL) on an 8ºC -35ºC thermal gradient. Lines carry *UAS-dicer-2, trpA1-AB-GAL4/+* (*trpA1-AB/+*, black, triangle marker), *UAS-MGAT-2-RNAi/+* (*MGAT-2-RNAi/+*, grey, round marker), *UAS-dicer-2/UAS-MGAT-2-RNAi; trpA1-AB-GAL4/+* (*trpA1-AB > MGAT-2-RNAi,* blue, round marker), *UAS-MGAT-3-RNAi/+* (*MGAT-3-RNAi/+*, grey, square marker) and *UAS-dicer-2/UAS-MGAT-3-RNAi; trpA1-AB-GAL4/+* (*trpA1-AB > MGAT-3-RNAi,* green, square marker) were examined, N=4-6. The data are presented as mean ± SEM.

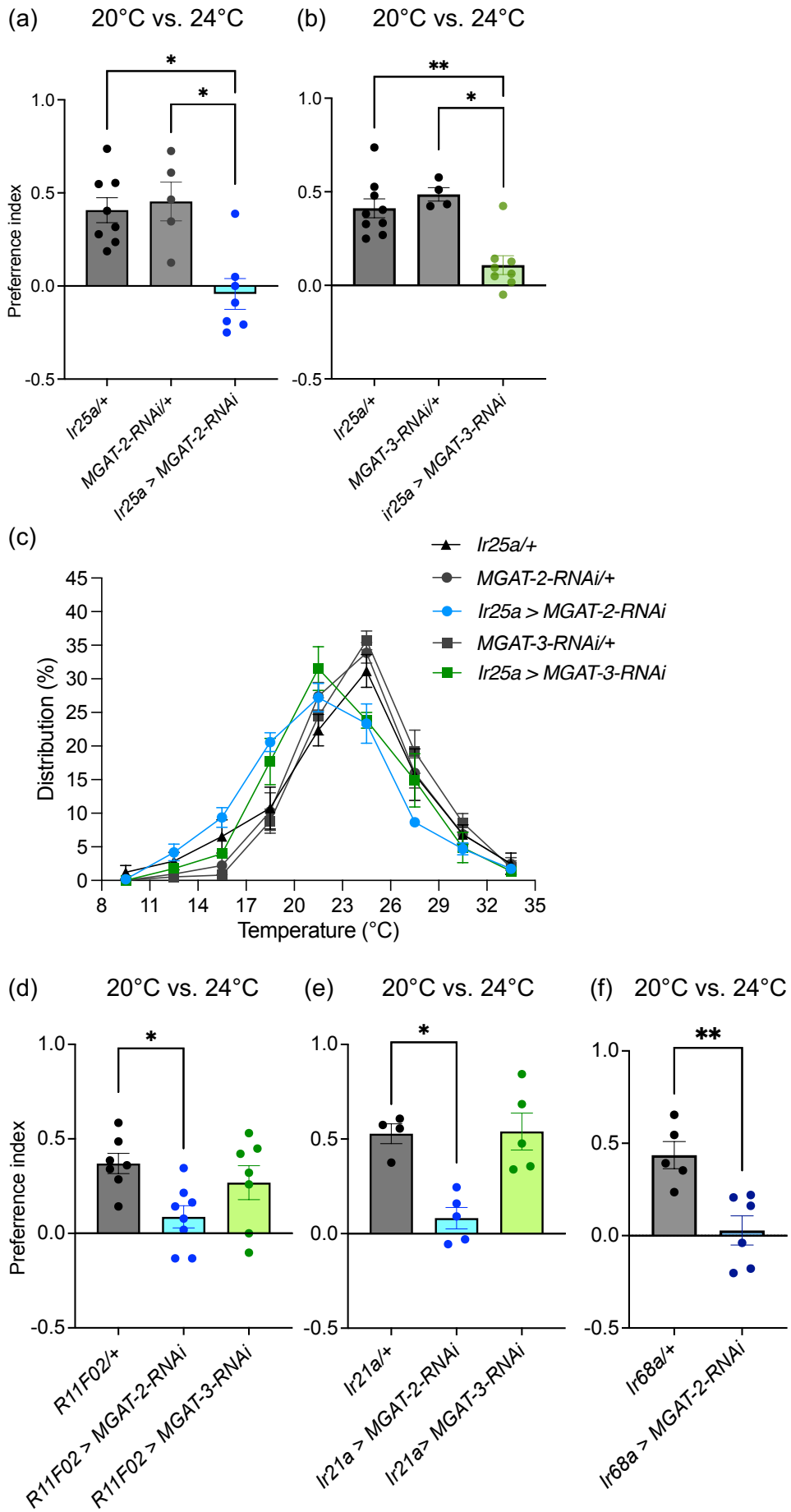
(a) 20°C vs. 24°C
(b) 20°C vs. 24°C
Preferrence index
1.0
0.5
0.0
-0.5
*
*
**
*
Ir25a/+
MGAT-2-RNAi/+
Ir25a > MGAT-2-RNAi
MGAT-3-RNAi/+
ir25a > MGAT-3-RNAi
(c)
Ir25a/+
MGAT-2-RNAi/+
Ir25a > MGAT-2-RNAi
MGAT-3-RNAi/+
Ir25a > MGAT-3-RNAi
Distribution (%)
45
40
35
30
25
20
15
10
5
0
8
11
14
17
20
23
26
29
32
35
Temperature (°C)
(d) 20°C vs. 24°C
(e) 20°C vs. 24°C
(f) 20°C vs. 24°C
Preferrence index
R11F02/+
R11F02 > MGAT-2-RNAi
R11F02 > MGAT-3-RNAi
Ir21a/+
Ir21a > MGAT-2-RNAi
Ir21a> MGAT-3-RNAi
Ir68a/+
Ir68a > MGAT-2-RNAi

Figure 24. *MGAT-2* was required for cool avoidance in DOCCs.

(a, b, d-f) PIs of 20°C versus 24°C condition two-way choice assay with indicated genotypes using early 3rd instar larvae (72 hours AEL). The data are presented as mean ± SEM.

(a) PIs were calculated using *UAS-dicer-2, Ir25a-GAL4/+* (*Ir25a/+,* black)*, UAS-MGAT-2-RNAi/+* (*MGAT-2-RNAi/+*, grey) and *UAS-dicer-2, Ir25a-GAL4/ UAS-MGAT-2-RNAi* (*Ir25a > MGAT-2-RNAi,* blue) lines, N=5-8. A statistical analysis was performed by Kruskal-Wallis test with Steel multiple comparison: *P<0.05.

(b) PIs were calculated using *UAS-dicer-2, Ir25a-GAL4/+* (*Ir25a/+,* black)*, UAS-MGAT-3-RNAi/+* (*MGAT-3/+*, grey) and *UAS-dicer-2, Ir25a-GAL4/UAS-MGAT-3-RNAi* (*Ir25a > MGAT-3-RNAi,* green) lines, N=4-9. A statistical analysis was performed by Kruskal-Wallis test with Steel multiple comparison: *P<0.05, **P<0.01.

(d) PIs were calculated using *UAS-dicer-2/+; R11F02-GAL4/+* (*R11F02/+,* black)*, UAS-dicer-2/UAS-MGAT-2-RNAi; R11F02-GAL4/+* (*R11F02 > MGAT-2-RNAi,* blue) and *UAS-dicer-2/UAS-MGAT-3-RNAi; R11F02-GAL4/+* (*R11F02 > MGAT-3-RNAi,* green) lines. A statistical analysis was performed by Kruskal-Wallis test with Steel multiple comparison: *P<0.05.

(e) PIs were calculated using *Ir21a-GAL4/+* (*Ir21a/+*, black)*, Ir21a-GAL4/UAS-MGAT-2-RNAi* (*Ir21a > MGAT-2-RNAi,* blue) and *Ir21a-GAL4/UAS-MGAT-3-RNAi* (*Ir21a > MGAT-3-RNAi,* green) lines. A statistical analysis was performed by Kruskal-Wallis test with Steel multiple comparison: *P<0.05.

(f) PIs were calculated using *UAS-dicer-2/+; Ir68a-GAL4/+* (*Ir68a/+,* black)*, UAS-dicer-2/UAS-MGAT-2-RNAi; Ir68a-GAL4/+* (*Ir68a > MGAT-2-RNAi,* blue) lines, N=5-6. A statistical analysis was performed by Mann-Whitney U test, **P<0.01.

(c) Distribution of early 3rd instar larvae (72 hours AEL) on an 8ºC -35ºC thermal gradient. Lines carry *UAS-dicer-2, Ir25a-GAL4/+* (*Ir25a/+,* black, triangle marker), *UAS-MGAT-2-RNAi/+* (*MGAT-2-RNAi/+*, grey, round marker), *UAS-dicer-2, Ir25a-GAL4/UAS-MGAT-2-RNAi* (*Ir25a > MGAT-2-RNAi,* blue, round marker), *UAS-MGAT-3-RNAi/+* (*MGAT-3-RNAi/+*, grey, square marker) and *UAS-dicer-2, Ir25a-GAL4/UAS-MGAT-3-RNAi* (*Ir25a > MGAT-3-RNAi,* green, square marker) were examined, N=4-6. The data are presented as mean ± SEM.

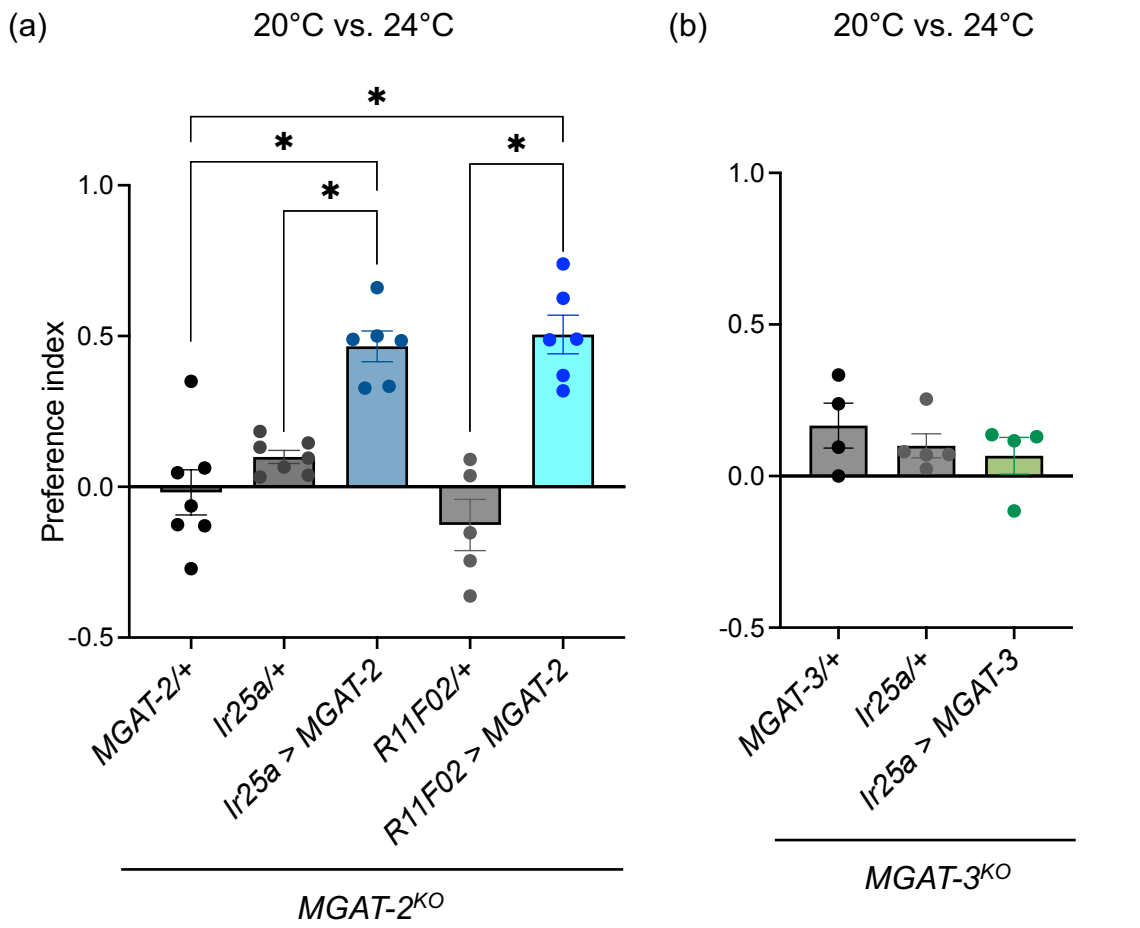
(a)
20°C vs. 24°C
(b)
20°C vs. 24°C
Preference index
1.0
0.5
0.0
-0.5
*
*
*
*
MGAT-2/+
Ir25a/+
Ir25a > MGAT-2
R11F02/+
R11F02 > MGAT-2
MGAT-2KO
MGAT-3/+
Ir25a/+
Ir25a > MGAT-3
MGAT-3KO

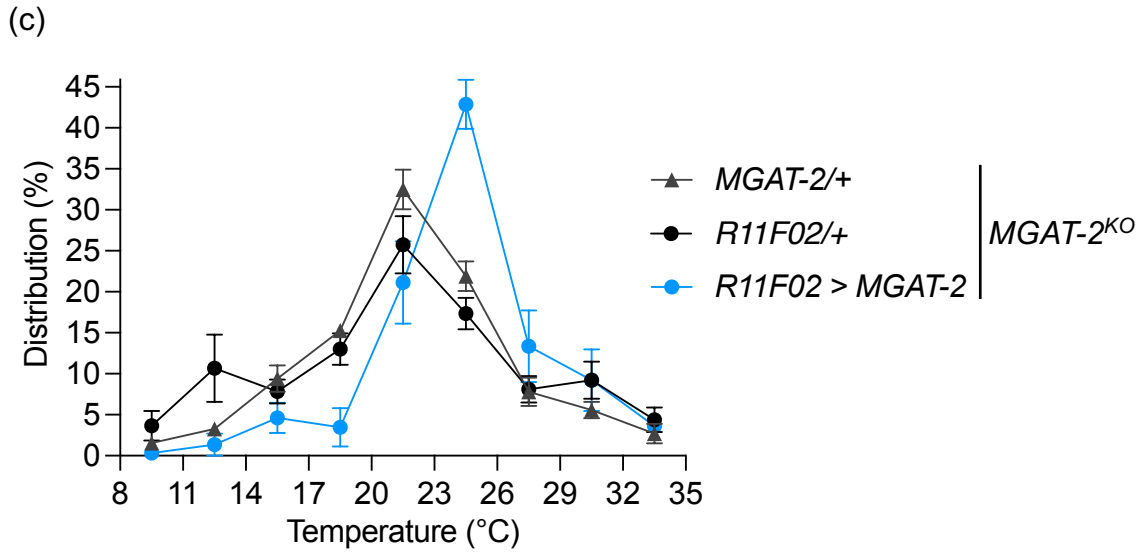
(c)
Distribution (%)
45
40
35
30
25
20
15
10
5
0
8
11
14
17
20
23
26
29
32
35
Temperature (°C)
MGAT-2/+
R11F02/+
R11F02 > MGAT-2
MGAT-2KO

Figure 25. *MGAT-2* primary functioned in DOCCs for cool avoidance.

(a, b) PIs of 20°C versus 24°C condition two-way choice assay with indicated genotypes using early 3rd instar larvae (72 hours AEL). The data are presented as mean ± SEM.

(a) All testing lines carry *MGAT-2^{KO}*. PIs were tested with *UAS-MGAT-2/+* (*MGAT-2/+*, black), *Ir25a-GAL4/+* (*Ir25a/+*, grey), *Ir25a-GAL4/+; UAS-MGAT-2/+* (*Ir25a > MGAT*-2, drak blue), *R11F02-GAL4/+* (*R11F02/+*, grey) and *R11F02-GAL4/+; UAS-MGAT-2/+* (*R11F02 > MGAT*-2, light blue) lines, N=5-7. A statistical analysis was performed by Kruskal-Wallis test with Steel-Dwass multiple comparison: *p<0.05.

(b) All testing lines carry *MGAT-3^{KO}*. PIs were tested with *UAS-MGAT-3/+* (*MGAT-3/+*, black), *Ir25a-GAL4/+* (*Ir25a/+*, grey), *Ir25a-GAL4/+; UAS-MGAT-3/+* (*Ir25a > MGAT*-3, green) lines, N=4-5. No asterisk indicates no significant difference based on one-way ANOVA with Tukey's multiple comparison.

(c) Distribution of early 3rd instar larvae (72 hours AEL) on an 8ºC -35ºC thermal gradient. All testing lines carry *MGAT-2^{KO}*. *UAS-MGAT-2/+* (*MGAT-2/+*, black, triangle marker) *R11F02-GAL4/+* (*R11F02/+*, black, round marker) and *R11F02-GAL4/+; UAS-MGAT-2/+* (*R11F02 > MGAT-2*, blue, round marker) larvae were tested in this assay, N=3-6. The data are presented as mean ± SEM.

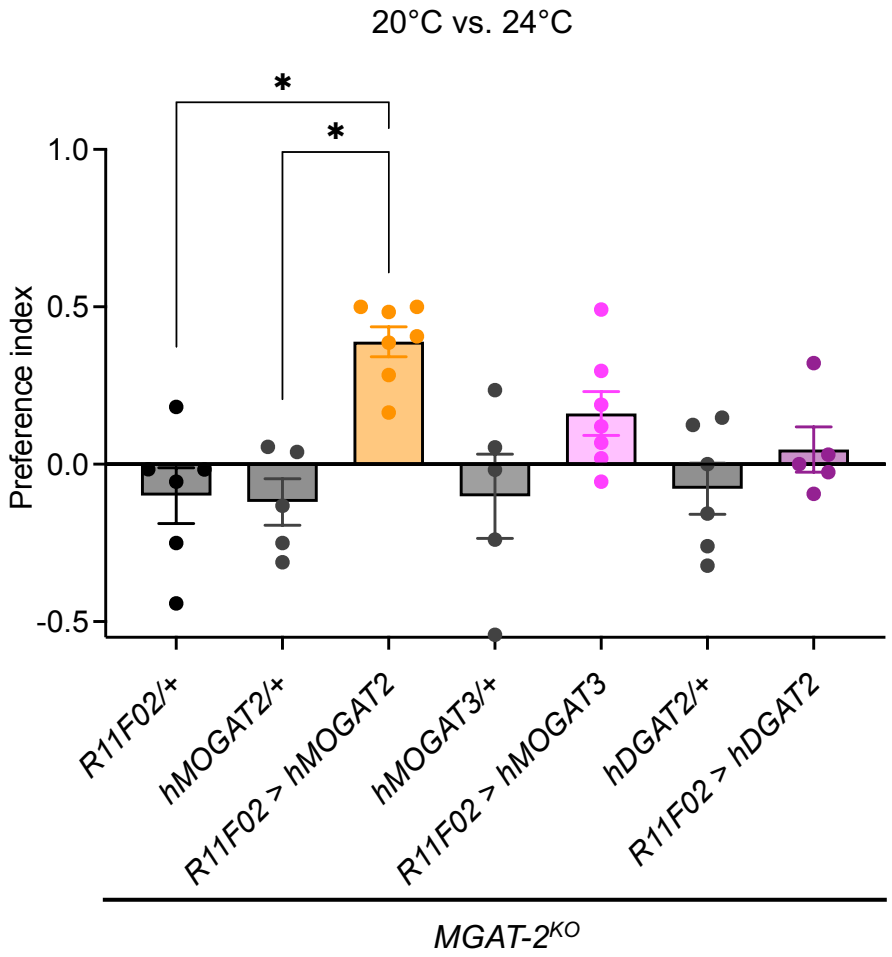

Figure 26. Function of *MGAT-2* in cool avoidance was compensated by human MOGAT2. PIs of 20°C versus 24°C condition two-way choice assay with indicated genotypes using early 3rd instar larvae (72 hours AEL). hMOGAT2: human MOGAT2; hMOGAT3: human MOGAT3; hDGAT2: human DGAT2. All testing lines carry *MGAT-2^{KO}*. PIs were tested with *R11F02-GAL4/+* (*R11F02/+*, black), *UAS-hMOGAT2/+* (*hMOGAT2/+*, grey), *R11F02-GAL4/+; UAS-hMOGAT3/+* (*Ir25a > hMOGAT-2*, orange), *UAS-hMOGAT3/+* (*hMOGAT3*, grey), *R11F02-GAL4/+; UAS-hMOGAT3/+* (*Ir25a > hMOGAT-3*, magenta), *UAS-hDGAT2/+* (*hDGAT2/+*, grey), and *R11F02-GAL4/+; UAS-hDGAT2/+* (*Ir25a > hMGAT-2*, dark red) larvae, N-5-7. A statistical analysis was performed by Kruskal-Wallis test with Steel-Dwass multiple comparison: *P<0.05. The data are presented as mean ± SEM.

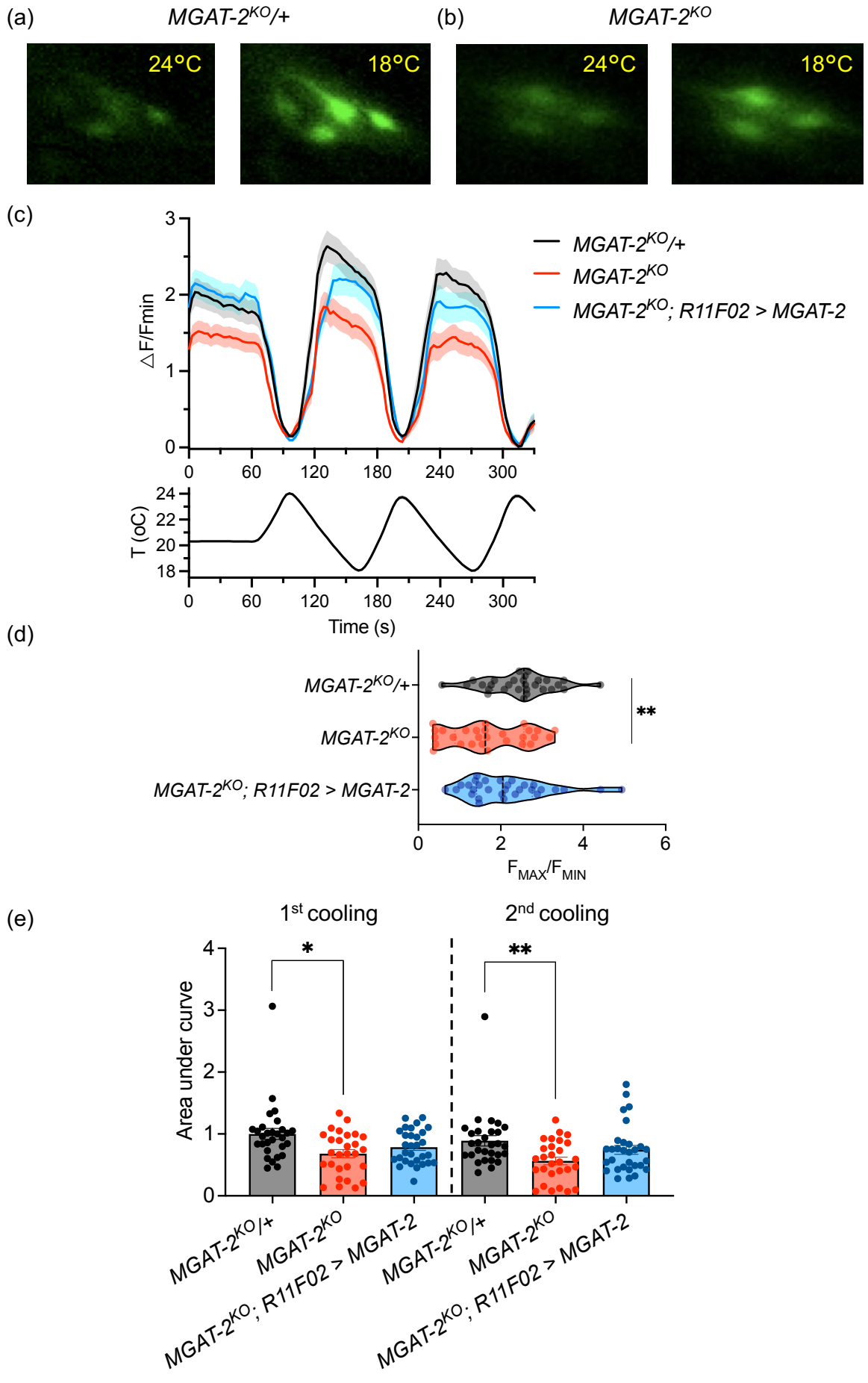
(a)
MGAT-2KO/+
24°C
18°C
(b)
MGAT-2KO
24°C
18°C
(c)
△F/Fmin
T (oC)
Time (s)
MGAT-2KO/+
MGAT-2KO
MGAT-2KO; R11F02 > MGAT-2
(d)
MGAT-2KO/+
MGAT-2KO
MGAT-2KO; R11F02 > MGAT-2
**
FMAX/FMIN
(e)
1st cooling
2nd cooling
*
**
Area under curve
MGAT-2KO/+
MGAT-2KO
MGAT-2KO; R11F02 > MGAT-2
MGAT-2KO/+
MGAT-2KO
MGAT-2KO; R11F02 > MGAT-2

Figure 27. Loss of *MGAT-2* caused the deterioration of cooling responses in DOCCs.
Experiments were conducted with early 3rd instar larvae (72 hours AEL), using GCaMP8m as a calcium indicator.
(a, b) Representative GCaMP-fluorescence images of *UAS-GCaMP8m*, *MGAT-2^{KO}*/+; *R11F02-GAL4*/+ (*MGAT-2^{KO}*/+, a) and *UAS-GCaMP8m*, *MGAT-2^{KO}*/*MGAT-2^{KO}*; *R11F02-GAL4*/+ (*MGAT-2^{KO},* b) under 24ºC and 18ºC.
(c) GCaMP-fluorescence changes in with *MGAT-2^{KO}*/+ (black), *MGAT-2^{KO}* (red) and *UAS-GCaMP8m*, *MGAT-2^{KO}*/*MGAT-2^{KO}*; *R11F02-GAL4*/*UAS-MGAT-2* (*MGAT-2^{KO}*; *R11F02 > MGAT-2*, blue) exposed to sinusoidal-like waves range from 18ºC and 24ºC. T (ºC): Temperature (ºC).
(d) Average ratio of maximum/minimum GCaMP-fluorescence (F_{MAX}/F_{MIN}) between 60-162 seconds and 168-270 seconds in *MGAT-2^{KO}*/+ (black), *MGAT-2^{KO}* (red) and *MGAT-2^{KO}*; *R11F02 > MGAT-2* (blue). A statistical analysis was performed by Kruskal-Wallis test with Steel-Dwass multiple comparison: **p<0.01, no asterisk indicates no significant difference.
(e) Relative area curves during 1st (96-162 seconds) and 2nd (204-270 seconds) warming in *MGAT-2^{KO}*/+ (black), *MGAT-2^{KO}* (red) and *MGAT-2^{KO}*; *R11F02 > MGAT-2* (blue) was normalized to the 1st cooling into 1. 1st cooling: a statistical analysis was performed by Kruskal-Wallis test with Steel-Dwass multiple comparison: *p<0.05, no asterisk indicates no significant difference. 2nd cooling: A statistical analysis was performed by one-way ANOVA with Tukey's multiple comparison: **P<0.01, no asterisk indicates no significant difference.
MGAT-2^{KO}/+: n=29 cells (from 12 animals); *MGAT-2^{KO}*: n=28 (11); *MGAT-2^{KO}*; *Ir68a > MGAT-2:* n=30 (13). The data are presented as mean ± SEM.

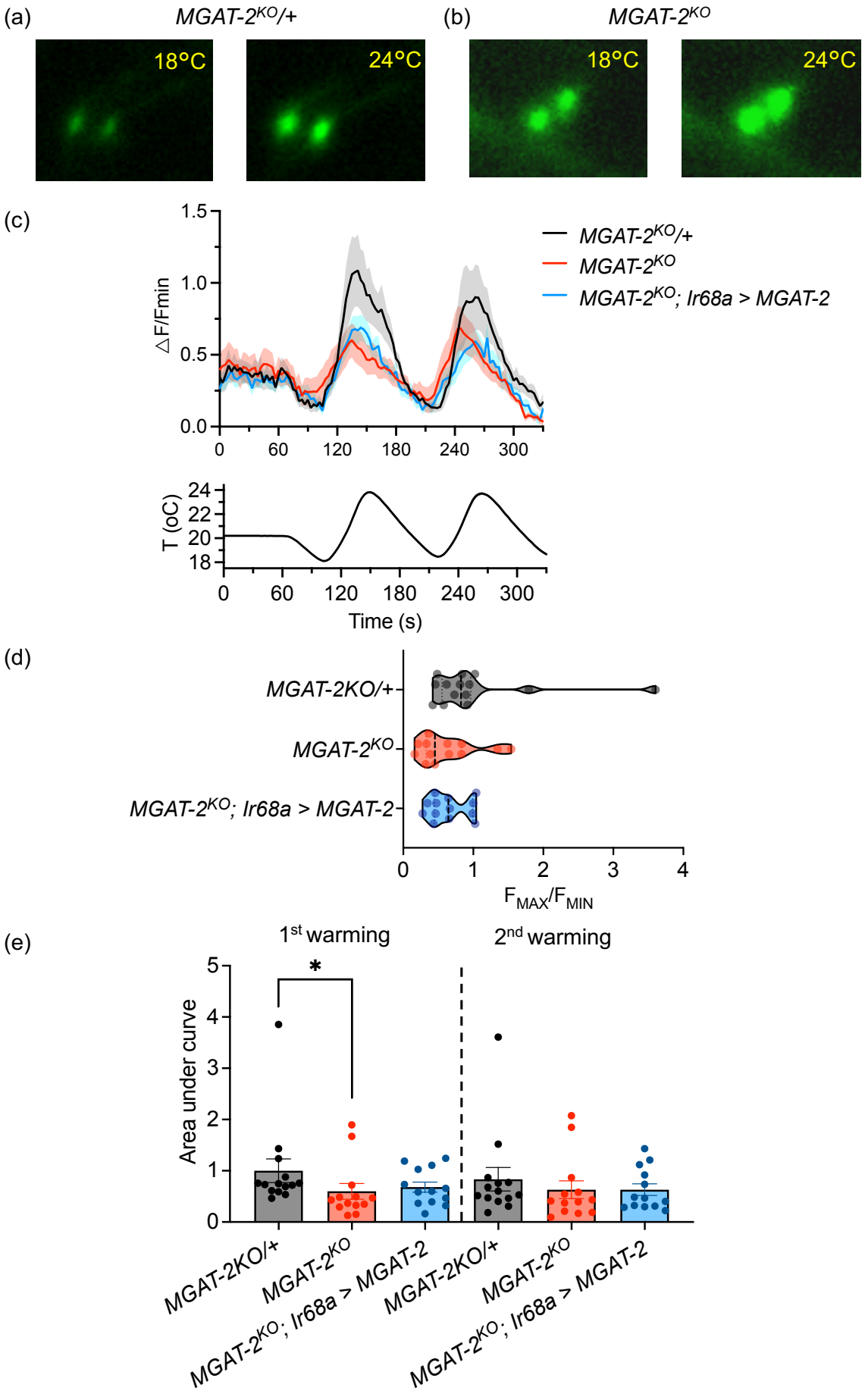
(a)
MGAT-2KO/+
18°C
24°C
(b)
MGAT-2KO
18°C
24°C
(c)
MGAT-2KO/+
MGAT-2KO
MGAT-2KO; Ir68a > MGAT-2
△F/Fmin
1.5
1.0
0.5
0.0
0
60
120
180
240
300
T (oC)
24
22
20
18
Time (s)
(d)
MGAT-2KO/+
MGAT-2KO
MGAT-2KO; Ir68a > MGAT-2
0
1
2
3
4
FMAX/FMIN
(e)
1st warming
2nd warming
*
Area under curve
5
4
3
2
1
0
MGAT-2KO/+
MGAT-2KO
MGAT-2KO; Ir68a > MGAT-2
MGAT-2KO/+
MGAT-2KO
MGAT-2KO; Ir68a > MGAT-2

Figure 28. Loss of *MGAT-2* caused the deterioration of warming responses in DOWCs.
Experiments were conducted with early 3rd instar larvae (72 hours AEL), using GCaMP8m as a calcium indicator.
(a, b) Representative GCaMP-fluorescence images of *UAS-GCaMP8m*, *MGAT-2^{KO}*/+; *Ir68a-GAL4*/+ (*MGAT-2^{KO}*/+, a) and *UAS-GCaMP8m*, *MGAT-2^{KO}*/*MGAT-2^{KO}*; *Ir68a-GAL4*/+ (*MGAT-2^{KO},* b) under 18ºC and 24ºC.
(c) GCaMP-fluorescence changes in with *MGAT-2^{KO}*/+ (black), *MGAT-2^{KO}* (red) and *UAS-GCaMP8m*, *MGAT-2^{KO}*/*MGAT-2^{KO}*; *Ir68a-GAL4*/*UAS-MGAT-2* (*MGAT-2^{KO}*; *Ir68a > MGAT-2*, blue) exposed to sinusoidal-like waves range from 18ºC and 24ºC. T (ºC): Temperature (ºC).
(d) Average ratio of maximum/minimum GCaMP-fluorescence (F_{MAX}/F_{MIN}) between 60-150 seconds and 174-264 seconds in *MGAT-2^{KO}*/+ (black), *MGAT-2^{KO}* (red) and *MGAT-2^{KO}*; *Ir68a > MGAT-2* (blue). No significant difference based on Kruskal-Wallis test with Steel-Dwass multiple comparison.
(e) Relative area curves during 1st (114-150 seconds) and 2nd (219-264 seconds) warming in *MGAT-2^{KO}*/+ (black), *MGAT-2^{KO}* (red) and *MGAT-2^{KO}*; *Ir68a > MGAT-2* (blue) was normalized to the 1st warming into 1. 1st warming: a statistical analysis was performed by Kruskal-Wallis test with Steel-Dwass multiple comparison: *P<0.05, no asterisk indicates no significant difference. 2nd warming: No significant difference based on one-way ANOVA with Tukey's multiple comparison.
MGAT-2^{KO}/+: n=14 cells (from 9 animals); *MGAT-2^{KO}*: n=13 (8); *MGAT-2^{KO}*; *Ir68a > MGAT-2:* n=13 (9). The data are presented as mean ± SEM.

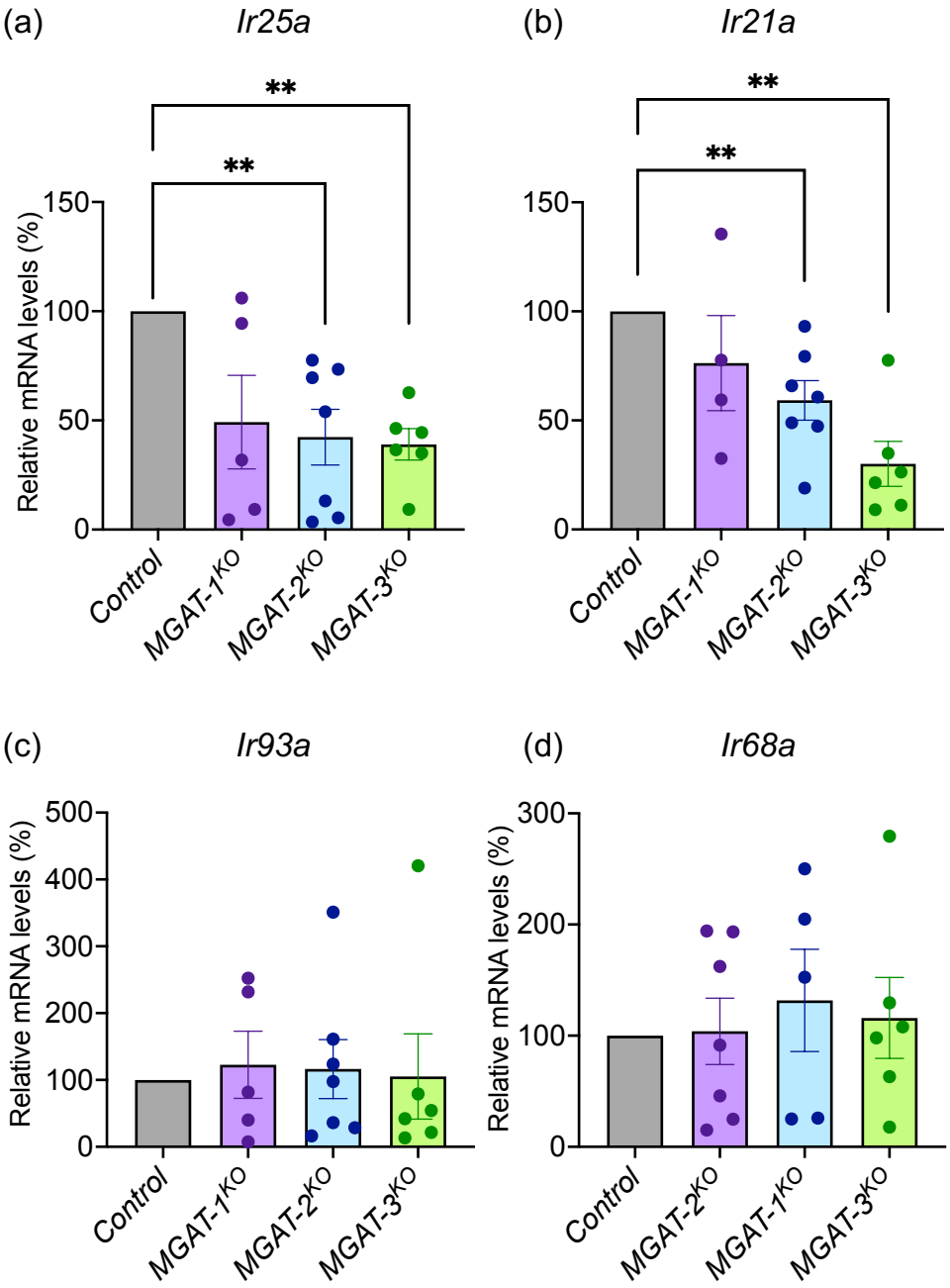
(a)
Ir25a
**
**
Relative mRNA levels (%)
150
100
50
0
Control
MGAT-1KO
MGAT-2KO
MGAT-3KO
(b)
Ir21a
**
**
150
100
50
0
Control
MGAT-1KO
MGAT-2KO
MGAT-3KO
(c)
Ir93a
Relative mRNA levels (%)
500
400
300
200
100
0
Control
MGAT-1KO
MGAT-2KO
MGAT-3KO
(d)
Ir68a
Relative mRNA levels (%)
300
200
100
0
Control
MGAT-2KO
MGAT-1KO
MGAT-3KO

Figure 29. *MGAT-2* and *MGAT-3* supported transcriptional level of *Ir25a* and *Ir21a* at the early 3rd instar stage.

(a-d) Relative mRNA levels in the anterior region of early 3rd instar larvae (72 hours AEL) were examined in control (w^{1118}, grey), *MGAT-1*^{KO} (purple), *MGAT-2*^{KO} (blue) and *MGAT-3*^{KO} (green). mRNA level in mutants were normalized to control into 100%. The data are presented as mean ± SEM.

(a-c) *Ir25a* (a, N=5-7), *Ir21a* (b, N=4-7) and *Ir93a* (c, N=4-7) (d, N=6) relative mRNA levels. Statistical analyses were performed by Kruskal-Wallis test with Steel multiple comparison: **P<0.01, no asterisk indicates no significant difference.

(d) Relative mRNA level of *Ir68a*. No significant difference based on one-way ANOVA with Dennett's multiple comparison.

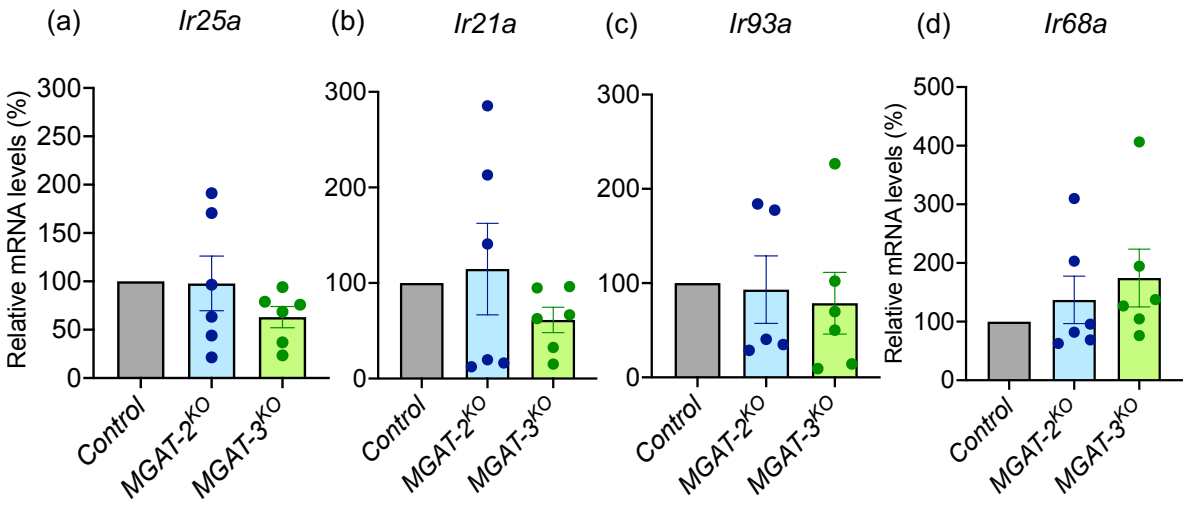

Figure 30. *MGAT-2* and *MGAT-3* did not affect *Irs* transcriptional level at the late 3rd instar stage.

(a-d) Relative mRNA levels in the anterior region of late 3rd instar larvae (120 hours AEL) were examined in control (w^{1118}, grey), *MGAT-2*^{KO} (blue) and *MGAT-3*^{KO} (green). mRNA level in mutants were normalized to control into 1. Data represent mean ± SEM.

Relative mRNA levels of *Ir25a* (a, N=6), *Ir21a* (b, N=6), *Ir93a* (c, N=5-6) and *Ir68a* (d, N=6) were examined. No significant difference based on one-way ANOVA with Dennett's multiple comparison. The data are presented as mean ± SEM.

(a)

Gene name	*MGAT-2*	*ir25a*	*ir21a*	*ir93a*
GATA-d	+	+	+	
broad	+	+		
pan		+	+	
Abd-B		+		
Dr		+		
exd		+		
Ubx				+
Vsx2				+

(b)

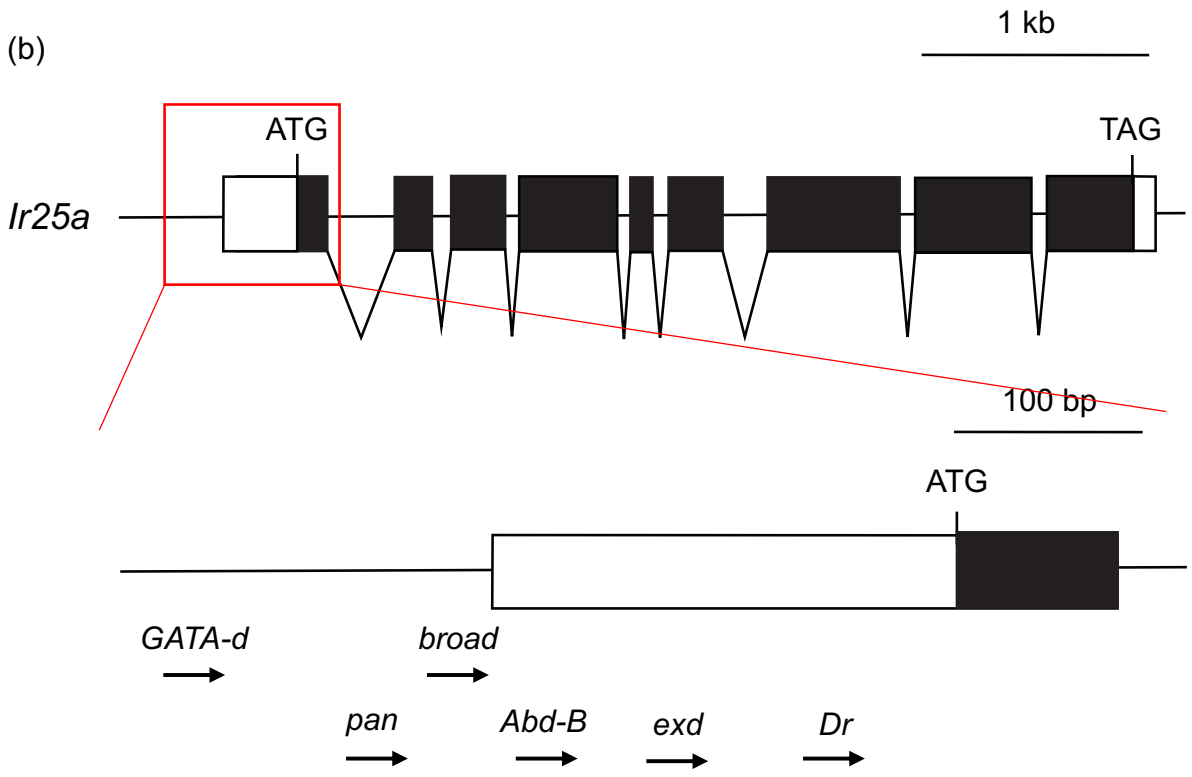

Figure 31. Predicted transcriptional factors at the upstream of *Ir25a* CDS.

(a) Transcriptional factor binding motifs of *GATA-d, broad, pan, Abd-B, Dr, exd, Ubx* and *Vsx2* (listed in the first column) were observed in *MGAT-2*, *Ir25a*, *Ir21a* or *Ir93a* (listed in the first row). "+" indicates the existence of binding motif in transcriptional factors in *MGAT-2*, *Ir25a*, *Ir21a* or *Ir93a.* This result in predicted by TFBS predictions in *Drosophila melanogaster* (genome: dm6) genome for all profiles in the JASPAR CORE insect's collection, with a minimum score of 425.

(b) Gene structure of *Ir25a* (upper) and positions of predicted transcriptional factor binding motifs upstream of *Ir25* start codon (lower). Broken lines indicate introns, black boxes indicate the CDS and white boxes indicate UTRs. "ATG" indicated the start codon and "TAG" indicated stop codon. The red rectangle highlighted 5' UTR and 1st exon which were shown in an amplified scale in the lower panel. Lower panel showed positions of predicted transcriptional factor binding domains of *GATA-d*, *broad*, *pan, Abd-B, exd* and *Dr*. Arrows indicate that predicted transcriptional factors' binding motif showed consistent direction to *Ir25a*.

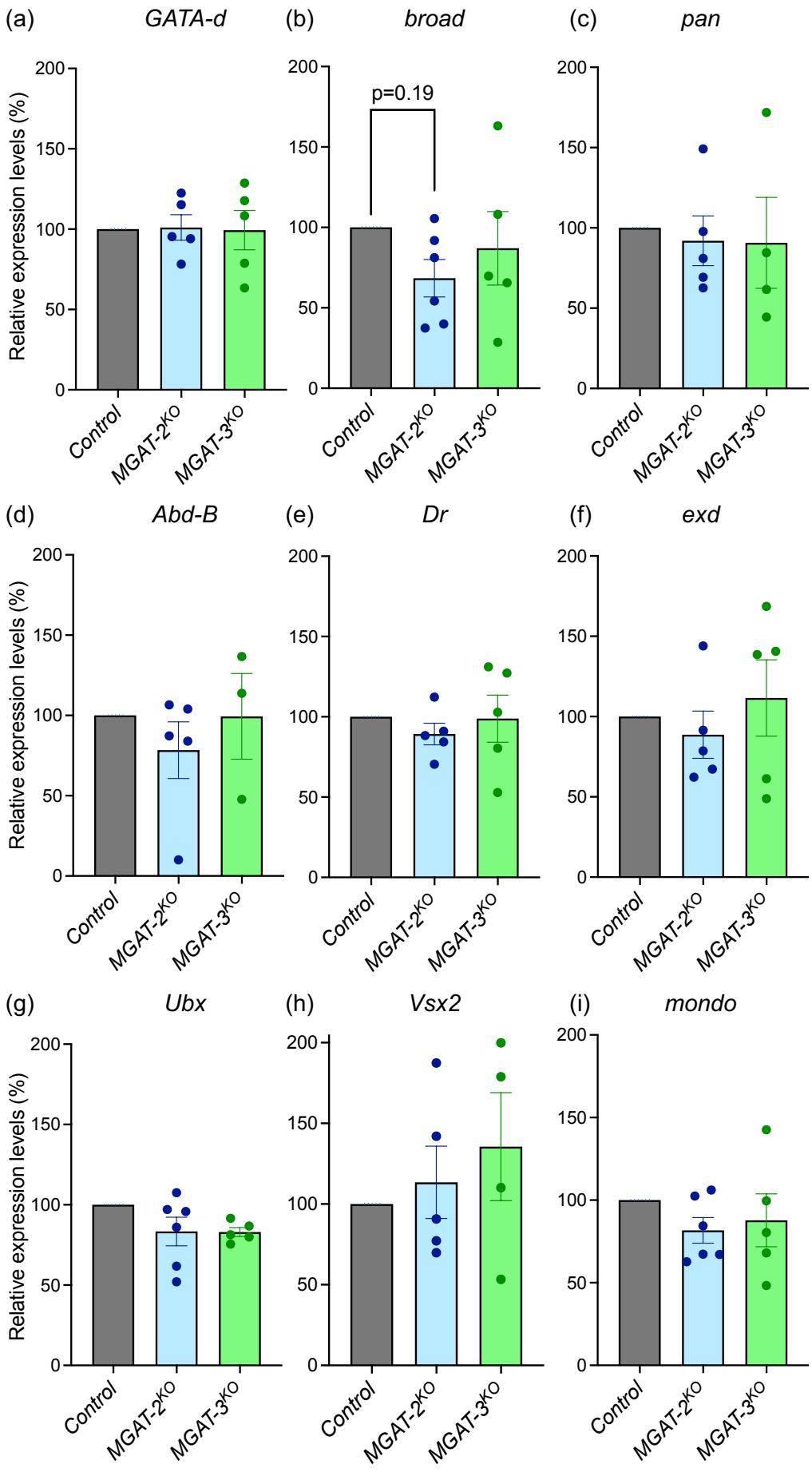
(a) GATA-d
(b) broad
(c) pan
(d) Abd-B
(e) Dr
(f) exd
(g) Ubx
(h) Vsx2
(i) mondo
Relative expression levels (%)
200
150
100
50
0
p=0.19
Control
MGAT-2KO
MGAT-3KO

Figure 32. *MGATs* affected the expression of *broad* at a transcriptional level in whole body. (a-i) Relative mRNA levels in the whole body of early 3rd instar larvae (72 hours AEL) were examined in control (w^{1118}, grey), *MGAT-2*^{KO} (blue) and *MGAT-3*^{KO} (green). mRNA level in mutants were normalized to control into 100%. Relative mRNA level of *GATA-d* (a, N=5), *broad* (b, N=5-6), *pan* (c, N=4-5). *Abd-B* (d, N=3-5), *Dr* (e, N=5), *exd* (f, N=5), *Ubx* (g, N=4-6), *Vsx2* (h, N=4-5) and *mondo* (i, N=4-5) were examined. No asterisk indicates no significant difference based on one-way ANOVA with Dennett's multiple comparison, P=0.19 in (b) indicates the statistical result of relative *broad* mRNA level in *MGAT-2*^{KO}. The data are presented as mean ± SEM.

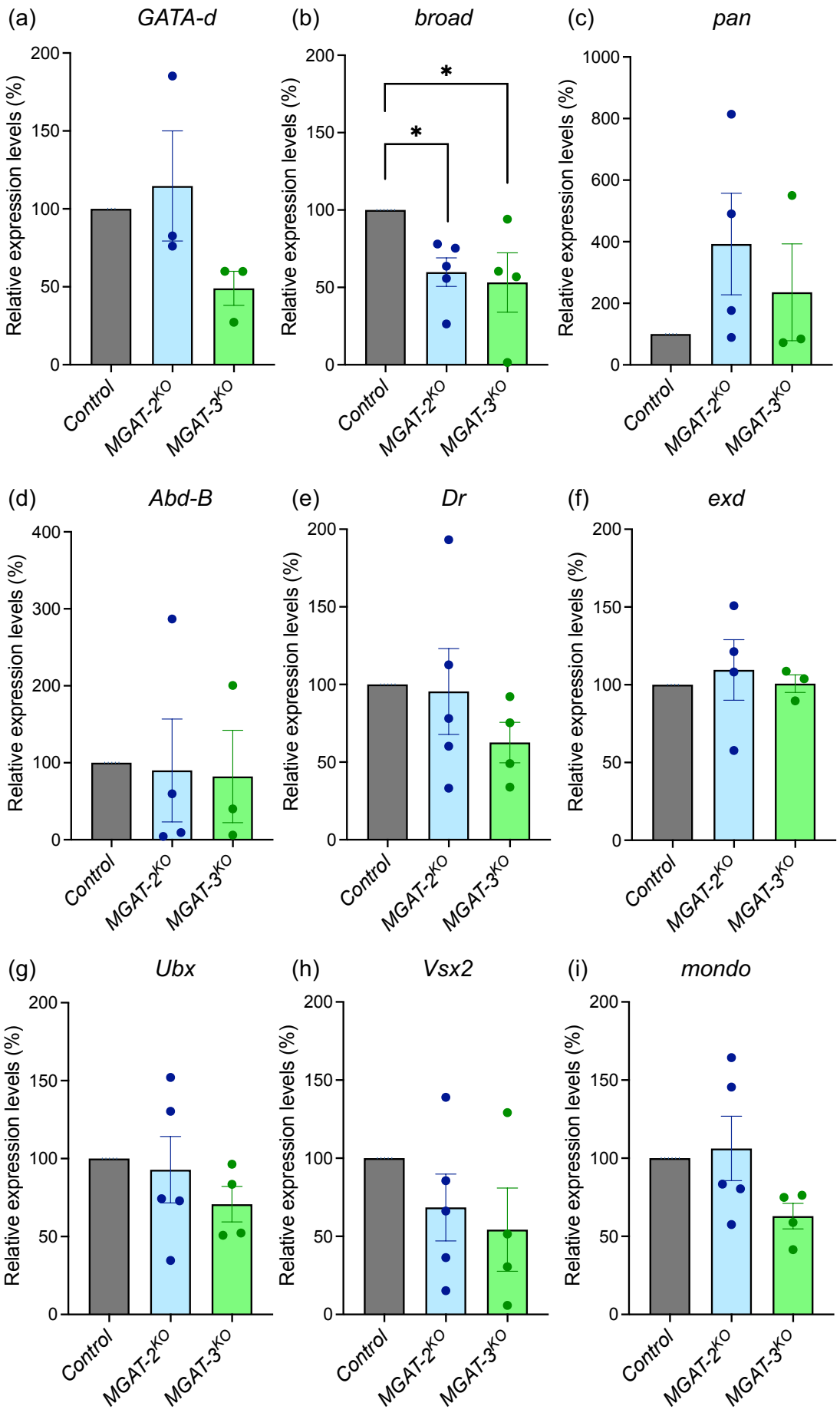
(a)
GATA-d
(b)
broad
(c)
pan
(d)
Abd-B
(e)
Dr
(f)
exd
(g)
Ubx
(h)
Vsx2
(i)
mondo
Relative expression levels (%)
Control
MGAT-2KO
MGAT-3KO
*
*

Figure 33. *MGATs* affected the expression of *broad* at a transcriptional level in DOCCs and DOWCs.

(a-i) Relative mRNA levels in the anterior region of early 3rd instar larvae (72 hours AEL) were examined in control (w^{1118}, grey), *MGAT-2*^{KO} (blue) and *MGAT-3*^{KO} (green). mRNA level in mutants were normalized to control into 100%. The data are presented as mean ± SEM.

(a, b) Relative mRNA level of *GATA-d* (a, N=3) and *broad* (b, N=5). Statistical analyses were performed by Kruskal-Wallis test with Steel multiple comparison: *P<0.05, no asterisk indicates no significant difference.

(c-i) Relative mRNA level of *pan* (c, N=3-4). *Abd-B* (d, N=3-5), *Dr* (e, N=4-5), *exd* (f, N=5), *Ubx* (g, N=5), *Vsx2* (h, N=4-5) and *mondo* (i, N=4-5). No significant difference based on one-way ANOVA with Dennett's multiple comparison.

7 Tables

Table 1. Primer list for vector construction (#1-12, #25-32) and genotyping (#25-32, #37-39).

Primer order (#)	primer name	Sequence (5'-3')
1	CG8839_gRNA_S	CTGTGATCGGGTTTTAGAGCTAGAAATAGC
2	CG8839_gRNA_AS	ATGCCATTCTCGACGTTAAATTGAAAATAGG
3	MGAT-1_gRNA_S	ACGTTTGCCAGTTTTAGAGCTAGAAATAGC
4	MGAT-1_gRNA_AS	CTGGCGACGCCGACGTTAAATTGAAAATAGG
5	MGAT-2_gRNA_S	GGCGTTCCAGGTTTTAGAGCTAGAAATAGC
6	MGAT-2_gRNA_AS	GACTGCAGATCCGACGTTAAATTGAAAATAG G
7	MGAT-3_gRNA_S	CGGGTTCCGCGTTTTAGAGCTAGAAATAGC
8	MGAT-3_gRNA_AS	GAGAGGAGCCCGACGTTAAATTGAAAATAGG
9	HDR_Arm1-F	CGTTTCACTTCTGAGTTCGG
10	HDR_Arm1-R	CTCTTATACGACATCACCGATG
11	HDR_Arm2-F	GCAGTATACGAGACCTATAGG
12	HDR_Arm2-R	GTATAGGAGACCTATAGTGTCTTC
13	CG8839_Arm1_F	CCATCGGTGATGTCGTATAGGAATAGCTGTCT GATGCGCACTC
14	CG8839_Arm1_R	CCTATAGGTCTCGTATACTGCCGGTGGAACAC TCTCACCC
15	CG8839_Arm2_F	GAAGACACTATAGGTCTCCTATACATCACAGA TGCCATTCTCTTGG
16	CG8839_Arm2_R	CATCGGTGATGTCGTATAAGAGACCTCTCTCA AGTGCTGTGCCAC
17	MGAT2_Arm1_F	CCATCGGTGATGTCGTATAGGAATTGGCGCTC CCATCGACGTG
18	MGAT2_Arm1_R	CCTATAGGTCTCGTATACTGCCAGAGGAACCC GCAGTGGTGC
19	MGAT2_Arm2_F	GAAGACACTATAGGTCTCCTATACGAACGCC GACTGCAGATACTGG

20	MGAT2_Arm2_R	CATCGGTGATGTCGTATAAGAGACAGTCCTG AAACCGTCGGAGC
21	MGAT3_Arm1_F	CCATCGGTGATGTCGTATAGGAAGCTTCCTCC CATTCCGACGACG
22	MGAT3_Arm1_R	CCTATAGGTCTCGTATACTGCGAACCCGGAGA GGAGCCCATTC
23	MGAT3_Arm2_F	GAAGACACTATAGGTCTCCTATACCGCTGGA ACGGCGGCTTC
24	MGAT3_Arm2_R	CATCGGTGATGTCGTATAAGAGACCATGGCTT CCTTGGCGCCAC
25	CG8839_genotype_F	AATTCTGAGTCCTAGTAGCTG
26	CG8839_genotype_R	CTCTTAAGTCTGGATCAACG
27	MGAT1_genotype_F	GAGGACCGTGCTACCAAGTAG
28	MGAT1_genotype_R	TGCGGTCTTGACCAGCTGTAC
29	MGAT2_genotype_F	ATCGCTGGCTTCCATATCATTC
30	MGAT2_genotype_R	CCAGCGACTCAATGACCTGT
31	MGAT3_genotype_F	ATAAGTACTCCACGTTACACCCTGG
32	MGAT3_genotype_R	TCTCCAATTGCTGCGGTAGAA
33	MGAT-2_UAS_F	AAAACTCGAGATGAAAATCGAGTGGGCACC AC
34	MGAT-2_UAS_R	TTCTAGACTAGTGTACAACTAGAGTGGCAC
35	MGAT-3_UAS_F	AAAACTCGAGATGACAATCGAATGGGCTC
36	MGAT-3_UAS_R	TTCTAGATCACTGTATTATAAGTTTGATATGC
37	vector_UAS_g_F	GCAGCTGAACAAGCTAAACAATC
38	MGAT-2_UAS_g_R	TGCCATCCACAACGGATTG
39	MGAT-3_UAS_g_R	CTCCGATTGCTGCGGTAGAAT

Table 2. Primer list for qPCR.

Primer order (#)	Primer name	Sequence (5'-3')
1	rp49__F	GACGCTTCAAGGGACAGTATCTG
2	rp49__R	AAACGCGGTTCTGCATGAG
3	CG8839_F	TGGACAATACAGCACGGAGG
4	CG8839_R	AAGAGTCCAGCTGTGTGCAG
5	MGAT-1__F	TGCGGTCTTGACCAGCTGTAC
6	MGAT-1__R	CTATTTCTTCGTTGCTGCCGTG
7	MGAT-2__F	CACCTTTGGCTTCCTCCCAT
8	MGAT-2__R	AGTGGCACTCTTCGAATTCTCC
9	MGAT-3__F	TGCCTCGCAGTAGCTATCCT
10	MGAT-3__R	CTCCGATTGCTGCGGTAGAAT
11	Ir25a__F	AGTCAGCGGGACAATGCGAC
12	Ir25a__R	CGTGACGAGATCAAAGGTTCCATAC
13	Ir93a__F	TCTAAATTGGAAGACCGCCGTTG
14	Ir93a__R	GTTCAGGGTCTCGGCTATTTCGATG
15	Ir68a__F	ATTGCCATCAGTCGGTATCGTTC
16	Ir68a__R	ATCATCGCTGTAGCCGAACAC
17	Ir21a__F	CTCAATAAATGCCCACCGGTC
18	Ir21a__R	TGCAATTGCAATCTATATGGCTCG
19	GATAd__F	AACTACGGCAAAGAGCACGGTC
20	GATAd__R	CCACAAACCACGTTGGGTAATC
21	br__F	CTACTTCCGCGAGCTGCTCAAG
22	br__R	AAGGACTGCAGGGACTTCTGGTG
23	pan__F	ATGAGCACGGAAGTCAGCTAAG
24	pan__R	CAATGTGGGTCGTTGCTGTG
25	Abd-B__F	CCACTGCATATACCCGCCAT
26	Abd-B__R	TCCGCTTCGTTCATGTAGGC
27	Dr__F	ATGTTTCCGGGAGCAGGATTC
28	Dr__R	AGCAGCTGCTGTGTTGTGAAG
29	exd__F	GCAACCCATATCCATCCGAAGAG
30	exd__R	TGGATAGCCCATGGAATCCTG

31	Ubx__F	GAGTCCCTATGCCAACCACC
32	Ubx__R	AGGCAGTCCTGTTTGTAGGC
33	Vsx2__F	CGAAATGCTCTCGCTGAAGAC
34	Vsx2__R	CCTTGGCCGACTTAAGGATCGTG
35	mondo__F	GCGATCCCATGCTAAACAGCAC
36	mondo__R	GTGGCTATGGCACTGACGGAAG

8 Acknowledgement

First, I would like to express my sincere appreciation to my supervisor Dr. Takaaki Sokabe, for his infinite patience and concern in my research and daily life. In the academic field, he offered me extensive guidance, which cultivated my knowledge and skills to explore biological mechanisms. He also guided me with the vision and taste of research, preserving my passion for challenging scientific problems. Outside of academia, his positive mind of life encouraged and supported me during times of hardship. I deeply thank for our encounter in the journey of science, my limited words are insufficient to express my gratitude.

Second, I would like to appreciate all the support that came from our Flyteam. All Flyteam members kindly support the stock maintenance which supported my experiments. Senior colleague Dr. Takuto Suito provided me selfless teaching in multiple techniques and gave me detailed suggestions to my research. Dr. Shoma Sato, PhD students Aliyu Mudassir Magaji and Hinata Yamanaka provided me with informative suggestions to my research project. Stuff members Naomi Fukuta and Terumi Hashimoto kindly supported me in molecular works.

My gratitude also extends to all lab members. Dr. Makoto Tominaga, Dr. Shigeru Saito and Dr. Jing Lei provided me constructive suggestions to my project. Claire Saito helped to improve my techniques in plasmid constructions. Yoshimi Ito handled a lot of my paperwork, which strongly ease my daily life. Other lab members, Dr. Makiko Kashio, Dr. Kenta Maruyama, Keiko Fukuoka, Dr. Derouiche Sandra, Dr. Tiangbang Li, Dr. Xiaona Feng, Dr. Nguyen Thi Hong Dung and Dr. Aykut Deveci accompanied and encouraged me during my PhD study.

I would like to thank my advisors Dr. Mikio Furuse and Dr. Michihiro Tateyama for their kind suggestions and encourages which helped my progress. Also, thanks to Dr. Craig Montell and Dr. Paul Garrity, who kindly provided me with fly stocks for experiments.

Finally, I thank my roommates Dr. Jing Lei and Yu Long who accompanied me for an enjoyable daily life in the shared-house. I also thank my family members who always respect my career and decisions. They healed my stress and gave me helpful suggestions from various perspectives.